Modifications to a Scanning Tunnelling Microscope

A thesis presented in partial fulfillment of the
requirements for the degree of

Master of Science

in

Physics

at Massey University, Palmerston North,
New Zealand

Mark Warwick Hunter
2001

Abstract

A scanning tunnelling microscope (STM), previously constructed as part of a PhD project, has been modified to improve its reliability and accessibility. Initially the aim was to obtain atomic resolution (~ 0.1 nm) on a routine basis but for an unknown reason this has not been obtained and thus far we are limited to a resolution of about 1 nm.

Improvements to the device that converts the tunnelling current into a voltage were made resulting in a 1 pA resolution with a 17 nA range. This resolution is an order of magnitude better than previously obtained, while the bandwidth (5 kHz) is essentially unchanged.

A major aspect of this work was the fabrication of the sharp tungsten tips used as the STM probe. Careful control of the chemical etching process resulted in reproducibly shaped tips, with a radius of curvature of less than 20 nm in some cases.

Acknowledgements

As with any lengthy project there is always a considerable number of people who have helped along the way.

Firstly my supervisor Dr. Craig Eccles for his patience and his consistently positive attitude. Thank you for your guidance. Dr. Henning Klank was the originator of this project and offered me considerable help and became a good friend.

To the electronics workshop staff, for all your help. It was very much appreciated, Udo von Mulert, Keith Whitehead and especially Peter Lewis. The mechanical workshop, Barry Evens, Steve Denby and Noel Foot were always willing to help. Robin Dykstra was always available to discuss my project. Doug Hopcroft from Hort Research for producing the SEM photos.

Paul Ryland is always helpful and I have enjoyed all the physics and all the music, thank you.

My lads, Craig Wallace, Daniel Pitchforth and David Ferry, thank you for all the laughter and friendship.

My parents Warwick and Jeannie, my siblings, Rosie, Nick and Jeremy for the encouragement and support.

Finally and most importantly my fiance Jillian, who at the time of printing will be my wife. Your support has been outstanding and a real blessing. I look forward to spending the rest of my life with you.

Contents

List of Figures

List of Tables

Chapter 1

Introduction

1.1 Background of project

In 1995 a project to build a digitally controlled Scanning Tunnelling Microscope (STM) was begun. This task was undertaken as a PhD project by Henning Klank and was supervised by Dr. Blair Hall, Associate Professor Robert O'Driscoll and in the later years, Dr. Craig Eccles. The project was a challenging one, requiring knowledge of electronics, programming, control theory and hardware design.

As the project was started from scratch, and its implementers were inexperienced in this field, the STM was very much a prototype and was designed so that changes could be made easily. Each part was constructed so that it would work simply and reliably, with the hope that the microscope would function as a whole. This was achieved in 1998 when the first image of graphite was obtained with atomic resolution.

The STM was beginning to work. Images were recorded of 3 nm high terraces on graphite, a gold sputtered transmission electron microscope grating replica and graphite atoms. However, as with many prototypes, the STM was rather unreliable, images were difficult to reproduce and the software was not easy to handle. The results and shortcomings of the project were detailed in Henning Klank's PhD thesis *Design of Digital Instrumentation for Scanning Probe Microscopy.*

1.2 This project

Two critical parts of the microscope were left in the prototype stage and this masters project aims to replace and improve these thereby increasing the performance and reliability of the STM. The two components are the

preamplifier, one of the most important parts of the STM electronics, and the STM probe, the most important and least understood piece of hardware in the STM. A third aspect of this work was the software interface that was tackled concurrently by Dr. Craig Eccles.

In some ways this thesis is a sequel to that of Dr. Klank's, but still with the goal of achieving atomic resolution on a regular basis. While the two major parts of this thesis should stand alone the driving motivation is to improve the STM.

1.3 Scanning Tunnelling Microscopy

A Scanning Tunnelling Microscope uses an imaging method similar to that used when reading braille. As a finger is scanned across a line, the various hillocks can be sensed by the finger tips and the words can be understood. In STM a very sharp metal probe, often called the tip, is scanned across a surface. However, instead of actually touching the surface to sense changes in height, a voltage between the tip and the sample is applied and a quantum mechanical effect called tunnelling occurs, in the form of a current. By measuring the tunnelling current the distance between the tip and the sample can be controlled. Many scans are performed to build up an image, similar to the pencil scans when making a pencil rubbing of an engraving.

1.4 The preamplifier

As in any instrumentation electronics, the performance of the first stage or preamplifier is critical in determining the overall noise and bandwidth of the system. In the STM the preamplifier is required to monitor the very small tunnelling current between the tip and the sample. This component is often referred to as a current-to-voltage converter.

A current-to-voltage converter for an STM has to amplify currents ranging from 10 pA to 10 nA. To convert very small currents such as these into reasonable voltages for analogue to digital conversion, a large gain is required.

Since high gain is essential this would usually require high valued feedback resistors. Because of this, small capacitances can have dramatic effects. Of particular importance is the reduction of the input capacitance, as this plays an important role in determining the final output noise. The most effective way of achieving this is to place the current-to-voltage converter as close as possible to the source. This creates its own challenges in STM.

1.5 STM tips

The tip in an STM is the very front end of the system, since it is the tip that determines the spatial resolution of the system and often the noise performance. Unfortunately the tip is easily damaged and therefore cheap, reliable tips have to be easy to manufacture.

It is now common place to achieve atomic resolution with such an instrument. To do this the tip must be *incredibly* sharp. The success of the STM as a tool relies on the nature of the tunnelling current. The tunnelling current decays exponentially with distance and it is this fact that is exploited to achieve high resolution. With a sharp tip and a flat surface the current is mostly contained within an area smaller than the surface area of the tip.

1.5.1 Fabrication of tips

Tips have to be constructed with a very small end radius, preferably less than 100 nm. This may seem like an almost impossible task and one requiring very specialised machining tools. However, this is far from the truth and although the manufacture of tips is still difficult, the process by which they are formed is relatively simple.

One starts with a simple wire, and electrochemically etches it until it breaks in two and hopefully a sharp tip remains. However some parameters can be varied to produce consistently good tips.

Good, reliable tips can dramatically improve the performance of a STM, not only in terms of resolution but also the signal to noise ratio.

Chapter 2

Scanning Tunnelling Microscopy

2.1 Background

2.1.1 Optical Microscopes

Microscopy takes its origins from the Greek words $\mu\bar{\iota}\kappa\rho\grave{o}\varsigma$, for small, and $\sigma\kappa o\pi\epsilon\check{\iota}$,to examine, and has come to mean the study of any process that looks at small things.

Optical microscopes were used by scientists as early the seventeenth century. In 1665 Robert Hooke published a book *Micrographica* that included sketches of specimens, including cat fleas, that he had observed with his microscope [44].

An advance in optical microscopy was made in 1830 when Joseph Lister produced lenses of a much higher quality. His developments improved the magnification from 200 times to about 2000 times. It was this improvement that enabled the French scientist Louis Pasteur to finally prove that disease is carried from person to person via bacteria. However, because of diffraction effects there is a limit to the magnification that can be obtained with an optical microscope. It is impossible to get a resolution of more that 200 nm i.e. one half of the minimum wavelength. This limit was reached during the 1930s and it was about this time that the first electron microscope was built.

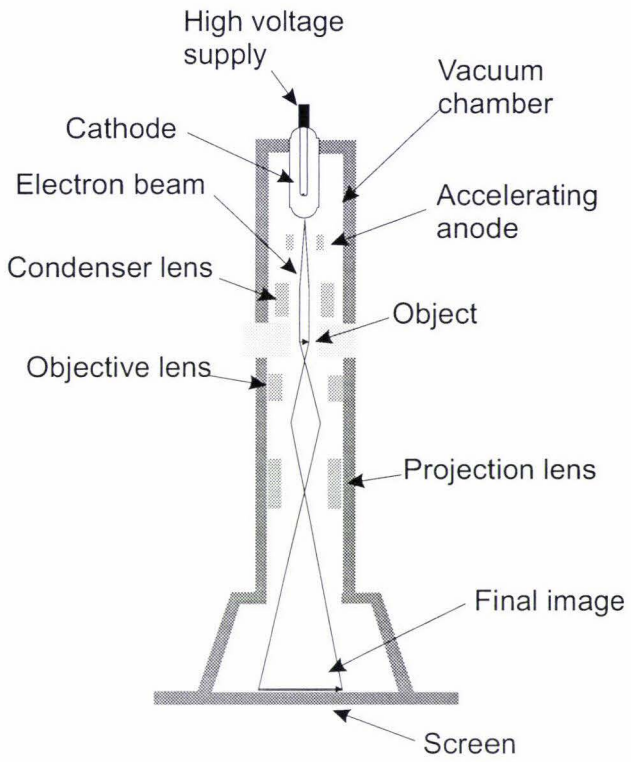

Figure 2.1: **The Transmission Electron Microscope:** Magnetic lenses direct a high energy beam of electrons in a similar manner to the way lenses direct light in an optical microscope. Reproduced from [51].

2.1.2 Electron Microscopes

Transmission Electron Microscope

Max Knoll and Ernst Ruska developed the first Transmission Electron Microscope (TEM) in 1931. A high energy[1] beam of electrons is used instead of light. The beam is focused through a series of 'lenses', usually electromagnets, the beam then strikes the specimen and parts of the beam are transmitted depending on the thickness and composition of the sample. The transmitted beam is projected onto the screen and this becomes the image (see figure 2.1). A TEM can achieve a resolution of approximately 0.2 nm [21], but only in some cases and then with careful sample preparation.

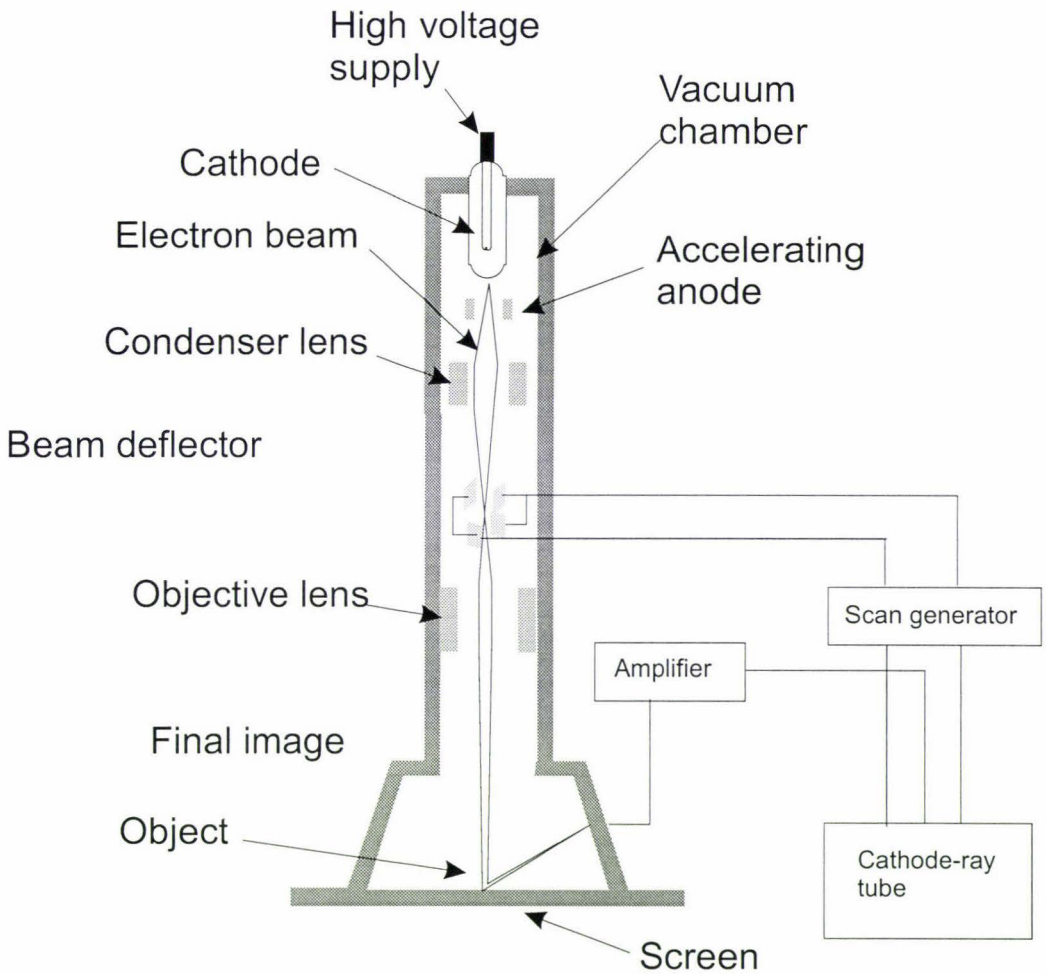

Figure 2.2: **The Scanning Electron Microscope:** An electron beam is scanned across the surface and secondary electrons are reflected onto a detector. The signal from the detector is scanned across a CRT with the same frequency as the beam deflection and an image is formed. Reproduced from [51].

Scanning Electron Microscope

In 1942 the first Scanning Electron Microscope (SEM) was built. In an SEM an electron beam is scanned across the sample using electric fields. As the electron beam strikes the surface lower energy electrons are scattered and detected to form an image (see figure 2.2). The resolution is of the order of a few nanometers. Although the resolution of a SEM is poorer than that of a TEM it offers an increased three dimensional perception since the reflecting of the electrons depends on the sample's surface.

Scanning Tunnelling Microscope

The Scanning Tunnelling Microscope (STM) was invented in 1982 by Gerd Binnig and Heinrich Rohrer of the IBM Zurich Laboratory [13] (see figure 2.3). The STM differs from the aforementioned SEM and TEM in that it uses electrons not as waves or particles reflecting or transmitting but measures the flow of electrons as a current between the sample and a probe, usually called the tip. A very sharp metal tip is placed very close to the sample (without touching) and a voltage is applied between the two, usually called the bias voltage. According to classical mechanics we would not expect any electron transfer. However, due to a quantum mechanical effect a current is observed between the tip and the sample. This is called a tunnelling current. It turns out that this current is very sensitive to the tip-sample distance, s. For example, if we double s we would expect to see the current become around ten times smaller.

To produce an image using this phenomenon the tip is placed very close to the sample and then moved across it in such a way that the tunnelling current remains constant (see figure 2.4). This is called a 'linescan'. During this scanning phase the vertical displacement of the tip is recorded. Many linescans are performed (often 512 or 1024) and then these linescans are combined and displayed on a computer as an 'image' (see figure 2.5). See appendix D for further reading.

Atomic Force Microscope

An Atomic Force Microscope (AFM) was invented by Binnig *et al.* in 1982 [50] and has become a very useful technique for looking at conducting and non conducting material. In AFM, a very small cantilever made of SiO_2, Si_3N_4 or Si with a pyramid-shaped tip is held near a sample. The

[1]high energy electrons have a short de Broglie wavelength and so produce smaller diffraction effects.

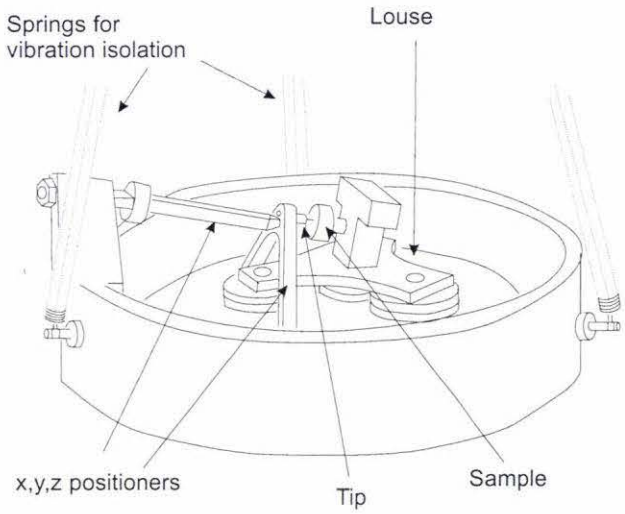

Figure 2.3: **The first STM:** Built by Binnig and Rohrer in 1982.

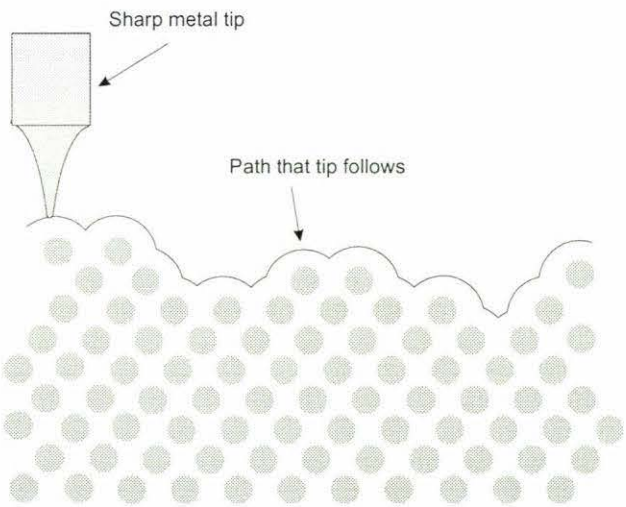

Figure 2.4: **An STM linescan:** The tip is scanned in such a way so that the tunnelling current and therefore, the tip sample distance, is constant. The vertical displacement of the tip is recorded as the scan. Several parallel scans make up an image.

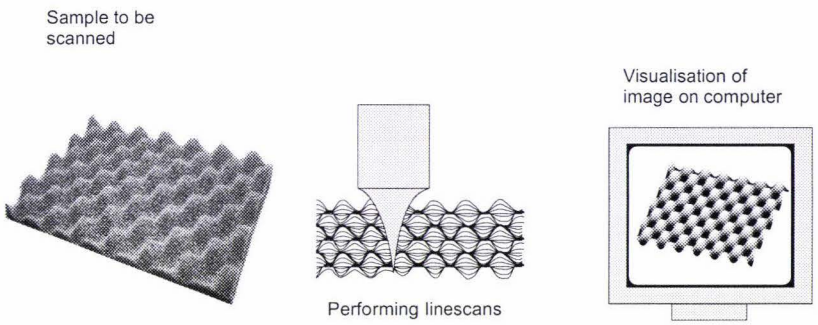

Figure 2.5: **Building an STM image:** The sample is scanned across many times and each scan is recorded. The scans can then be presented as a computer image.

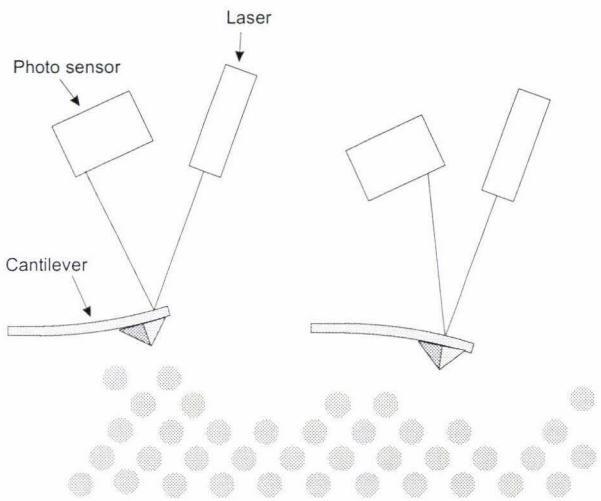

Figure 2.6: **Atomic Force Microscopy:** As a small cantilever is scanned across a surface the amount of deflection is measured, giving a topography of the sample.

interatomic forces will deflect the tip and if this deflection is measured an image can be created. The deflection of the cantilever is most commonly measured by the deflection of a reflected laser beam. See figure 2.6.

2.2 Theory of Tunnelling

2.2.1 One dimensional tunnelling through a barrier

The simplest explanation of the quantum mechanical tunnelling effect comes from a classical analogy. Imagine a ball rolling on a frictionless surface with kinetic energy, E_k. In its path is a shallow hill. If the ball was at the top of the hill and stationary, its potential energy would be E_h. We can say that

the hill acts as a potential barrier of 'height' E_h. We refer to 'height' as the amount of energy needed to get over the hill. If the kinetic energy of the ball, E_k, is greater than the 'height', E_h of the hill, then the ball would roll up the side of the hill, slow down, and then roll down the other side and carry on with kinetic energy E_k. If the kinetic energy of the ball, E_k is less than E_h the ball will roll up the hill, slow down, stop and then roll back down moving in the other direction with energy E_k. Imagine we are rolling the ball again towards the hill with a kinetic energy E_k that is less than E_h. We expect to see the ball turn round and come back because it doesn't have enough energy to climb over the hill. However when it is approaching the hill we are distracted and look another way. When we look back at the ball it is now on the *other* side of the hill, still with the same kinetic energy, E_k. We know that the ball didn't have enough energy to climb over the hill and back down again so we say it must have *tunnelled* through the barrier.

Although this behaviour is not allowed by classical mechanics it is predicted by quantum mechanics. An electron's motion in a potential is described by the Schrödinger equation. A simple example is the particle in a finite potential well.

The one-dimensional time-independent Schrödinger equation for an electron in a potential $V(z)$ is

$$\left(-\frac{\hbar^2}{2m}\frac{\mathrm{d}^2}{\mathrm{d}z^2} + V(z)\right)|\psi\rangle = E|\psi\rangle. \tag{2.1}$$

where

$$V(z) = V \quad \text{for} \quad z > a,$$

$$V(z) = V \quad \text{for} \quad z < -a,$$

$$V(z) = 0 \quad \text{for} \quad -a < z < a.$$

This gives us two different areas in which to solve the Schrödinger equation (see figure 2.7). There may be several $|\psi\rangle$, corresponding to discrete or *quantised* energy levels. Inside the well where E is greater than V gives a wavefunction, $|\psi\rangle$ that is sinusoidal. Outside the well E is less than V and the wavefunction is given by,

$$|\psi\rangle \propto e^{-\kappa z}, \tag{2.2}$$

where

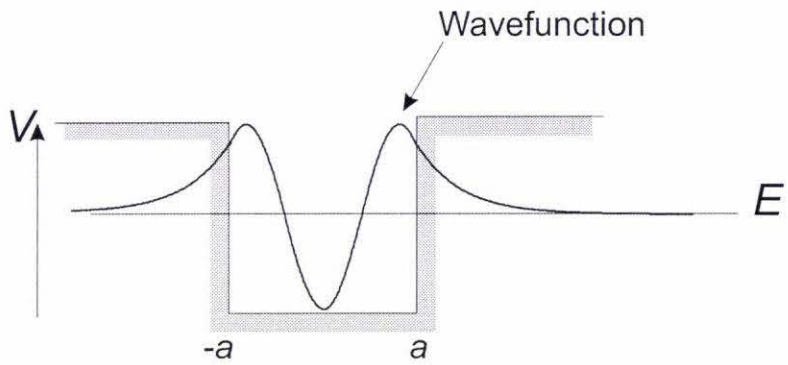

Figure 2.7: **A quantum well:** A wave function for an electron in a finite potential well.

$$\kappa = \frac{\sqrt{2m(V-E)}}{\hbar}. \tag{2.3}$$

To find the total wave function we must apply the boundary conditions that the wavefunction and its derivative must be continuous. The modulus squared of this wavefunction then describes the probability for finding the electron at that position. Figure 2.7 shows the wavefunction for the second excited state of the electron.

If one side of the well is replaced by a finite barrier we see that the wavefunction of the electron can extend into the free space to the right (see figure 2.8). This means there is a possibility of finding the electron in this region. Classically the electron does not have enough energy and would never escape but quantum mechanics predicts that it can move though the barrier. This is like going though a hill rather than over it. Hence the electron is said to 'tunnel' through the barrier. By comparing the modulus squared of the wavefunctions on either side, we can find the probability that the electron will tunnel through the barrier.

One dimensional tunnelling between metals

So far we have only considered a single electron in a well with a barrier on one side and the possibility that it will tunnel beyond the barrier.

The conducting bands of metals are closely packed states, so much so that they can be approximated as continuous.

Metals are filled up to their Fermi energy with electrons (see section A.2). The amount of energy needed for electrons to escape from the surface of the metal is given by the work function (see figure 2.9). When two metals are placed in electrical contact a transfer of electrons takes place to reach an

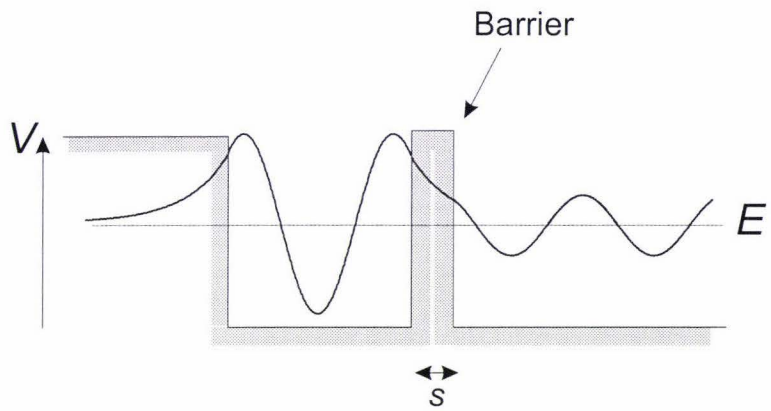

Figure 2.8: **A quantum well with one side replaced by a barrier:** When the Schrödinger equation is solved for the above potential the wave function is as above. i.e there is a certain probability that the electron will tunnel through the barrier.

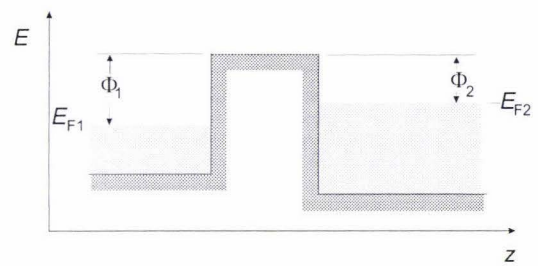

Figure 2.9: **Two metals:** Two metals both with electrons filled up to their Fermi energy.

equilibrium and the Fermi energies of the two metals become equal [3]. The potential barrier between them is sloped (see figure 2.10). If, however, a bias voltage is applied between the two metals the barrier becomes more sloped and the Fermi energies are offset by eV_{bias}. Electrons are now able to tunnel from the high energy to the lower energy (see figure 2.11).

The only electrons that tunnel from metal 1 are the ones that have a place to go in metal 2. That is the electrons in the energy region from E_{F1}-eV_{bias} to E_{F1}. The current due to this electron flow will be:

$$I_{\mathrm{t}}(s) \propto \sum_{E_\mu = E_{\mathrm{F1}} - eV_{\mathrm{bias}}}^{E_{\mathrm{F1}}} |\psi_\mu(0)|^2 e^{-2\kappa s}, \tag{2.4}$$

where the summation is over all the wavefunctions ψ_μ that are in the specified energy range. The wave is written as $\psi_\mu(0)$ since, referring to figure 2.11, the barrier on the right of metal 1 has been defined as $z = 0$.

The summation in the above equation can be expressed in a simpler way

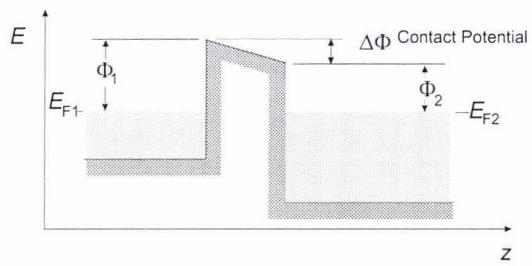

Figure 2.10: **Contact potential:** If two metals are joined in such a way that permits electron flow, for example a conducting wire, the Fermi energy's of each metal will become the same and there will be a net potential between the two metals.

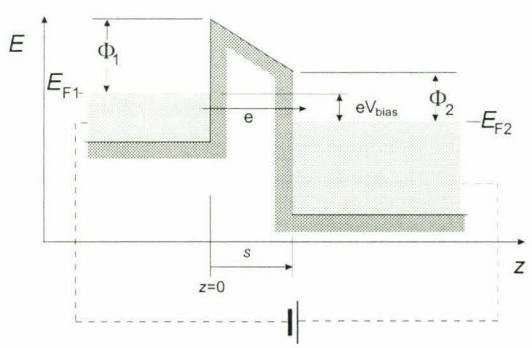

Figure 2.11: **Two metals with a bias voltage between them:** Applying a bias voltage between the two metals allows a current to flow.

using the local density of states (LDOS). The general expression for the LDOS is (see appendix A.1 for details)

$$\rho_1(z, E) = \frac{1}{\epsilon} \sum_{E_\mu = E-\epsilon}^{E} |\psi_\mu(z)|^2 . \tag{2.5}$$

Substituting $z = 0$, $E = E_{\mathrm{F1}}$ and the energy range $\epsilon = eV_{\mathrm{bias}}$ into the above equation we have,

$$\rho_1(0, E_{F1}) = \frac{1}{eV_{\mathrm{bias}}} \sum_{E_\mu = E_{\mathrm{F1}} - eV_{\mathrm{bias}}}^{E_{\mathrm{F1}}} |\psi_\mu(0)|^2 , \tag{2.6}$$

This expression for the LDOS can now be substituted into equation 2.4 to give.

$$I_{\mathrm{t}} \propto eV_{\mathrm{bias}}\, \rho_1(0, E_{\mathrm{F1}})\, e^{-2\kappa s} . \tag{2.7}$$

This simple example shows that STM images are not specifically of atoms but of the *local density of states*, which can be interpreted as a density of electrons over space and energy. The most commonly imaged surface is that of highly orientated pyrolytic graphite (HOPG) and the surface of graphite is well known to be like a hexagonal honeycomb. However, STM images of graphite can look more like tightly packed oranges in a fruit vendors display. This is because, due to the influence of multiple layers of HOPG, the maximums in the LDOS do not show the same symmetry as the lattice (see figure 2.12).

For further reading in interpreting images from STM refer to Chen [13] or Bai [5, 50].

2.2.2 Lateral resolution

The ability of STM to obtain much better lateral resolution that the corresponding dimensions of the tip arise from the nature of the tunnelling current. A simple calculation was performed by Binnig in 1978 [13].

The very end of the tip is assumed to be spherical with a radius, r, at a distance s from the surface, as in figure 2.13.

Over a small region of x, the shape of the tip can be approximated as parabolic. This means the tip sample distance z, as a function of x, can be written as

$$z = s + \frac{x^2}{2R}.$$

Substituting this into 2.7 we get

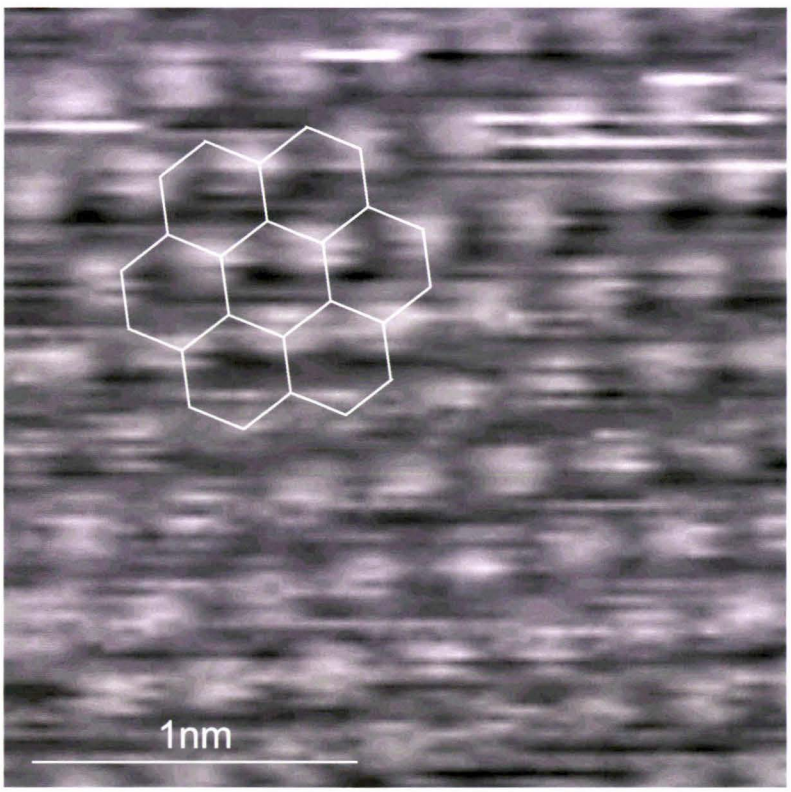

Figure 2.12: **STM image of graphite:** An STM image recorded in our laboratory of highly orientated pyrolytic graphite (HOPG). This does not show the well known honey comb lattice shape of graphite. This is because the image recorded is of the local density of states of graphite and this can be calculated to give the above result [42]. The white overlay shows the lattice shape of the graphite.

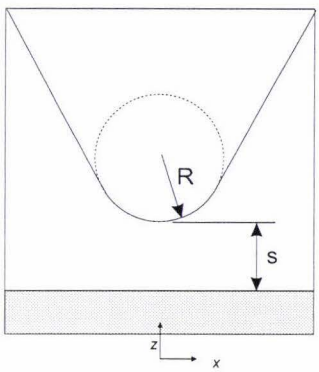

Figure 2.13: **Estimating the lateral resolution:** The tip is assumed to have a spherical shape at its apex. The surface is the shaded region. A simple calculation shows that the majority of the current is contained in a small spatial area.

$$I(x) = I_0 e^{-2\kappa \frac{x^2}{2R}},$$

where κ is typically $1\,\mathring{A}^{-1}$ [13]. For $R = 100\,\text{nm}$ this gives $x = 2.6\,\text{nm}$ for a one half drop in current. The actual resolution achieved is much smaller than this due to local protrusions at the end of the tip and it is not uncommon to get a lateral spatial resolution of $0.2\,\text{nm}$.

Chapter 3

Background of microscope operation

3.1 Operation of microscope

Implementing an STM presents some challenges. A tip with an ultra sharp point has to be fabricated, this tip then has to be held very close to the surface of a sample and a very small tunnelling current has to be measured. The tip must then be scanned over the surface at constant height and the topology recorded. Tip manufacture is discussed in detail in chapter 5, measuring the tunnelling current in chapter 4 while this chapter will focus on positioning the tip. Once the tip is in place scanning routines can then be implemented to obtain an image.

3.1.1 Approach

Positioning the tip close to the sample is executed in two stages, the coarse and the fine approach. In our case, as in many other STM's both stages of approach are performed using the properties of a 'piezoelectric' material.

A piezoelectric material is one which will change shape in the presence of an electric field. This deformation is relatively linear and easy to predict. For the fine approach, using a piezo 'actuator' is the most straightforward method. The piezo actuators are available in hollow tubes with electrodes on the inside and outside. The inner wall is grounded and the outer electrode is broken up into four separate quadrants (see fig 3.1). To scan horizontally, two of the quadrants are connected to ground while the other two receive a positive and negative signal. To extend, all four electrode are held negative with respect to ground and to retract, the electrodes are made positive. This movement is used for the fine approach, which has a vertical range of 470 nm

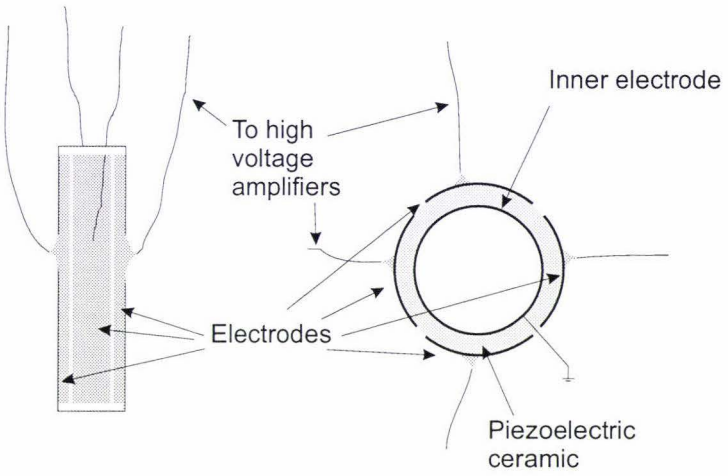

Figure 3.1: **The piezoelectric actuators:** The inner electrode of the actuator is grounded and a separate voltage (up to ±70 V) can be applied to each outer electrode. This creates an electric field across the piezo which causes the material to reshape. This effect can be used to obtain vertical and horizontal movement of the actuator.

in 0.001 nm steps and for the scan, which has a horizontal range of ± 1.9 μm in 0.008 nm steps, at zero vertical extension[1]. See figure 3.2.

Piezo crystals can also be used for the coarse approach of the probe. This time three legs are connected to the probe head so that they look like a 'beetle' [24]. The beetle stands on a disk that is divided into three sections, one section per leg. Each section is sloped. The beetle can be made to walk in a clockwise direction and thus down the ramp. Walking from the top of the ramp to the bottom lowers the probe head by 0.4 mm. See figure 3.3.

'Walking' is achieved in the following way. Each leg of the beetle has a ball bearing attached to it. This acts as its 'foot'. If a step voltage is applied to the actuator it bends very quickly and the foot slips out from underneath. However, the probe head stays still due to its inertia. The voltage on the actuator is then ramped down slowly so that the actuator straightens while keeping the 'foot' in contact with the ramp. See figure 3.4.

To obtain a tunnelling current without crashing,[2] a number of coarse steps (typically 30) are taken by the beetle and then the fine approach by the centre piezo. This process is repeated until a current is found. Once a tunnelling current is found we can then obtain an image by scanning the

[1] these figures are for a power supply of ± 70 V and sensitivities of $r_v = 3.36\,\mathrm{nm/V}$ and $r_h = 27\,\mathrm{nm/V}$. The step sizes are the peak to peak noise levels. The number of steps possible is 2^{20}.

[2] that is, accidentally ramming the tip into the sample, destroying the tip and degrading the sample.

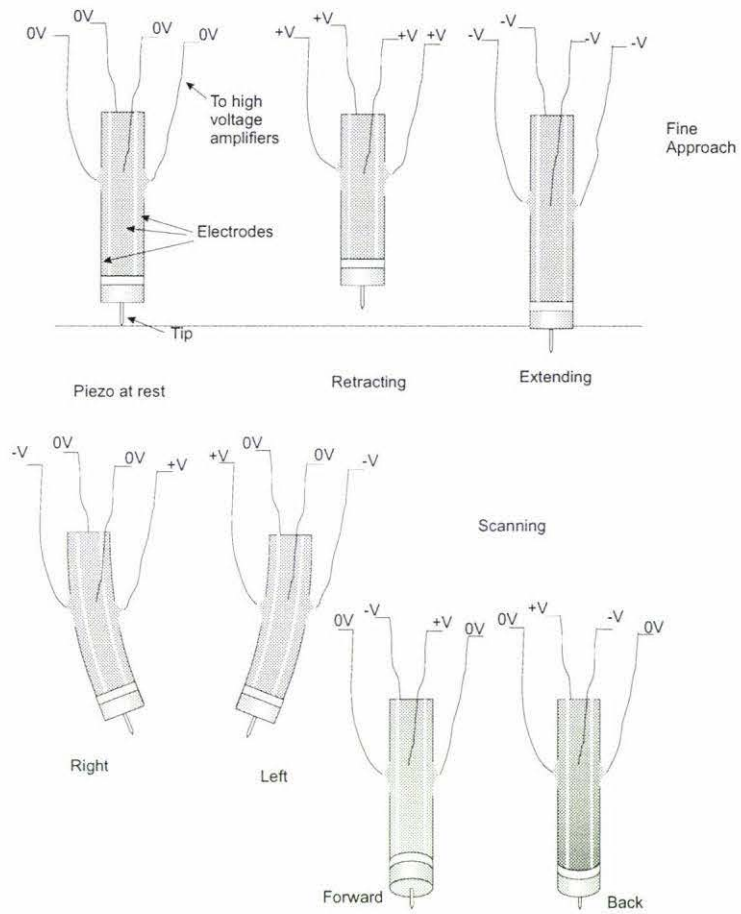

Figure 3.2: **The fine approach and scanning:** A negative voltage on all electrodes extends the piezo and a positive voltage will contract it. This gives us a vertical range of 470 μm with a resolution of 0.001 nm. Applying opposite polarity voltages to opposite electrodes will cause the actuator to bend, giving x and y movement. When the piezo is extended or retracted the scanning movement is restricted.

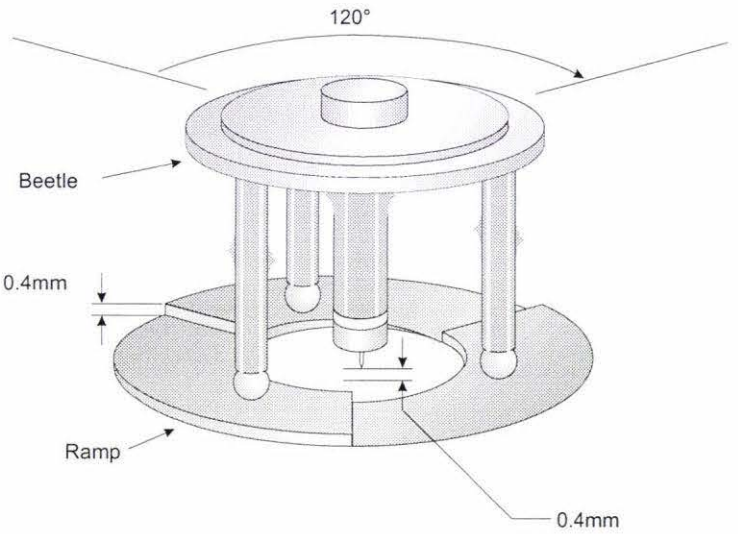

Figure 3.3: **The beetle positioned on the ramp:** The three-legged beetle with a center piezo sits on top of a tungsten carbide ramp. The ramp is divided into three sections with each section having a gradient of 0.4 mm over 120°. As the beetle rotates clockwise, it will walk down the ramp and therefore lower its position by 0.4 mm. The beetle can also be made to move in the transverse direction, permitting a coarse approach in the x-y plane.

sample.

The beetle is not the only method of coarse approach, other commonly used designs include the 'louse' [8] or a stepper motor [7]. The beetle design was chosen because of its minimal thermal drift and superior vibration isolation.

3.1.2 Vibration isolation and thermal drift

Vibration isolation

To make measurements with the tip only nanometers from the sample, exceptional vibration isolation is required. Vibrations can occur through the air acoustically or through the mounting of the STM. Buildings typically have resonant frequencies around 10 to 30 Hz and to minimise the effect of these vibrations the STM should ideally be on a ground floor or basement, although our unit is on the second floor.

Vibration isolation is often achieved in the following manner. Instead of mounting an object directly on a vibrating surface, thus transmitting all vibrations, the object is rested on a large inertial mass and connected to the surface via a spring and a damping device. The transmitted vibration will be reduced, depending on the values of the spring constant, the mass, the

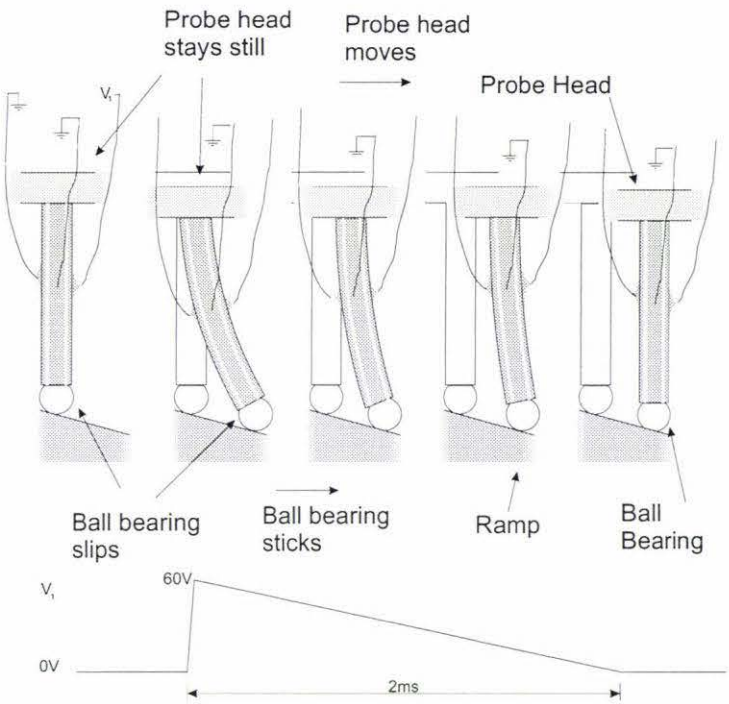

Figure 3.4: **The slip-stick motion of the coarse approach:** The initial step in voltage is enough to bend the actuator with such a force that the friction between the ball bearing 'foot' and the ramp is overcome. During this movement the probe head stays still due to its own inertia. The voltage is then slowly ramped down so that as the actuator straightens out, the friction between the 'foot' and the ramp holds the foot still. The probe head moves and once the actuator is straight, one complete step has been taken. The outlined shape shows the initial position of the leg. With the voltage waveform indicated here, the probe head moves by 10 nm for each step. Reversing the voltage polarity makes the probe head walk up the ramp.

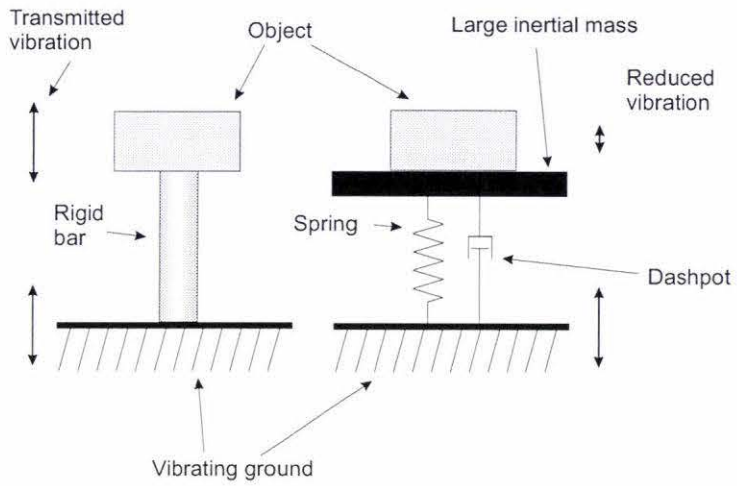

Figure 3.5: **Vibration isolation:** On the left an object is connected to ground via a rigid bar. In this case the vibration is completely transmitted. If the object is mounted on a spring and dashpot system, the transmitted vibration can be significantly smaller.

damping factor and the frequency of the vibration. See figure 3.5.

In our system, vibration isolation is performed in two stages. Firstly, to filter out the low frequency vibrations, the STM is mounted on an air table [37]. This table is essentially a large slab of stainless steel resting on four columns of compressed air contained within the legs. Higher frequencies are filtered out because the probe head sits on a stack of three brass plates separated by viton 'O' rings (see figure 3.6).

Each stage of vibration isolation will have its own unwanted resonant frequency. The beetle itself will also have horizontal and vertical resonant frequencies. Resonant responses are often characterised by two variables, the 'damping factor' and the resonant frequency ω_0. By carefully choosing these variables during the design of the system, the vibration between the tip and the sample can be minimised.

Figure 3.7 shows the response of the system as modelled by Dr. Klank [30]. The probe head is designed to have a high resonant frequency which can be filtered out by the air table and the mass stack. The response has since been improved by using plates of different mass [45].

Once the probe head has been isolated from ground vibrations there is now the problem of passing signals to and from the probe. Very thin wires must be used to reduce the mechanical coupling from the ground to the probe head. In addition the probe head must also be free to move 120° around the ramp. To achieve this successfully the thick cables from the DSP are mounted on a frame which sits on the air table. Very thin copper wires,

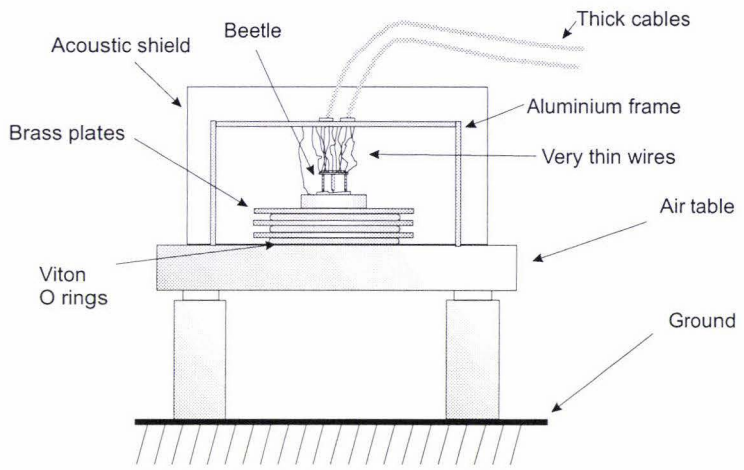

Figure 3.6: **Vibration isolation:** To minimise the transmission of vibrations from the ground to the beetle, the STM is mounted on a stack of brass plates and viton O rings. This stack then sits on an air table.

with a diameter of 0.06 mm, are used to pass signals from the frame to the probe head.

Thermal drift

Materials will expand or contract due to a change in temperature. This increase or decrease is usually a small percentage of the overall dimensions, but it is a problem that needs to be overcome in STM since length changes in the system could increase or decrease the tip-sample distance during a scan, giving the false impression that the sample is contoured.

The STM 'beetle' has good thermal properties because the piezo actuators, whose coefficients of expansivity are not well known, are in parallel and the change in length of each one will be similar, leaving the tip position relatively unaffected by temperature variation (see figure 3.8).

The thermal drift was calculated by Dr. Klank as $13 \pm 30\,^{\mathrm{nm}}/_{\mathrm{K}}$. Effects due to this drift have not been a significant problem.

3.2 Our System

3.2.1 Design

The STM is controlled by a Digital Signal Processor (DSP). This contains the control algorithms, and scan routines. The microscope operator uses a computer to call these routines on the DSP. The DSP then implements these

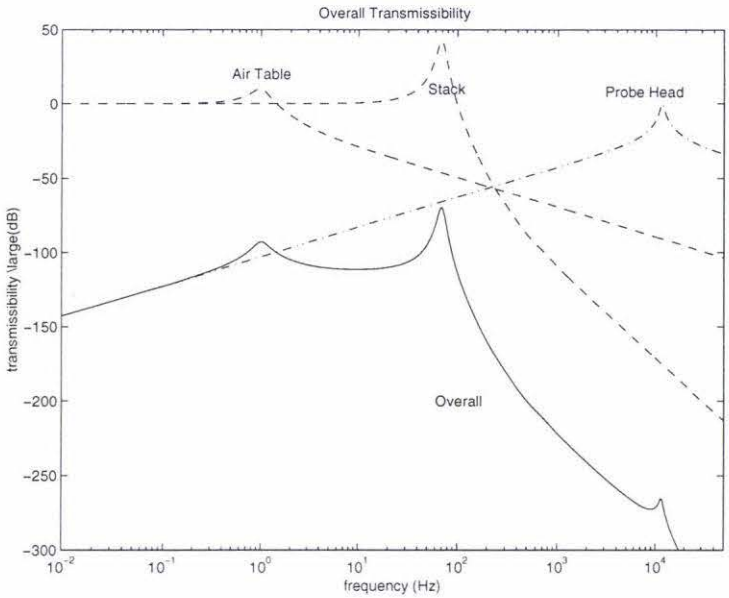

Figure 3.7: **Transmissibility:** The transmissibility is a measure of the transmitted vibration. The combination of the air table, mass stack and the probe head give an indication of the vibration transmitted from the ground to the tip-sample distance as a function of frequency.

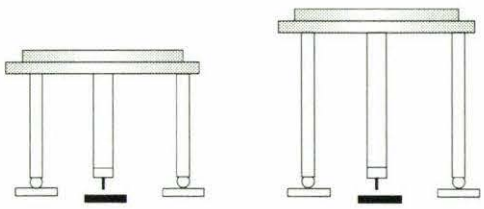

Figure 3.8: **Mechanical Thermal drift:** A grossly exaggerated and simplified schematic drawing showing the effects on the probe due to a change in temperature. As the piezo's expand, they do so together, so that although the probe head moves, the movement of the tip is minimised. The effect of the thermal drift on the ramp and the sample holder also has to be taken into account.

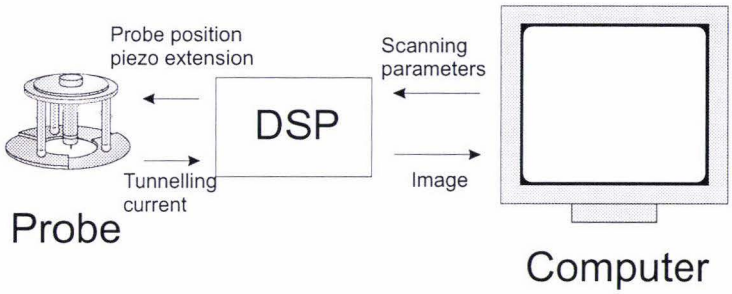

Figure 3.9: **A DSP controlled STM:** The DSP receives instructions from the computer and then executes them e.g. walking down, then finding a tunnelling current. The DSP sends the probe head signals to move the piezos and walk down the ramp, as well as receiving the tunnelling current as data. The DSP then transfers the data to the computer.

routines and collects the data. The data is then uploaded to the computer where it can be visualised (see figure 3.9 and appendix C).

3.2.2 Digital Control

To perform a linescan (see section 2.1.2 and figure 2.4) the distance between the tip and the sample is kept constant while the piezo is moved horizontally. During this time the vertical movement of the piezo is recorded. The distance is controlled by measuring the tunnelling current, so obviously the current-to-voltage converter required to do this is a very important part of the system. Keeping a variable constant in a process is a common problem, e.g. keeping the temperature constant in a room or keeping a vehicle's speed constant in a cruise control system, and it is usually performed using negative feedback (see figure 3.10). In many cases such as these, there is no direct control over the variable, e.g. the temperature is kept constant by switching a heating or cooling element on or off.

Consider the case of a cruise control system. To keep the speed constant using feedback control, the desired speed is set by the user, and then the difference between the desired speed and the actual speed, the error, is fed into the controller. The controller will then send a signal to the accelerator to slow down or speed up accordingly. The controller cannot adjust the speed directly but can only increase or decrease power to the accelerator. Also affecting the speed will be the 'load' on the system. The load symbolises any system that may change the speed of the car. For example, if the car is approaching the bottom of the hill, the car will slow down. The error would then become positive and the controller would tell the engine to speed up to keep the speed at the desired set-point. This is how the controller works against the 'load'. See figure 3.11.

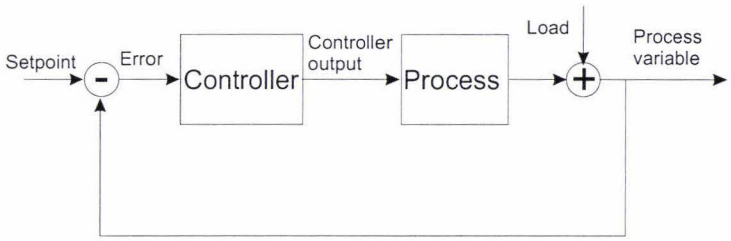

Figure 3.10: **A typical feedback control system:** The controller tries to keep the process variable close to the set-point to counter the effects of the load.

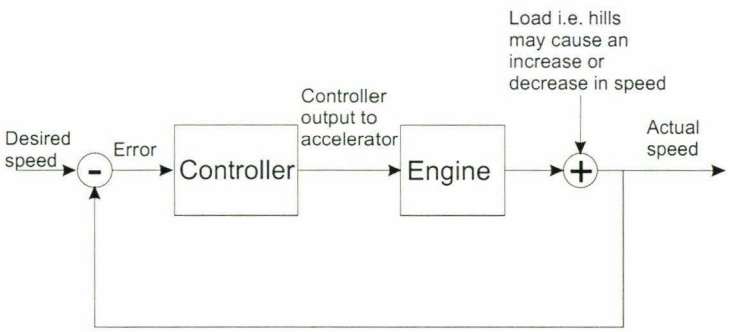

Figure 3.11: **Using feedback to keep constant speed:** The controller works against the 'load' to keep the speed constant. If the 'load' is a steep hill, the controller will sense the drop in speed and send a signal to accelerate the engine until the desired speed is reached.

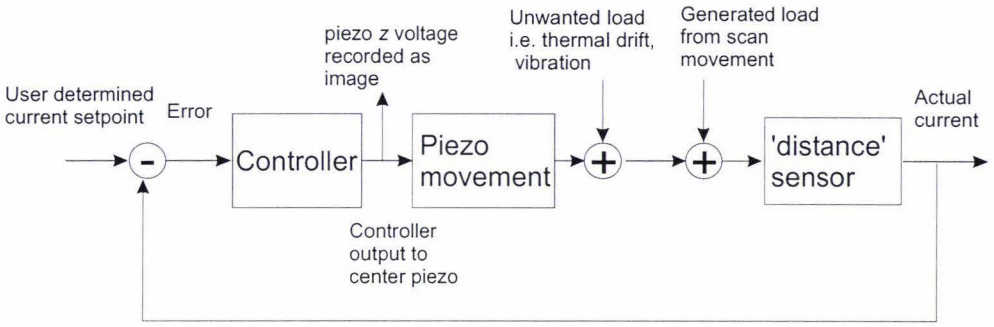

Figure 3.12: **The STM as a control system:** As the controller keeps the current constant the z voltage on the piezo is recorded. The 'distance sensor' is actually a current to voltage converter.

The controller in the STM works in a slightly different way. Although the current should remain constant during a scan, what is really useful is determining the change in the extension of the piezo required to do this. If this extension is recorded it can be used to form the image. In this case the 'load' is generated by the scan i.e. the tip is sitting above the sample at the desired set-point and moving the tip may cause a change in tip-sample distance. This is the 'generated load' of figure 3.12. If the tip is instructed to move to the right, the 'distance' sensor will output a different current and the controller will see an error signal. Once the controller has corrected for this, the voltage on the center piezo is recorded.

The controller also provides a measure of protection against thermal drift and vibration. If the STM is tunnelling and the piezo expands due to thermal drift, the controller will retract the piezo to keep the current constant, thus preventing the tip from crashing into the sample. However, this will still degrade the quality of images.

PID control

A PID (proportional, integral, differential) controller responds to the error signal by forming a linear combination of the error, the differential of the error and the integral of the error. Considering the cruise control again, the controller could be set to increase the power to the engine, $E(t)$, by an amount proportional to the error, $e(t)$, where the proportionality constant is P. This is proportional control. If the speed set-point is set to $100\,^{\mathrm{km}}/_{\mathrm{h}}$ and the actual speed is $80\,^{\mathrm{km}}/_{\mathrm{h}}$, the controller will increase the power to the engine by

$$E(t) = P.e(t)$$

As the car accelerates it may slowly approach the set-point or the speed may overshoot and oscillate around the set-point. However with only proportional control the set-point is never reached. If, for example, the set-point is again $100\,^{\mathrm{km}}/_{\mathrm{h}}$ and the car is travelling at $98\,^{\mathrm{km}}/_{\mathrm{h}}$, the power applied to the engine will be

$$E(t) = P.2^{\mathrm{km}}/_{\mathrm{h}}$$

This power might only be enough to overcome the friction in the engine and driveshaft and so the car will not accelerate. The controller will apply the same power to the engine and again the car will not accelerate. To get as close to the set-point as possible a very large proportional gain could be used but this could result in a very large overshoot since the controller and engine cannot respond at an infinite rate. Another way to avoid steady state errors is with the integral term. If the proportional term has a steady state error and this error is integrated then the integral will increase. The power in the engine can then be set to

$$E(t) = P.e(t) + I.\int e(t)dt$$

where I is the weighting of the integral of the error. Because of its summing action, the integral term is most sensitive to low frequency errors. To increase the response time of the controller, the differential of the error signal can be weighted by a term D and added to the power signal. As the speed gets close to the set-point, and the rate of change in the error is slower, the proportional and integral terms take over. Differential control tends to reduce the overshoot, although it is very sensitive to noise.

By choosing the coefficients of each term carefully, the controller can be tuned to suit the application. However, not all combinations of coefficients can be used. For our STM often the I term is the only one used, with a value of around 0.1.

In a control system it is very important to know the magnitude and phase response of each component or else the system may be driven into instability. It is vital to avoid a loop gain of one, with a $360\,^{\circ}$ phase shift.

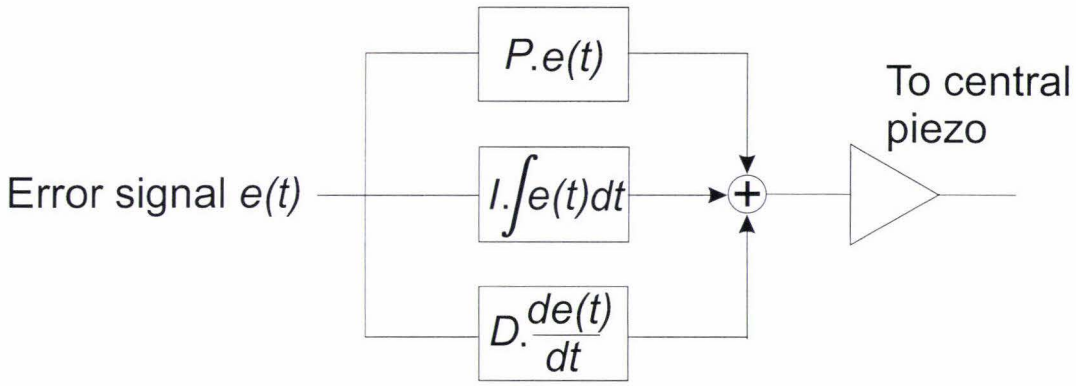

Figure 3.13: **A PID controller:** The controller treats the error in three ways. The error is weighted with a factor P, the error is differentiated and weighted by D and integrated and weighted by I. These factors are then summed and sent to the piezo. The response of the controller depends critically on the choice of these three factors.

Chapter 4

Preamplifier improvements

4.1 Introduction

The first component of any measurement system is often referred to as the preamplifier and is usually the most critical in terms of the overall signal to noise ratio which can be expected at the output. Subsequent amplification stages are of far less importance since any noise injected at this point undergoes less amplification than input noise in the first stage.

Considerable improvements in the performance of a system can therefore often be achieved by carefully redesigning this most important component.

4.2 Our needs

The controlling parameter in the STM is the tunnelling current. A bias voltage is applied between the sample and the tip and a small tunnelling current results. A *transimpedance* preamplifier (or current-to-voltage converter) is required to convert this tiny current into a useful voltage. Typical maximum currents are around 1 to 10 nA and so a very large gain of around 10^8 to 10^9 V/A is required. Also, because of this small current the input bias current into the operational amplifier (opamp), which is used in the current-to-voltage converter, needs to be as small as possible. Other requirements for the current-to-voltage converter are a low noise output level corresponding to less than 1 pA and a reasonable bandwidth of between 5 and 10 kHz. These values should enable us to obtain good quality atomic resolution images at a reasonable speed.

High gain transimpedance amplifiers are commonly used for photodiode transducers or pH probes, but in these cases the required bandwidth is only a few Hertz. It is not often that one needs a current-to-voltage converter

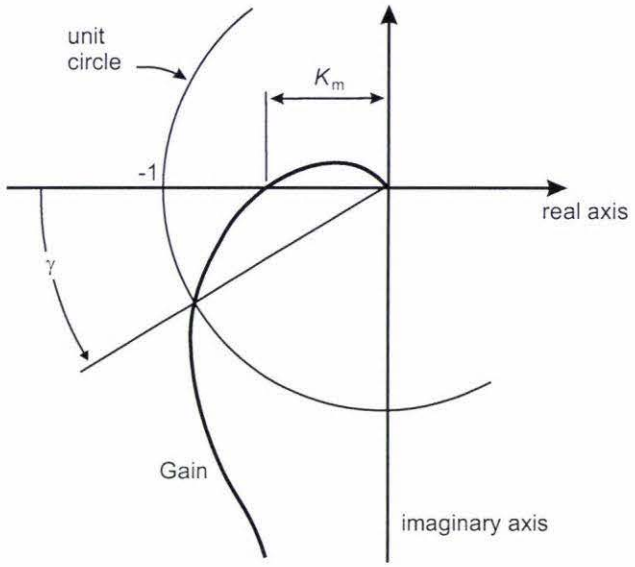

Figure 4.1: **Gain Margin:** This graph shows the gain of a system decreasing as the phase increased. The gain margin is given by $1/K_m$ and the phase margin is given by γ.

with such a high gain *and* a significant bandwidth.

4.2.1 The current-to-voltage converter as part of a control loop

As shown figure 3.12, the current-to-voltage converter is part of a control loop. The closed loop gain of the whole system has to be designed so that the loop is stable. Instabilities arise when the loop has a gain near 1 and the phase shift is close to 180°. As a guide, the phase margin needs to be $\geq 30°$ and gain margin $\geq 8\,\mathrm{dB}$ [4] (see figure 4.1). This is true for any system so it can be applied to the control loop or individual components such as the current-to-voltage converter.

When considering the stability of the loop, phase shifts come from the current-to-voltage converter, controller or the movement of the probe head[1]. It is hoped that the introduction of the current-to-voltage converter preserves loop stability without significantly reducing the bandwidth.

[1]Phase shifts from the probe head are dependent on frequency and will reach 90° if the probe is driven at resonance.

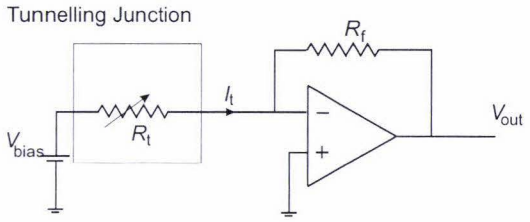

Figure 4.2: **The Ideal current-to-voltage converter:** The tunnelling junction behaves like a variable resistance. The bias voltage, V_{bias}, is connected to the sample and the current-to-voltage converter is connected to the tip.

4.2.2 The role of the current-to-voltage converter

The circuit that needs to be built is a current-to-voltage converter and will be referred to as such. However, its place in the STM can be considered to fulfil a different role. The controller performs its task by keeping the tip-sample distance constant. This height is 'sensed' using the tunnelling current between the tip and the sample. A known bias voltage is applied to the sample and the current is measured with a current-to-voltage converter (see figure 4.2). In effect the controller keeps the resistance between the tip and sample, R_t, constant. For this reason, the tunnelling resistance will be considered part of the circuit and will be included in the circuit analysis. The tunnelling resistance can vary from 1 MΩ to 1 GΩ [30] and for testing, a resistance of 29 MΩ will be used. This enabled easy comparison with the pre-existing current-to-voltage converter, which was also tested using the same resistor.

4.3 The Circuit

4.3.1 Ideal current-to-voltage converter

The ideal circuit is a very simple one, an operational amplifier with a large resistor for negative feedback (See figure 4.2). Unfortunately, a real circuit is a little more complicated as parasitic capacitances have to be considered and the non-ideal properties of the opamp have to be taken into account (see figure 4.3).

Source capacitance

The source capacitance comes from the distance between the tip and the sample. This is assumed to have little effect because, with the exception

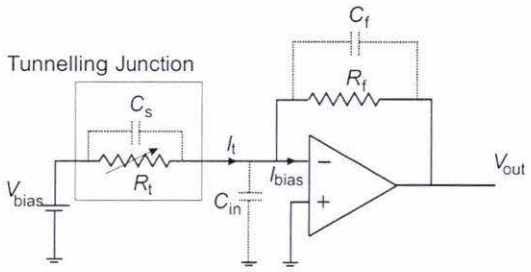

Figure 4.3: **The Real Preamplifier:** The tunnelling junction is like a variable resistance. Parasitic capacitances are shown as dotted lines. C_s is the source capacitance and is between the tip and the sample. C_f is the capacitance of the feedback resistor and C_{in} is the capacitive coupling between ground and the input of the amplifier. I_{bias} is the input bias current to the opamp.

of recording I-V curves, the sample voltage is held constant. The source capacitance is estimated to be about 200 fF.

Feedback capacitance

The feedback capacitance, C_f, arises because any resistor will have a certain amount of inter-electrode capacitance (see figure 4.4). With small resistors this is not usually a problem, but for applications requiring large valued resistors and frequencies significantly higher than dc it is important to have a very small parasitic capacitance[2]. It is shown in appendix B that the transfer function of the real current-to-voltage converter is equivalent to a damped resonant circuit and the damping factor depends on the feedback capacitance. If the feedback capacitance is large enough to over-damp the circuit, then it will reduce the bandwidth, but for a well chosen resistor this will not be the case.

Input capacitance

An input capacitance exists between ground and the wire carrying the signal from the source to the input stage of the amplifier. The longer this wire, the more capacitance there will be (see figure 4.5). Surprisingly, the input capacitance to ground is one of the major factors in determining the output noise and also is the dominant factor in determining the bandwidth of the current-to-voltage converter (see section 4.4.2). Other parasitic capacitances may also exist and indeed there is a small capacitance between the tip and the electrodes of the centre and outer piezos (see section 4.6.4).

[2]e.g. if a 100 MΩ resistor has a parasitic capacitance of ~ 0.1 pF, then the capacitance will have a comparable impedance at around 15 kHz.

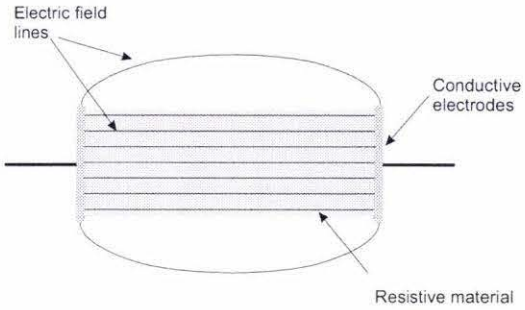

Figure 4.4: **The feedback capacitance:** All resistors will have a small parallel capacitance as a consequence of the electric field between the two electrodes. The field lines are shown as thin lines. To reduce this capacitance a ground plane could be placed near the resistor to minimise the external field.

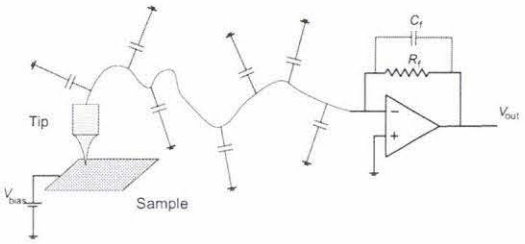

Figure 4.5: **The input capacitance:** Any physical distance between the source and the input of the preamplifier will include some parasitic capacitance to ground. To minimise this effect the preamplifier is usually mounted as close as possible to the source.

Input bias current

Because the current being measured is so small, a significant portion of it may be undesirably sourced into the opamp as bias current. This would be manifested as an offset on the output voltage. To avoid this, an opamp must be chosen that has a very small bias current when compared with likely tunnelling currents.

4.4 Circuit analysis

4.4.1 Transfer function

If we assume that I_{bias} is negligible, then the transfer function of the circuit shown in figure 4.3 is[3]

[3]see appendix B equation B.13.

$$\frac{V_{\text{out}}}{V_{\text{bias}}} = -\frac{R_{\text{f}}}{R_{\text{t}}}(1 + j\omega C_{\text{s}} R_{\text{t}})\frac{\omega_0^2}{\omega_0^2 - \omega^2 + j\omega 2\delta}, \tag{4.1}$$

where

$$\omega_0^2 = \frac{\omega_u}{R_{\text{f}} C_{\text{tot}}}, \tag{4.2}$$

ω_{u} is the unity gain bandwidth of the opamp and

$$2\delta = \frac{1}{C_{\text{tot}}}(\omega_u C_{\text{f}} + \frac{1}{R_{\text{t}}} + \frac{1}{R_{\text{f}}}). \tag{4.3}$$

Hence the response of the circuit will be similar to a damped resonance circuit with a dc gain of $-R_{\text{f}}/R_{\text{t}}$. C_{tot} is the sum of the three capacitances and is most likely to be dominated by the input capacitance C_{in}. The extra term in equation 4.1, $(1 + j\omega C_{\text{s}} R_{\text{t}})$, will have little effect on the transfer function as its characteristic frequency is well above ω_0.

The feedback capacitance affects the circuit in two ways. If the resonant circuit is very heavily damped, then the bandwidth is given by (see section B.2)

$$\frac{1}{R_{\text{f}} C_{\text{f}}},$$

which is undesirable. If the feedback capacitance is reduced so than the circuit is no longer over-damped, then a resonant peak begins to appear and the bandwidth is approximated by ω_0. In this situation the input capacitance is the dominant factor in determining the bandwidth.

For the resonance to be critically damped we need

$$\delta = \frac{\omega_o}{\sqrt{2}}. \tag{4.4}$$

This is usually achieved by altering C_{f}.

When designing a current-to-voltage converter with a high gain, the input capacitance has to be determined first. Ideally it would be zero but this is never the case. Once the input capacitance is known, or estimated, then as long as the feedback capacitance can be made small enough for near critical damping, the choice of R_{f} becomes a trade off between gain and bandwidth, according to equation 4.2, (since $\omega_{\text{u}} \sim 1\,\text{MHz}$ for most suitable opamps).

4.4.2 Noise and the input capacitance

The noise gain of the current-to-voltage converter can be found by replacing the bias voltage with its ideal impedance and placing a noise generator on the

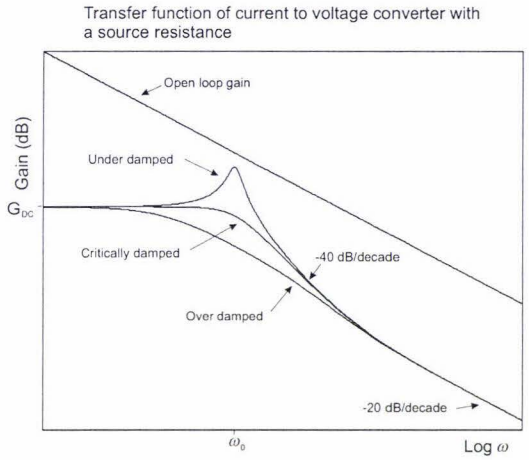

Figure 4.6: **Frequency response of current-to-voltage converter model:** The three graphs show when the circuit is under-damped i.e with a peak, over-damped with a reduced bandwidth and critically-damped. The final response will depend on the values chosen for the circuit. The frequency of the peak depends on $\sqrt{\frac{\omega_u}{R_f C_{tot}}}$ and the damping factor on $\frac{1}{2C_{tot}}(\omega_u C_f + \frac{1}{R_t} + \frac{1}{R_f})$. The total capacitance, C_{tot}, will be dominated by the input capacitance. Ideally the circuit would be critically damped. The final roll-off of -20 $^{dB}/_{decade}$ is a consequence of the extra term in equation 4.1, $(1 + j\omega C_s R_t)$, which dominates at high frequencies.

non-inverting input (see section 4.7.2 and figure B.4). The resulting transfer function is calculated in appendix B.1.1 and is

$$\frac{V_{out}}{v_n} = \frac{R_f + R_t}{R_t}(1 + j\omega C_{tot} R_t || R_f)\frac{\omega_0^2}{\omega_0^2 - \omega^2 + j\omega 2\delta} \tag{4.5}$$

where δ and ω_0 are as given above.

The noise gain has the same resonant response as the signal gain but because of the non-inverting amplifier configuration, has a higher dc gain of $\frac{R_f+R_t}{R_t}$. The difference is in the second term on the right of equation 4.5. Even if the resonant term is critically damped, as a consequence of this extra term the gain will increase at 20 $^{dB}/_{decade}$ above a characteristic frequency until it hits the open loop gain. The net effect is to form a peak in the noise gain spectrum which largely depends on the size of the input capacitance. As C_{in} increases, the peak position decreases in frequency and gets wider and higher. The total noise seen in the time domain is related to the area under the graph and this will also increase with an increase in input capacitance.

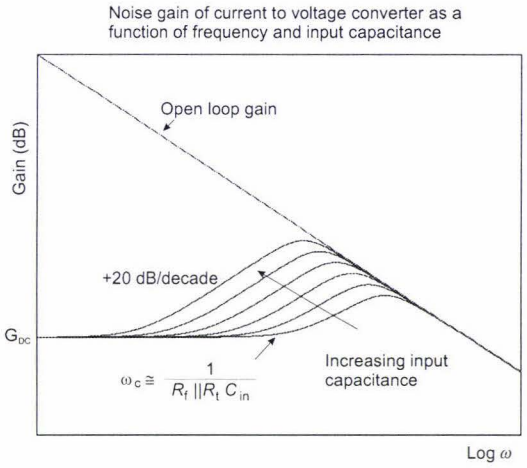

Figure 4.7: **Noise gain of model:** Although the resonant factor is critically damped a peak is still present due to the extra term in the equation. As C_{in} increases (C_{f} was also increased to ensure critical damping), the peak becomes larger and so the total noise, which is the area under the graph, becomes larger too.

Model	Bias Current (fA) max	Unity Gain (MHz)	Input Voltage Noise ($\frac{\text{nV}}{\sqrt{\text{Hz}}}$)	Input Current Noise ($\frac{\text{fA}}{\sqrt{\text{Hz}}}$)
OPA129	100	1	17 (1 kHz)	0.1 (10 kHz)
AD549	250	1	35 (1 kHz)	0.22 (1 kHz)

Table 4.1: **Two low bias current operational amplifiers:** The AD549 was the opamp chosen for the original circuit. The OPA129 was not available at the time of original construction but was recommended for future designs.

4.5 The Pre-existing Circuit

The mounting of the previous current-to-voltage converter contributed to most of its problems. The signal was passed from the tip to the current-to-voltage converter via a coaxial cable of around 30 cm in length. This gave rise to an input capacitance of approximately 66 pF. This restricted the choice of R_{f} to 90 MΩ giving a bandwidth of 7 kHz. A gain of $1\,^{\text{V}}/_{\text{nA}}$ would have been preferred for a better signal-to-noise ratio but this reduced the bandwidth to less than 1 kHz. An AD549 was chosen and in Dr Klank's thesis [30] it was noted that for future designs of the current-to-voltage converter the opamp OPA129 could be used (see table 4.1).

From the previous section it can be seen that a major consideration in redesigning the current-to-voltage converter was to attempt to reduce the

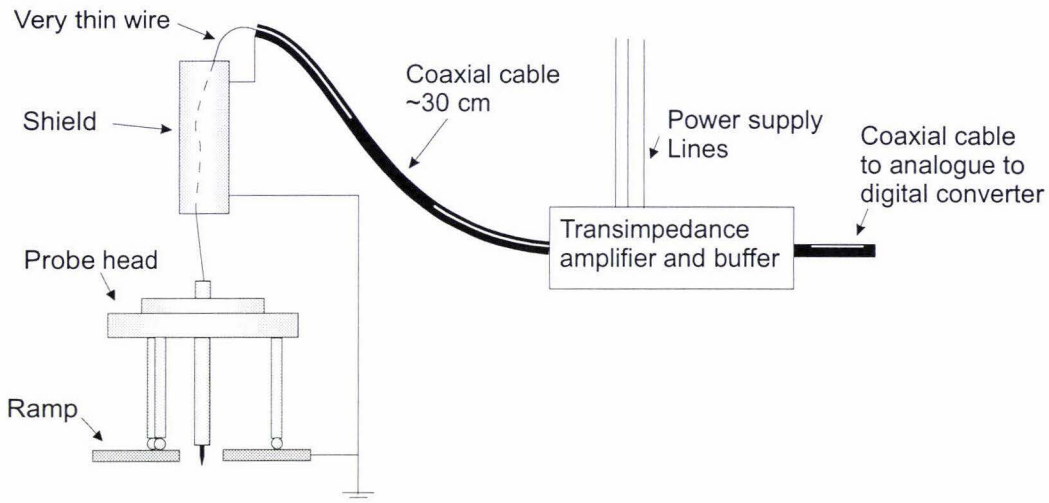

Figure 4.8: **The pre-existing current-to-voltage converter:** The preamplifier was mounted remotely from the probe head which resulted in a significant input capacitance.

input capacitance. A value of 5 pF should be aimed for as this is estimated to be the capacitance between the opamp pins. Since most of the input capacitance comes from transferring the signal from the tip to the current-to-voltage converter via a coaxial cable (see figure 4.8) the current-to-voltage converter needs to placed as close to the source as possible. Also suggested was the possibility of increasing the gain since this increases the signal to noise ratio. A gain of $1\,^{V}/_{nA}$ could be considered if the bandwidth was not significantly reduced (the problem in the original design).

4.6 The improvements

4.6.1 Reducing the input capacitance

Mounting the current-to-voltage converter closer to the probe head and eliminating the need for the shielded coaxial cable was one method that was considered (see figure 4.9). However, it was found that the input capacitance was still significant [23]. Additional noise was also observed due to the unshielded input wire.

Another option was to mount the current-to-voltage converter *on top of* the probe head (see figure 4.10). It would not be necessary for the buffer to be close to the probe head so this could be mounted elsewhere. For this to be an effective solution several aspects had to considered.

- the extra mass on top of the probe head might reduce the resonant

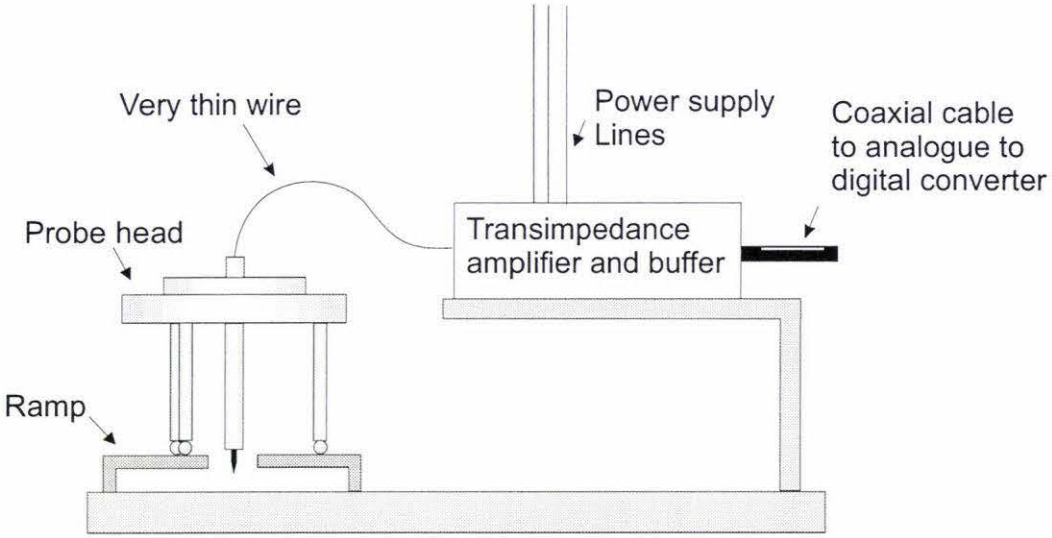

Figure 4.9: **One idea:** Mounting the current-to-voltage converter closer to the probe head would reduce the input capacitance, but the noise pickup from the input wire would be unacceptable.

frequency of the probe head to a value which is unacceptable.

- inside the circuit, care must be taken so that no part of the circuit can vibrate at an unwanted frequency,
- the extra mass might make the slip stick motion more difficult,
- passing the signal from and the power to the current-to-voltage converter must be done without significant mechanical coupling.

As a consequence of the first three points listed above, the current-to-voltage converter with its shielding box needs to be as light and as rigid as possible (see figure 3.7). Increasing the mass might increase the static friction between the legs and the ramp, therefore preventing the 'slipping' phase described in section 3.1.1. However, it is assumed that the added mass would have to be significant to have any effect. As an advantage, the increased mass might allow for a faster 'stick' phase. The signal and power can be passed to the circuit via very thin copper wires with a diameter of 0.06 mm. These wires are insulated and are light enough to avoid significant mechanical coupling.

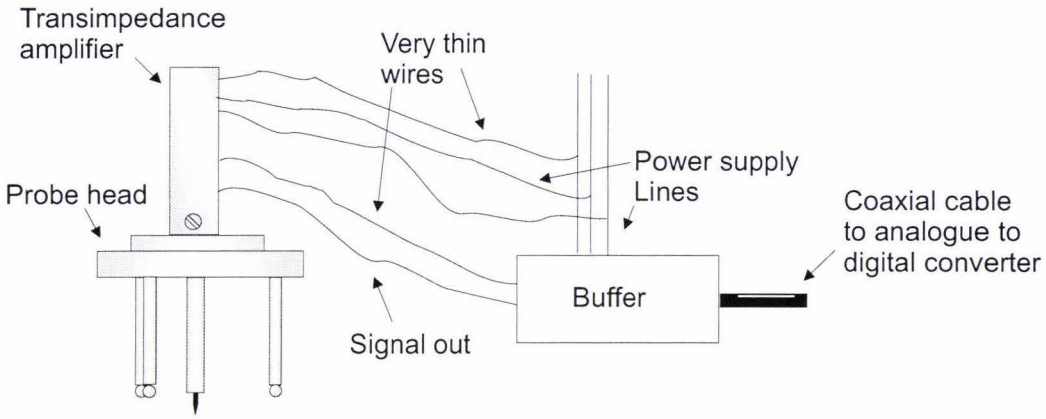

Figure 4.10: **The final design:** The preamplifier is mounted on top of the probe head and is connected to a buffer which drives a coaxial line to the analogue to digital converter.

4.6.2 Choosing the feedback resistor

In Dr Klank's thesis, section 5.4.2, the choice of feedback resistor, R_f, was discussed and it was noted that the signal increases with R_f while the Johnson noise is proportional to $\sqrt{R_f}$, so this gives a signal to noise ratio of

$$\frac{s}{n} \propto \frac{R_f}{\sqrt{R_f}} = \sqrt{R_f}$$

for the current-to-voltage converter.

Therefore, increasing the feedback resistance will increase the signal to noise ratio. The disadvantage of doing this would be the decrease in bandwidth due to the increased feedback at higher frequencies caused by the feedback capacitance (equation 4.1).

As mentioned earlier, the feedback resistor is critical since a small capacitance in parallel with a very large resistance can still have a low cut-off frequency. A resistance of 1 GΩ was aimed for and an attempt was made to sufficiently reduce the feedback capacitance so that this capacitance would not restrict the bandwidth. Because of the consequent high gain, the circuit needed to be shielded from 50 Hz noise.

4.6.3 The printed circuit board and leakage current

Because the current-to-voltage converter is measuring such small currents, it is very important to try and reduce the leakage current from the input terminals of the opamps. Any leakage current into the opamp will give an offset voltage on the output. When the opamp is mounted on a standard printed circuit board, surface contaminants can give rise to a current as large

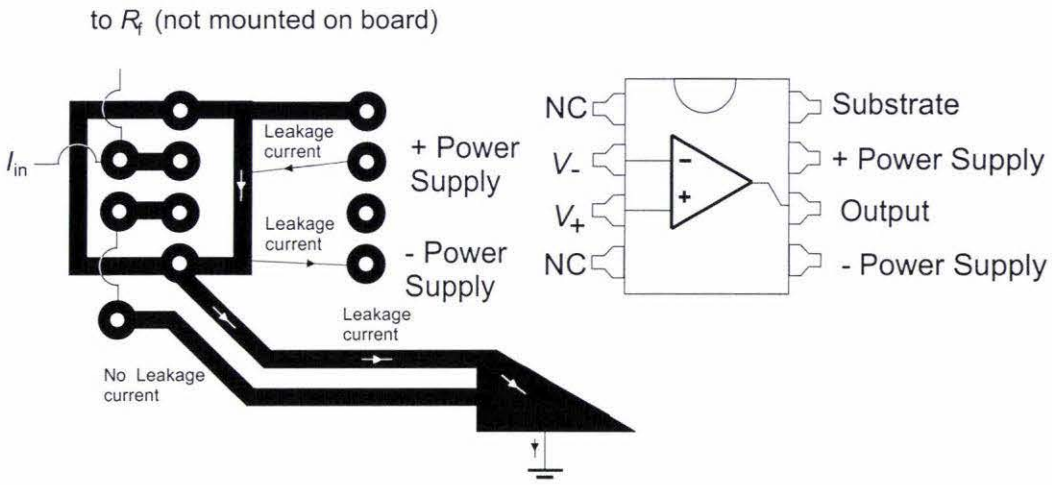

Figure 4.11: **Leakage current guard:** The guard ring protects the inputs from leakage currents from the power supply pins. Surface contaminants can give rise to currents as large as 12 pA. Since the guard ring is at the same potential as the inputs of the opamp, no current will flow.

as 12 pA. Simply keeping the surface clean is not enough since humidity can readily decrease surface resistance.

To avoid the surface leakage the input terminals should be guarded from external potentials. One option is to use a 'stand off'. This is a piece of material with *very* high resistance that is attached to the circuit board and the connection that needs protection. Teflon is often used as it has a resistivity of around 10^{16} Ωm. See fig 4.12. It is very important to clean the teflon effectively, otherwise contaminants on the surface can significantly reduce the resistance. To clean the teflon, and indeed the whole circuit board, it must be swabbed with iso-propropyl alcohol, rinsed with de-ionised water and left to dry in a low humidity environment. It *is* necessary to use a stand off and not just simply float the input in space because of triboelectric charges than can occur through friction and movement [29]. An alternative solution, and the one used here, is to use a guard ring. A guard ring is a ring of conducting material, such as circuit board tracks, completely enclosing the input terminals on both sides of the circuit board. The ring should be at the same potential as the non-inverting input but *not* connected directly to it. The connection should be made via a ground 'mecca' or 'star point'. Any leakage current from the circuit board will be sourced away through ground. No current will occur between the guard ring and the inputs because they are at the same potential (see figure 4.11). This solution also has the advantage of minimizing stray capacitance between input and output. The input capacitance to ground will be slightly, but not significantly, increased.

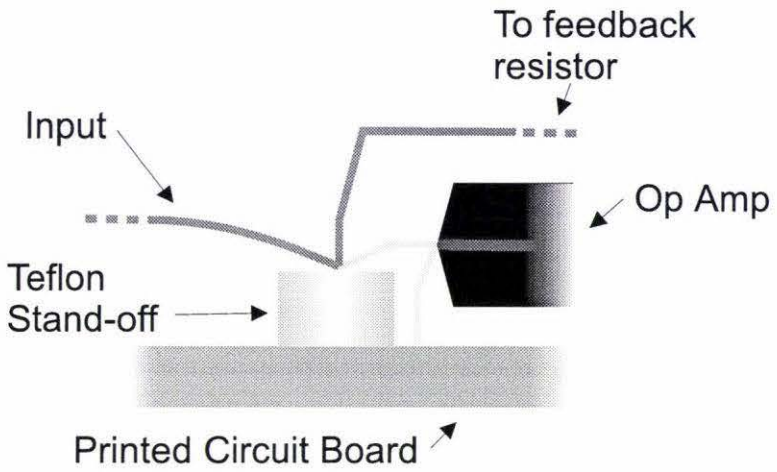

Figure 4.12: **Teflon Standoff:** The Telfon standoff is another a way of reducing the leakage current from the power supply pins.

Another source of leakage current is from the electrodes on the centre piezo. The electrodes on the centre piezo are separated from the tip holder by a slice of macor 1.2 mm thick. Although the resistance of the macor is very high, any surface contaminants will conduct a small amount of current. So again, the macor needs to be rinsed with iso-propyl alcohol and de-ionised water. With the electrodes held at 70 V and the macor uncleaned, offset voltages as large as -80 mV where observed. This corresponds to a resistance between the electrodes and the tip holder of around $10^{11}\,\Omega$. This resistance is very dependent on humidity - if the probe head was placed near a container of a humidity reducing agent, the offset would reduce to around -5 mV. To minimise this resistive coupling a guard ring similar to that using on the circuit board must also be used. In fact, this shield is more important because the shielding is from much higher voltages that before. A very small ring was painted on to the macor using conductive paint (see figure 4.16). The ring was grounded using the same fine wires that were used for the piezo control lines.

The guard ring eliminated the residual leakage current between the piezo electrodes and the current-to-voltage converter reducing the offset of the current-to-voltage converter to 0.09 ± 0.03 mV. This corresponds to a input bias current of 90 fA.

4.6.4 Stray capacitance

Piezo legs

There will be a certain amount of capacitive coupling between the tip holder, that is, the input of the current-to-voltage converter, and the electrodes on the centre and outer piezos. This stray capacitance, together with the current-to-voltage converter, will act as an inverting differentiating amplifier of the control signals. When the signals are changing rapidly, such as the slip phase in the coarse approach, a spike in the output of the current-to-voltage converter of up to -8 V can be observed.

Center piezo

During the slip-stick phase of the coarse approach the tunnelling current is not being monitored, so the coupling between the current-to-voltage converter and the outer piezos is inconsequential. However, there is also coupling between the tip holder and the electrodes on the centre piezo. During the fine approach, the voltage on the centre piezo is ramped down to extend the piezo. The current-to-voltage converter will differentiate this ramp and an offset on the output will be observed. At low frequencies the response of the capacitively coupled system is

$$V_{\text{out}} = -R_{\text{f}} C_{\text{p}} \frac{dV_{\text{piezo}}}{dt}.$$

Applying a ramp of 430 $^{\text{V}}/_{\text{s}}$ to the electrodes on the centre piezo results in an offset on the current-to-voltage converter of 35 mV. From this, a parasitic capacitive coupling of 84 fF can be inferred. During the fine approach, the DSP will begin to control once the tunneling voltage[4] has reached a preset value and so as long as this preset value is above the offset from the capacitive coupling, then the problem is not of immediate concern. However, the capacitive coupling also forms another unwanted feedback path in the control loop. As the piezo is moved to compensate for an error, the output from the current-to-voltage converter will change due to a change in tip-sample distance. In addition, the output of the current-to-voltage converter will also change because of the capacitive coupling from the electrodes. The controller will not know the difference between the two effects and will try and correct for both of them. Depending on the nature of the capacitive coupling, this could cause instabilities.

[4]While the term 'tunnelling voltage' is not strictly correct, it can be interpreted as the output from the current-to-voltage converter from a tunnellng current.

During a raster scan, a ramp is applied to the two electrodes of the center piezo to provide motion along the x-axis but because the ramps are equal and opposite, the pick-up due to the capacitive coupling cancels out.

The calculated and measured frequency response of the capacitively coupled electrode to tip holder system is shown in figure 4.14. There is a broad peak around 5 kHz. There are various ways to reduce this unwanted effect. If a ground plane is placed between the electrodes and the tip holder in the form of a shield (see figure 4.13), the capacitive coupling will be reduced. A simple experiment showed that this reduced the coupling by a factor of almost two (see figure 4.15). Alternatively, the output of the current-to-voltage converter could be filtered at some frequency below 5 kHz. Although this is not desirable as the bandwidth would be reduced, this is the solution that is presently used. Finally, if the behaviour is well known it could be corrected for in software. As the controller moves the piezo, the programme could calculate the expected current-to-voltage converter response from the capacitive coupling and then subtract it from the measured response.

Reducing the capacitive coupling would be a priority if the probe were to be redesigned. The macor layer could be split into two with a ground plane in between. Careful design could almost eliminate the capacitive coupling completely (see figure 4.23).

Bias voltage

The capacitance from the bias voltage to the input of the current-to-voltage converter can, in most cases, be ignored since the bias voltage is held constant. However, when recording V-I curves the bias voltage is ramped and the capacitance together with the current-to-voltage converter will act as a differentiator. We have

$$V_{\text{out}} = -R_{\text{f}} C_{\text{bias}} \frac{dV_{\text{bias}}}{dt}$$

where C_{bias} is the capacitance between the tip and the sample.

By adding a sine wave to the bias voltage and measuring the peak current frequency, C_{bias} was calculated as 200 ± 50 fF.

When recording V-I curves the slope on the bias voltage is around $2.2\,\text{V/s}$ which would produce an offset of about 0.4 mV. This will have little effect on the V-I curves recorded.

4.6.5 Buffer amplifier

To buffer the output of the OP129 opamp an OP27G was used. The output of the OP129 was connected to the non-inverting input of the OP27G and

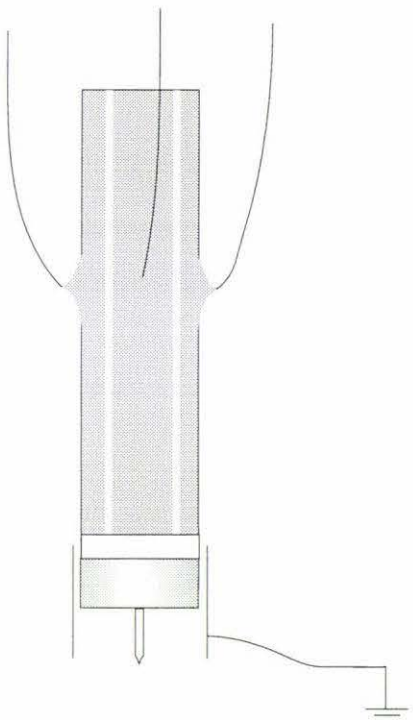

Figure 4.13: **Shielding from piezo electrodes:** Placing a grounded shield between the piezo electrodes and the input reduces the capacitive coupling.

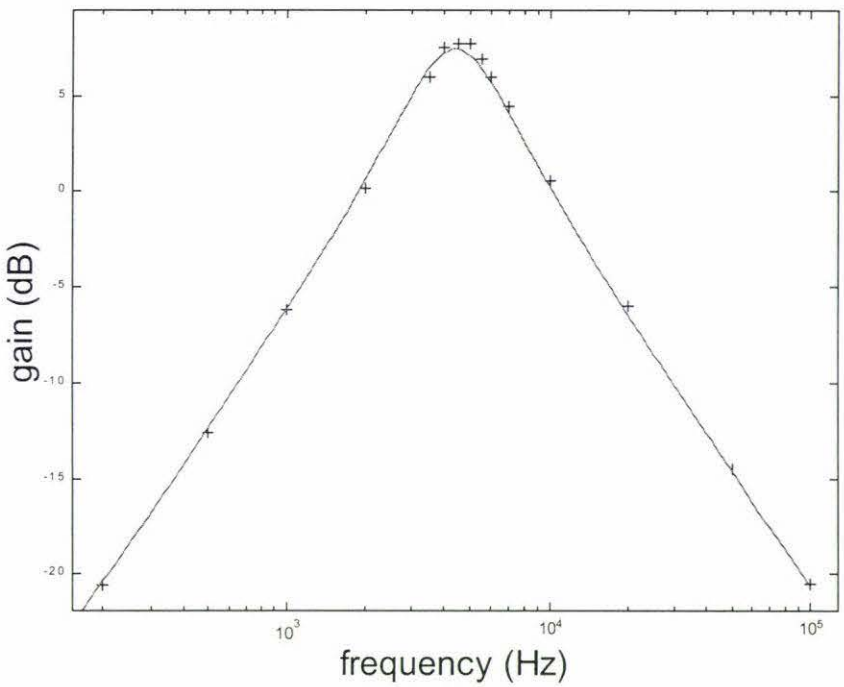

Figure 4.14: **Measured and modelled frequency response from piezo coupling:** This provides unwanted feedback into the system. To avoid this the output of the current-to-voltage converter is filtered at a frequency below 5 kHz

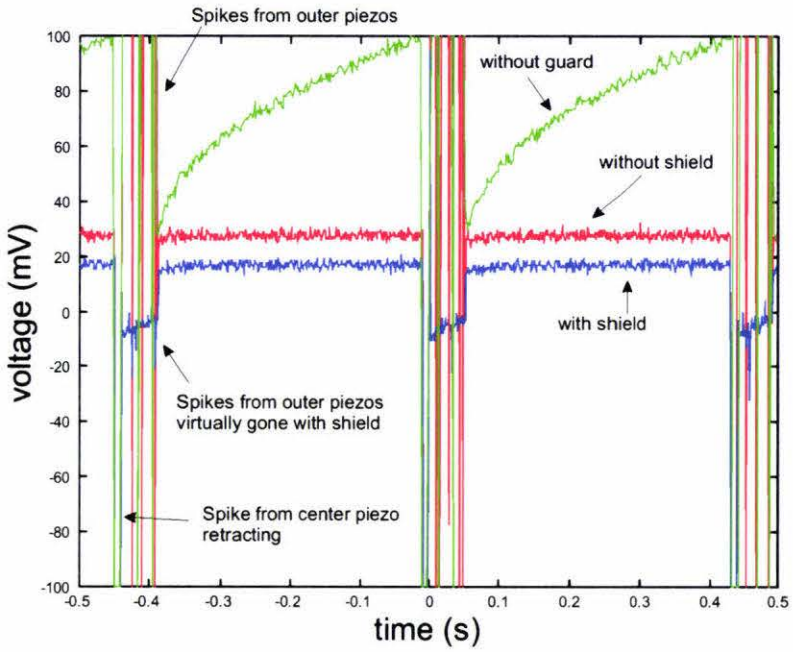

Figure 4.15: **Output of current-to-voltage converter during walking, with and without shield:** The capacitance between the input of the current-to-voltage converter and the piezos forms a differentiator with the current-to-voltage converter. During the fine approach, the center piezo extends steadily and so a dc level is observed from the current-to-voltage converter. Reducing the capacitance by adding a grounded shield (see figure 4.13) reduces this by almost a factor of 2. Also shown is the current-to-voltage converter output before the leakage current guard was used (see section 4.6.3). This effect made it difficult for the program to identify when a tunnelling current had been found.

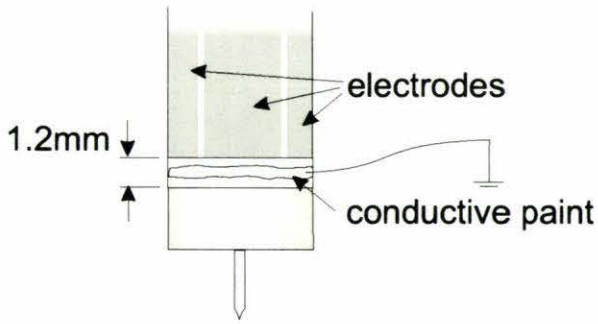

Figure 4.16: **Guard from piezos:** Similar to the guard from the power supply pins to the input of the opamp, this grounded guard ring protects the current-to-voltage converter from any surface leakage current from the piezos.

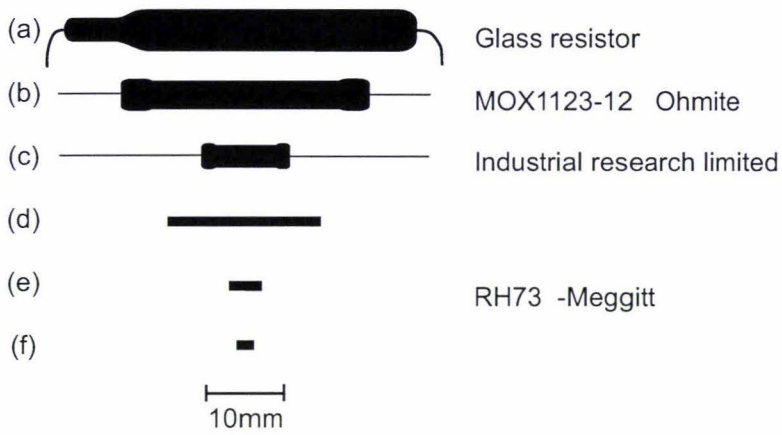

Figure 4.17: **Resistor sizes:** The silhouettes of various 1 GΩ resistors and resistor configurations. (a) Glass resistor provided by the Institute of Fundamental Sciences electronics workshop (b) Metal oxide resistor from Ohmite, part no. MOX1123-12. (c) Resistor from Industrial Research Limited. (d) 10 × 100 MΩ resistors from Meggitt, series RH73. (e) 2 × 500 MΩ resistors. (f) 1 × 1 GΩ Note: (d-f) are surface mount resistors 0805 with a thickness of 0.4 mm.

the inverting input was connected to the output giving a gain of 1. The rms noise was not measurable on a Fluke 8050A digital multimeter and can be assumed to be negligible (less than 10 μV). The voltage offset was $30 \pm 10\,\mu$V which is consistent with the typical value given in the data sheet.

4.7 Results

Several different resistor combinations were tried (see figure 4.17) using a circuit built with the OPA129 opamp. The transfer functions for three combinations are shown in figure 4.18. The final combination of two 500 MΩ chip resistors in series was used since this gave a response fairly close to the ideal possible with this configuration (see figure 4.19). In fact to avoid a peak altogether the feedback capacitance would need to be increased slightly. From the data, parameter values were estimated using the relationships given in equation 4.1 and B.2. Uncertainties were estimated by varying the values while still maintaining a reasonable curve fit,

$$C_{\mathrm{f}} = 35 \pm 2\,\mathrm{fF}$$

$$C_{\mathrm{s}} = 70 \pm 5\,\mathrm{fF}$$

$$C_{\mathrm{in}} = 8.9 \pm 0.8\,\mathrm{pF}$$

$$R_{\mathrm{f}} = 920 \pm 10\,\mathrm{M\Omega}$$

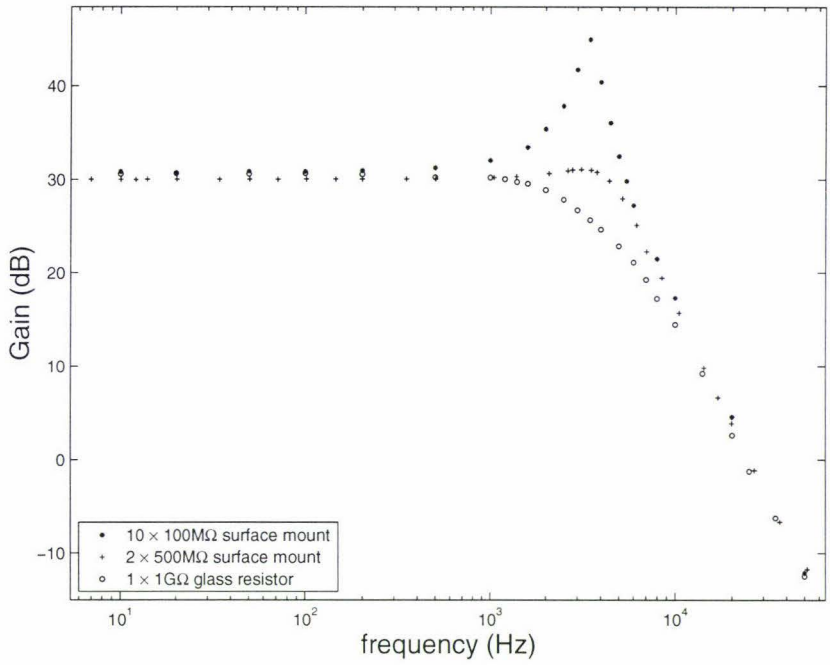

Figure 4.18: **The measured frequency response of the preamplifier with different 1 GΩ resistors :** Different resistor combinations result in different frequency responses and here we see one over-damped system and two under-damped. The final combination used was the one marked as +. The source resistance used was 29 MΩ

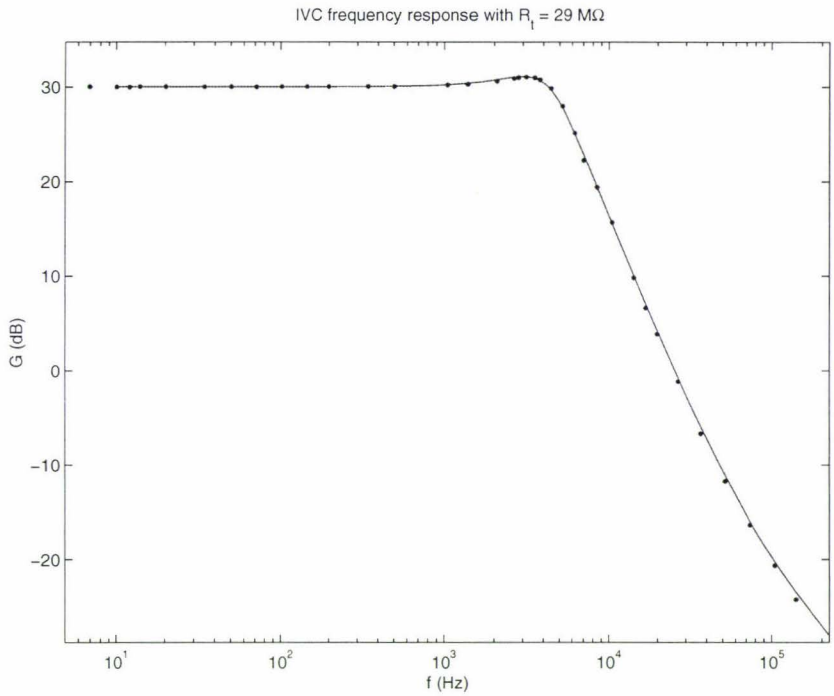

Figure 4.19: **The measured and modelled frequency response of the current-to-voltage converter:** Using the relationships given in appendix B.2, a resonance curve was fitted. This gives an indication of the parasitic capacitance values. $C_{\mathrm{in}} = 8.9 \pm 0.8\,\mathrm{pF}$, $C_{\mathrm{f}} = 35 \pm 2\,\mathrm{fF}$, $C_{\mathrm{s}} = 70 \pm 7\,\mathrm{fF}$. The feedback resistor R_{f} appears to be only 920 MΩ.

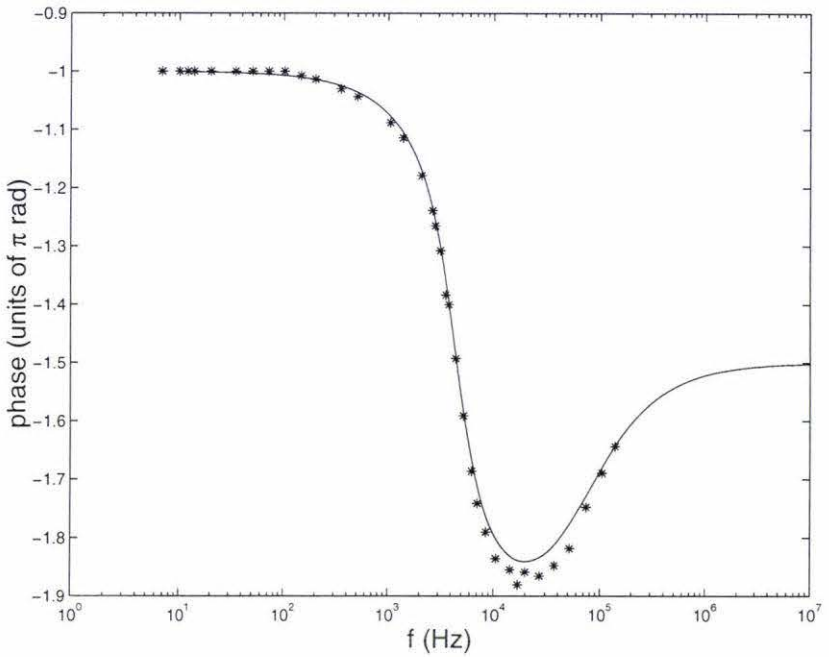

Figure 4.20: **The measured and modelled frequency response of the current-to-voltage converter phase:** The phase shift at dc is 180° because the current-to-voltage converter is an inverting amplifier. The final phase shift of 225° is because of the extra term in the transfer function.

$$R_s = 29 \pm 2\,\mathrm{M}\Omega$$

If the input capacitance were to be reduced further, then a feedback resistor with less parasitic capacitance, such as ten 100 MΩ resistors could be used. This would increase the bandwidth of the current-to-voltage converter. The box containing the current-to-voltage converter was originally designed to be large enough to hold the large glass resistor. Since the final solution used the surface mount resistors, the shielding box could now be made significantly smaller.

The phase response using the 29 MΩ source resistor is shown in figure 4.20. The dc phase shift of -180° is because the current-to-voltage converter is an inverting amplifier. This could have been corrected for by using a buffer with a gain of -1 or more simply correcting in software.

4.7.1 Tunnelling resistance and the transfer function

The current-to-voltage converter was tested using a 29 MΩ resistor. This enabled a comparison to the pre-existing current-to-voltage converter which was tested using the same resistor. From this, values for the input capacitance,

feedback capacitance and feedback resistance could be estimated. However, in actual use, the tunnelling resistance will be determined by the bias voltage and the current set-point. This will mean that the feedback capacitance will be such that the circuit may no longer be critically damped. Figure 4.21 shows a graph of the feedback capacitance needed for critical damping for different tunnelling resistances.

As a future option it may be desirable to be able to adjust the feedback capacitance in software. This could be an automatic adjustment that would make sure that the current-to-voltage converter was critically damped for whatever tunnelling resistance was chosen. The feedback capacitance of 10 100 MΩ resistors in series was as low as 4 fF which would mean we would need a variable capacitor in parallel that could be changed from 0.02 pF to 0.05 pF. This could be achieved by using a very small capacitor, in series with a voltage controlled capacitor such as a reverse bias diode. Finding suitable components would be difficult and it might be easiest to fix the feedback capacitance to 0.055 pF which would cause reasonable damping over a range of tunnelling resistances (see figure 4.21).

4.7.2 Noise calculation

All opamps contain resistors and transistors that generate thermal noise, shot noise and flicker noise. A convenient way of modelling these is to assume that the opamp is noiseless and then add a voltage noise generator at the non-inverting input and a current noise generator between the non-inverting and the inverting input [15] (see figure B.4). The details of the noise generators will be different for each opamp and are specified in data sheets. The noise level will generally depend on frequency.

The noise gain of the amplifier due to the voltage source was given as a function of frequency in section 4.4.2. To find the total noise, the noise gain must be multiplied by the rms input noise level, $v_n(\omega)$, squared and then integrated over the bandwidth of the amplifier.

$$V^2_{\text{amplifier}} = \int (G_n(\omega) v_n(\omega))^2 d\omega,$$

where $G_n(\omega)$ is the noise gain and v_n is the input noise level.

The noise level is given in the data sheet [12] and can be approximated by

$$v_n(\omega) = N(1 + j\sqrt{\frac{\omega_n}{\omega}}),$$

where a typical value of $N = 17\,^{\text{nV}}/\sqrt{\text{Hz}}$ and $\omega_n \approx 300\,\text{rad}$.

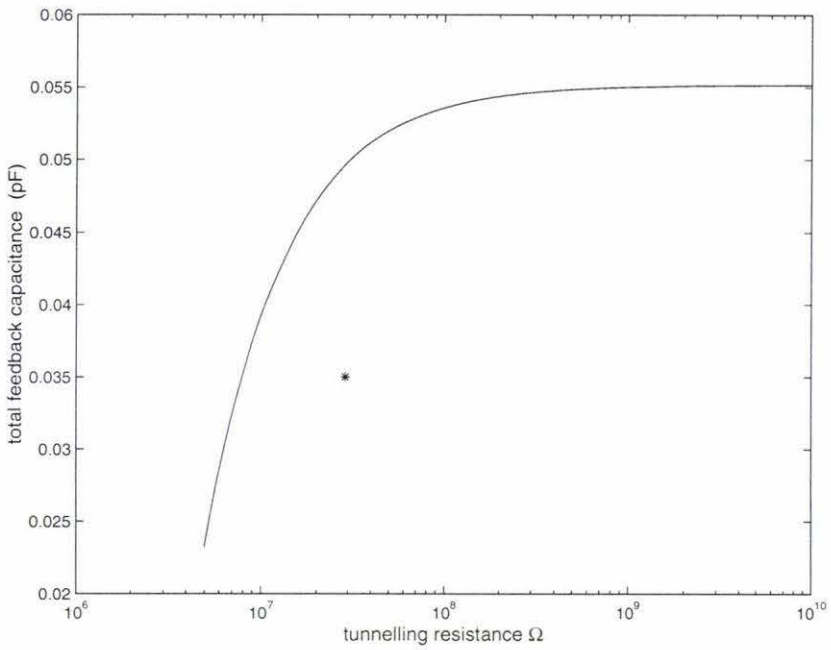

Figure 4.21: **The feedback capacitance required for critical damping with different tunnelling resistances:** If large tunnelling resistances are to be used it would appear that a feedback capacitance of 0.055 pF would critically damp the circuit over a wide range. The star shows the feedback capacitance of the current-to-voltage converter as it was tested on a source resistance of 29 MΩ. Since it is not on the line, the circuit is not critically damped although referring to figure 4.19 it would seem that the peak is acceptable (see section B.3 for more explanation of this graph).

The other major source of noise in the current-to-voltage converter is the Johnson noise from the large feedback resistor, R_f. This is given by

$$V_{\text{Johnson}} = \sqrt{4R_f k_B T \Delta f}$$

where Δf is the bandwidth, k_B is Boltzmann's constant, and T is the temperature in Kelvin.

Because noise sources are uncorrelated the total root mean square noise is the square root of the sources squared.

$$V_{\text{total noise}} = \sqrt{V^2_{\text{Johnson}} + V^2_{\text{amplifier}}}$$

The noise level was measured while artificially increasing the input capacitance with $R_t = \infty$. Figure 4.22 shows the measured data with the calculated noise. A best fit was obtained with a value of N of $17\,^{\text{nV}}/\sqrt{\text{Hz}}$ and $\omega_n = 60\,\text{rad}$. From this graph it can be seen, for the current-to-voltage converter with an input capacitance of 8.9 pF, that the noise due to the voltage noise generator is less than the Johnson noise from the feedback resistor.

4.8 Conclusions

Although the target for C_{in} of 5 pF was not quite met, the current-to-voltage converter is such that the noise "due to" C_{in} has been significantly reduced, the gain has been successfully increased to $.920\,^{\text{V}}/_{\text{nA}}$ while preserving a reasonable bandwidth of 5.5 kHz. This is a significant improvement over the pre-existing current-to-voltage converter which had a gain of $.090\,^{\text{V}}/_{\text{nA}}$ and a bandwidth of 7 kHz.

The current-to-voltage converter was unconditionally stable and could be integrated in with the rest of the loop. Further work is needed to increase the bandwidth of the total loop while maintaining stability.

The final rms noise output from the current-to-voltage converter measured using the same multimter used to record the graph of figure 4.22 is approximately $400 \pm 50\,\mu\text{V}$. Referring again to figure 4.22 it would appear that the input capacitance has risen to 10 pF or more. This could be because of the increased capacitance from the guard ring between the piezos and the current-to-voltage converter input. Future design of the probe could eliminate the need for this guard ring and possible reduce the input capacitance further (see figure 4.23). A much smaller box could also be used especially if a surface mount opamp were used. The true rms, measured using a Fluke 8050A digital multimeter, was $600 \pm 50\,\mu\text{V}$ which corresponds to an input current noise of $0.60 \pm .05$ pA which is within the desired range. The offset voltage is $120 \pm 40\,\mu\text{V}$ which is low enough to be insignificant.

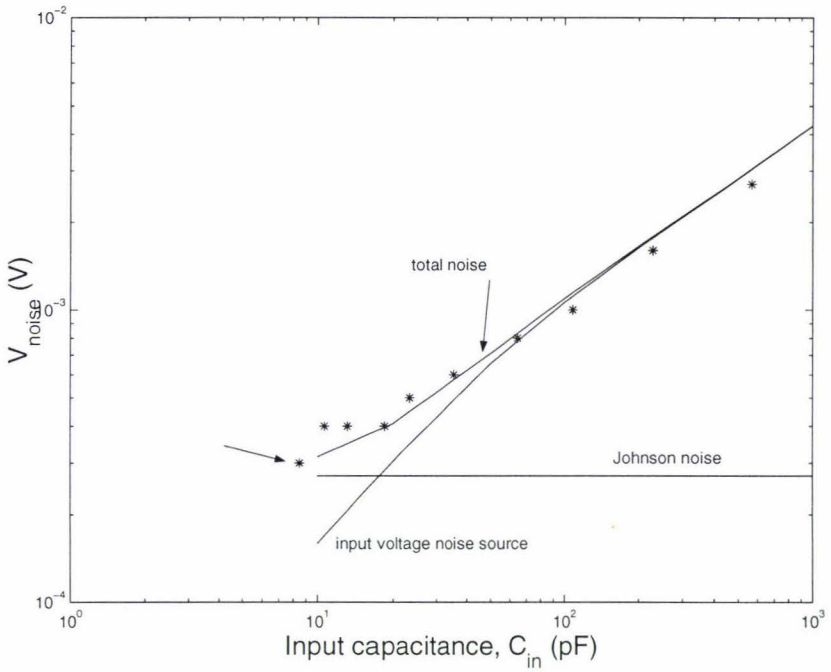

Figure 4.22: **The measured and modelled noise levels of the current-to-voltage converter for different input capacitance:** Various sized capacitors were added on the input stage of the current-to-voltage converter. The noise was modelled by performing the numerical integration detailed in section 4.7.2. The arrowed point on the far left of the graph is with no capacitance added, hence the input capacitance is sufficiently low that the Johnson noise is the major contributor to noise. Nothing except for the capacitance was connected to the input. Note that these voltages were recorded with a multimeter that does not give true rms readings so the above reading could be in error by 10-20%.

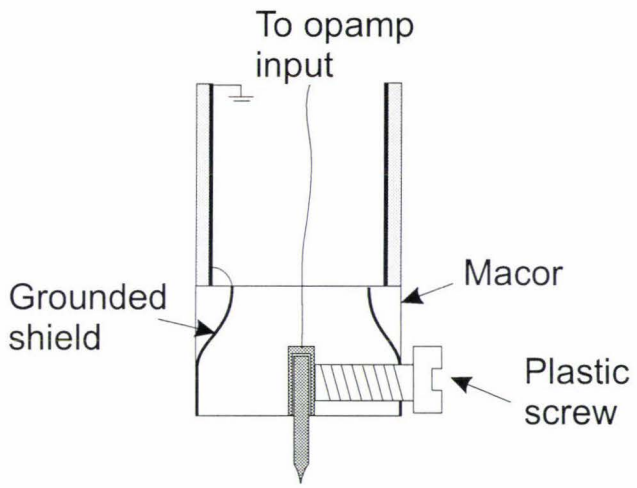

Figure 4.23: **Redesign of probe:** In order to eliminate coupling from the piezoelectrodes, a grounded shield must be used (shown in black). However to avoid increasing the input capacitance the shield must be far away from the input (shown in dark grey).

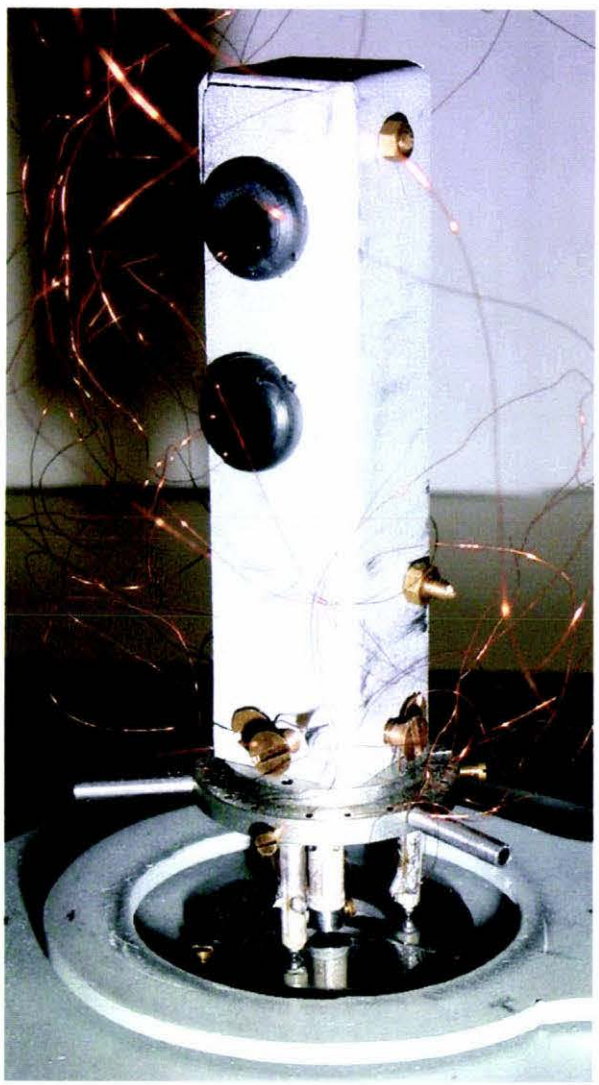

Figure 4.24: **Photo of probe head and current-to-voltage converter:** The shielding box was originally designed to be able to hold a resistor of length 4 cm so the box could now be replaced with a much smaller one. The rubber grommets were used to protect the wires passing into the box. The 'rat's nest' of fine wires are the control lines for the piezos. The overall height of the box is 4.5 cm. The metal ring at the base of the probe is used to lift the probe off the ramp.

Chapter 5

Fabrication of tips

5.1 Introduction

As described in section 2.1.2, the operation of a scanning tunnelling microscope relies on a very sharp metal probe being manipulated over a sample while the tunnelling current is monitored. This metal probe is referred to as the *tip*. For STM, "very sharp", takes on a new meaning. To obtain atomic resolution with an STM it is necessary to have a tip that has a single atom at the very end [42]. Therefore the tunnelling current will primarily exist between the sample and one atom at the apex of the tip.

No technique exists for reliably manufacturing tips with a single atom at the apex. The process of making tips is best described by the title of a review written by Melmed [33] "The art and science of making tips".

The previous method for making tips developed by Dr. Klank [30] was a simple one chosen for ease of construction and to be consistent with the prototyping environment described in section 1.1. An introduction to tip making and a summary of the literature, including on overview of Dr. Klank's technique will be presented below followed by the new method that has been investigated in this work.

5.1.1 'Good' tips

Tips for STM should be very sharp but this is not the defining factor in producing a good tip. A tip is only classed as good if it is able to obtain 'good' images, i.e. low noise, high vertical and lateral resolution. The most common method for classifying a tip as good is to state whether or not atomic resolution of Highly Orientated Pyrolytic Graphite (HOPG) was obtained.

The most reliable way of making a tip 'good' is to make sure it is sharp. This may seem contradictory to the preceding paragraph but the reason for

this is as follows.

The sharpness of a tip is characterised by the radius of the tip when observed in a Scanning Electron Microscope (SEM). It is hoped that on the apex of this radius there is a small 'minitip' or 'asperity'. These are small groups of maybe 1, 3 or 5 atoms that will contain most of the tunnelling current. If the radius of the apex is small, it is more likely that there will only be one minitip. A tip with a large radius could have multiple minitips that would give rise to many tunnelling sites which would reduce resolution and produce imaging artifacts (see figure 5.1).

The first step in fabricating a tip is therefore to make sure it is sharp. The sharper the tip, the greater chance of there being a single atom at the apex, and if the tip obtains atomic resolution, it is 'good'. A radius of less than 100 nm is usually aimed for.

Once a tip has been manufactured and placed in an STM, the quality of the tip can be determined by whether atomic resolution is obtained. If it is, the resolution can be estimated to be around 2 Å, in other words a single atom is acting as the tip [42].

5.2 Background

Scanning tunnelling microscopy places other requirements on tips;

- to avoid significant vibrations of the tip, the taper must be short (see figure 5.2),
- the tip must be constructed from a conductive material that is rigid and resistant to corrosion,
- to obtain reasonable vertical range the tip must be narrow [25].

What follows, is a review of the methods for making tips that is relevant to us and also a brief look at the previous technique for tip making used in this laboratory. This is not intended as a complete review or a history of making STM tips, for this, refer to Melmed [33].

5.2.1 Electrochemical etching

Sharp tips are not unique to STM, they have been required for field ion microscopy (FIM) and even earlier, field electron emission microscopy (FEEM) [33]. In these cases, however, tip sharpness was not so crucial, up to 100 nm for FIM and 1000 nm for FEEM. Tip lengths for FIM were generally around 1

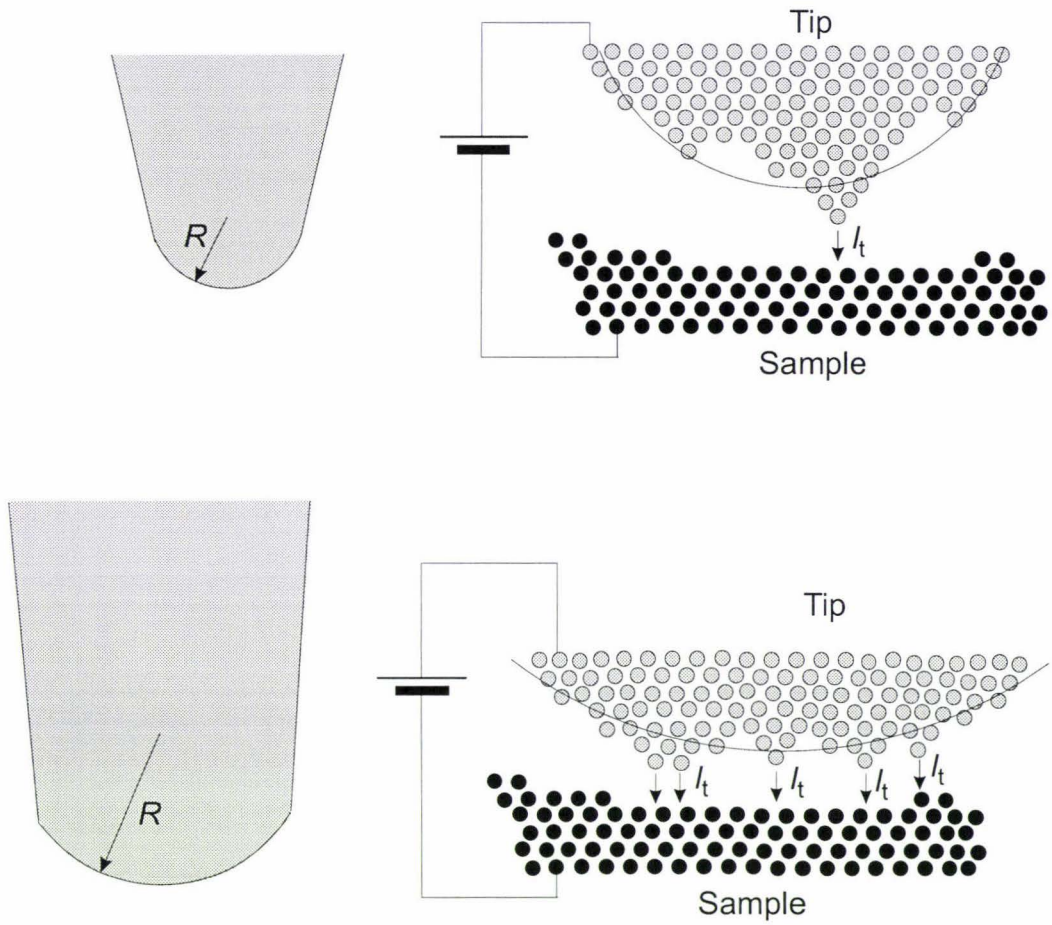

Figure 5.1: **Characterisation of a tip:** On the left is a schematic diagram of what a tip observed in an SEM might look like. The very apex of the tip can be described as a sphere with radius R. Every attempt to make this radius as small as possible is made. On the right is what is hoped for, a small minitip, with a single atom at the end that will act as the source. If the radius of the tip is made as small as possible, there is a greater chance that single minitips will occur. Below shows a bad tip. The radius is very large which gives many minitips and so a lot of tunneling sites. This could produce a noisy tunnelling current, low resolution and/or multiple images.

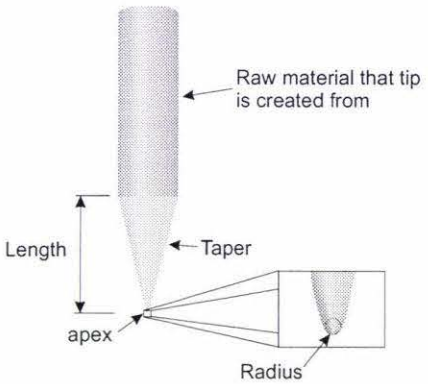

Figure 5.2: **Tip properties:** The length of the tip is the distance from the raw material to the apex. To avoid unwanted vibrations this length should be as small as possible. The most preferable shape is not the one pictured here but one in which the taper gets narrow very rapidly and produces a thin apex.

to 2 mm. STM requires sharper and shorter tips than those previously used for FIM.

Methods for producing STM tips are wide and varied. The two most common methods in use today are an electrochemical etching technique and a mechanical technique, cutting.

The cutting technique is very simple. A piece of wire is snipped by a pair of side cutters at an appropriate angle. It is hoped that the rough edge will produce one single protrusion, which will then act as the tip. Although cutting has been thought of as non-reproducible and unsuitable for forming "good" tips [22, 33], it is routinely used for making tips from a Pt-Ir alloy. For reasons described below (section 5.2.3) the option of fabricating tips from Pt-Ir was unavailable to us and so will not be described in detail in this report.

Tungsten tips were very commonly used in FEEM and so were the natural choice for STM. The tips are almost exclusively prepared by electrochemical etching[1]. A sample of tungsten wire is placed in a bath of a base, such as NaOH or KOH and a voltage is applied between the wire and a counter electrode. This causes a chemical reaction to take place that removes material from the wire (see figure 5.3).

For tungsten the reaction is

$$6H_2O + 6e^- \rightarrow 3H_{2(g)} + 6OH^-$$

at one of the electrodes and

[1]Due to the crystalline structure of tungsten mechanical cutting is not an option.

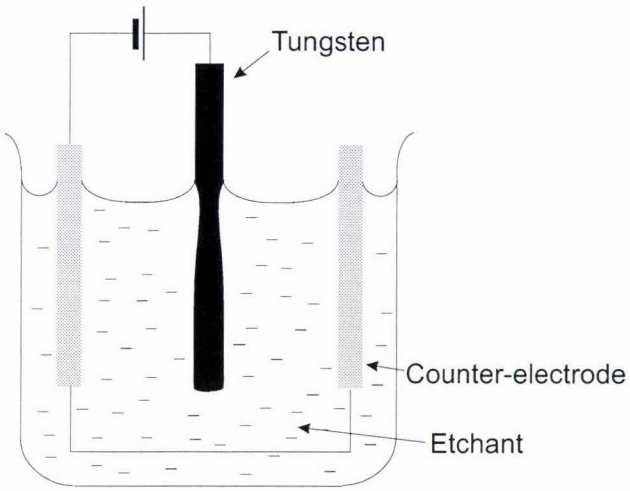

Figure 5.3: **Electrochemical etching:** A piece of tungsten wire is etched in a solution. Although a dc potential is shown here, sometimes ac is used. The configuration of tungsten, counter-electrode and etchant is known as the cell. This particular technique is known as the standard drop-off technique.

$$W_{(s)} + 8OH^- \rightarrow WO_4^{2-} + 4H_2O + 6e^-$$

at the other.

The reaction occurs most strongly at the surface of the liquid, so much so, that the wire is etched through until the thinnest part fractures from the weight of the wire below it. This event is known as the "drop-off". This results in two tips, the upper and the lower tip (see figure 5.4). The fracture tears the wire and it is believed that very small asperities remain on the tip and this is where most of the tunnelling occurs.

The necking-in effect results from reaction by-products flowing down the wire, thereby protecting the lower half of the wire from etching [28]. Because of this, the lower half of the etching profile, which becomes the lower tip, has a rather drawn out taper, which is a slight disadvantage in STM since it might have a resonant frequency which is low enough to be unacceptable. The upper tip will have a much more desirable shape.

When the drop-off occurs, the upper tip will remain connected to the etching power supply and be left in the solution and so will continue to etch (see figure 5.5). This action will blunt the tip as the asperities are etched away [10]. On the other hand the lower tip is removed from the circuit and so will not be susceptible to extra etching and will consequently remain sharp.

Mounting requirements in the STM dictate the length of the lower tip. However, in the electrochemical etching process this length is also constrained.

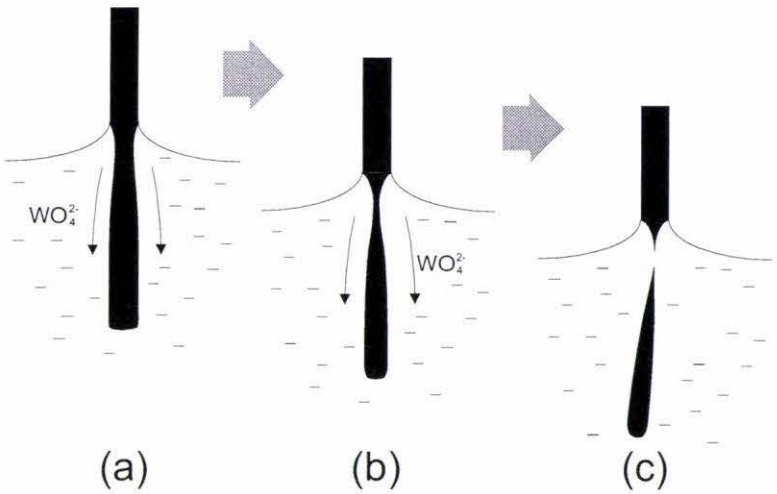

Figure 5.4: **The "necking in" effect:** The reaction occurs most vigorously at the air interface boundary. The tungsten oxide flows down the lower part of the wire and shields it. The wire then etches through and breaks off leaving two tips.

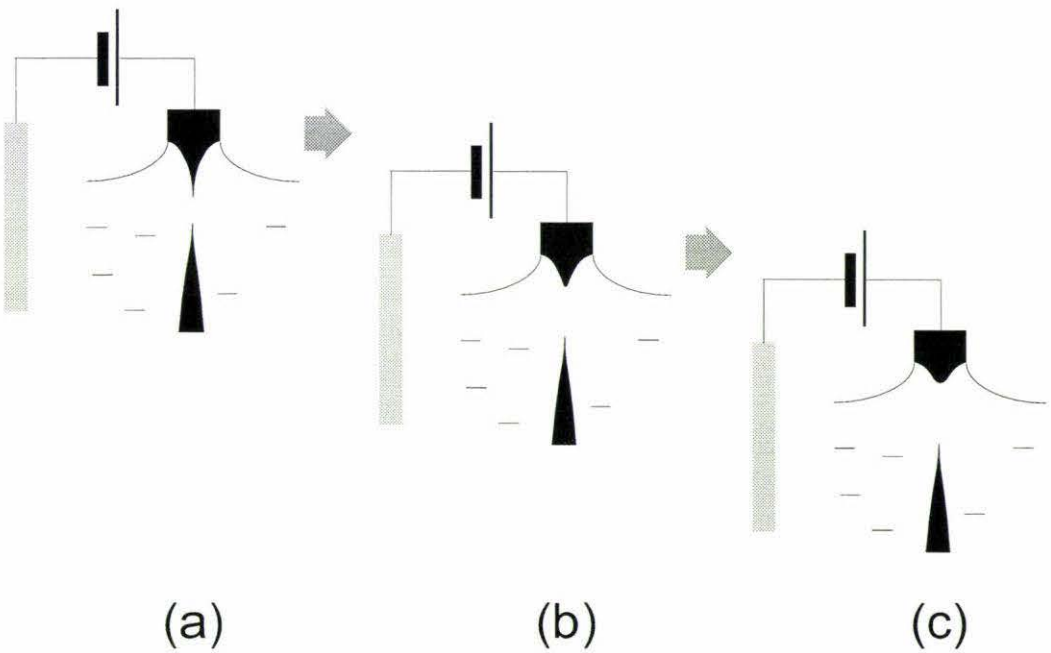

Figure 5.5: **Extra etching of the upper tip:** After the drop-off the lower tip is disconnected from the circuit and so will remain sharp (a). The upper tip, however, is still connected and etching will continue. This will blunt the tip (b)-(c).

Firstly, the tungsten wire is the working electrode of the cell and so its surface area will affect the local current density and therefore, the etching profile. Consequently, the amount of wire beneath the surface must be chosen to give the best shape. Secondly, the drop-off occurs as the wire fractures under its own weight, so obviously the mass of wire beneath the surface will have an effect on the way the tip fractures and hence will effect the tip morphology.

An additional problem is that as the reaction proceeds, the wire beneath the surface will be etched and so will be reduced in diameter, possibly non-uniformly; this can also cause problems when mounting the lower tip in the STM.

In short, the upper tip is the most reproducible and has the most favourable shape but is blunt. The lower tip is sharp but has an undesirable shape.

5.2.2 Upper or lower tip?

Lower tip

If the etching can be limited to the necking-in area then two of the problems with the lower tip are avoided; the wire below the surface no longer effects the etching shape and the lower tip will not be reduced in diameter.

Bryant *et al.* [10] solve this problem by arranging the wire so that the lower half is in an air column that is trapped in a capillary tube. When the tip is formed the lower tip drops down onto a bed of polystyrene. The etching was performed with an ac current (although their diagram shows dc) in KOH. It was mentioned that the upper tip might still be sharp enough for field ion use if an electronic cut-off circuit was used.

Upper tip: cutting off the etching current

Ibe *et al.* [28], as a follow-on from Bryant's paper, stated that the upper tip could, in fact, be used if a very fast current cut-off circuit was built. This has the advantage that the sharp asperities would remain on the tip. This idea was first mentioned by Nagahara *et al.* [35] as a way of electrochemically producing Pt-Ir tips for in-liquid STM. Unfortunately no details of the cut-off circuit or its speed were given. Ibe *et al.* confirmed that any extra etching subsequent to the drop-off would blunt the tip and thus highlighted the need for a very fast cut-off circuit.

Using the upper tip allows the length of wire beneath the surface to be varied freely, thus the length of wire beneath the surface giving the best shape and radius can be found.

This idea was studied in detail by Oliva *et al.* [39], using similar experimental apparatus to Ibe *et al.* It was found that a large length (5 mm) of wire immersed under the surface produces sharp upper tips. However, differing results were found by Ibe *et al.* who suggested that too greater load will tend to snap the wire prematurely since the tensile strength is exceeded and in fact, they suggested only 1 or 2 mm [28]. Oliva *et al.* suggested that shorter tips can be made by using tungsten wire of a large diameter [39].

An idea presented by Fainchtein and Zarriello [20] was to try and shape the tips by using a computer to slowly withdraw the wire from the solution during the etching process. A cut-off method similar to that devised by Ibe *et al.* was used, except that it was controlled by the computer and cut-off via a relay. This limited the cut-off time to the switching time of a relay - around 50 ms. In any case, slowly withdrawing the wire would only serve to make the tip longer, which is undesirable.

A mechanical cut-off technique that enabled the upper tip to be used was suggested by Bourque and Leblanc [9]. The lower half of the tip is covered with heat shrink tube and further sealed with silicone glue. The wire is then suspended in the solution in such a way that when the drop-off occurs the meniscus is dragged down by the lower part of the wire. As a result of this, the upper tip is then not in the solution and so no further etching will occur. Although this is a novel solution and does not rely on an electronic circuit it has two disadvantages, preparation of the wire is time consuming and most importantly, the effective cut-off time is too slow.

Rao and Mathur [43], using a very similar cut-off circuit to that designed by Ibe *et al.*, claimed a success rate of around 70% with an etching potential of 5 V dc. Rao and Mathur define success as a tip with a curvature of less than 100 nm.

The cut-off circuit

Anwei *et al.* [2] pointed out that cut-off circuits similar to that of Ibe *et al.* had a design flaw. To understand this we must first look at how these circuits operate.

Firstly, the etching current is converted to a voltage, V_{etch}, and as the reaction proceeds, V_{etch} slowly drops. When the drop-off occurs, V_{etch} drops very quickly, since the surface area of the wire reduces rapidly. The cut-off is achieved by triggering a switch once V_{etch} has dropped below a preset reference etching voltage V_{ref}. The problem is that it is not possible to know the value of V_{etch} when the drop-off occurs, so setting V_{ref} is difficult. If V_{ref} is set too high, the circuit will switch the etching off before the drop-off has occurred. If V_{ref} is set too low then the upper tip will be etched slightly

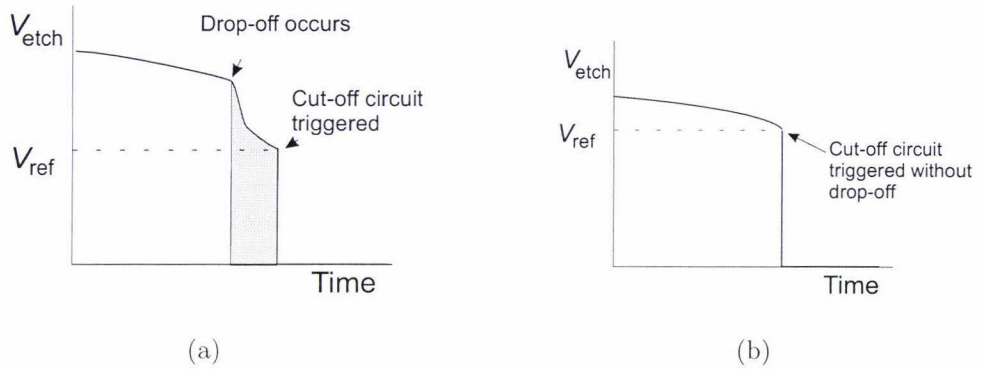

Figure 5.6: **Switching off the etching current:** Once the current is converted into a voltage V_{etch} it is compared against a preset reference voltage V_{ref}. If V_{etch} falls below V_{ref}, the etching is switched off. Graphs (a) and (b) show the disadvantage of this system. The etching voltage when the drop-off occurs can only be estimated and so it is difficult to set V_{ref}. If the reference voltage is set too low, as in graph (a), the upper tip will continue to be etched for a short while before V_{etch} drops below V_{ref}. The shaded region indicates the extra etching that will blunt the upper tip. If the reference voltage is set too high, as in graph (b), the etching current will be cut off before the drop-off has occurred.

before the current is switched off (see figure 5.6). Although the circuit has a cut-off speed of 500 ns, this is not an accurate indication since the circuit is not triggered by the actual drop-off event but some time after it. Any amount of extra etching after the drop-off will blunt the tip. This type of cut-off circuit is therefore unsatisfactory.

Anwei *et al.* [2] described a different, superior method for triggering the cut-off circuit. Instead of comparing V_{etch} to a reference voltage, V_{etch} is differentiated. When the drop-off occurs and V_{etch} drops suddenly, the differential of V_{etch} changes very sharply and it is this pulse that can be used to trigger a switch. Unfortunately, the speed of the circuit was not given but in can be inferred that since the circuit triggers on the drop-off, and not microseconds after it, that the overall cut-off time will be quicker.

This type of cut-off, using a differentiator, was reported at the same time by Dickmann *et al.* [18] as a technique for etching silver tips. The switch that was used, however, was a relay, which is several orders of magnitude slower than a solid state device.

Using the upper tip with the etching cut-off by a detection circuit has become an acceptable method of producing tips for STM. If the circuit is fast enough the tip will be sharp enough.

During the research phase of this project a paper was published by Nakamura *et al.* [36] which described a circuit that cut the etching current off in

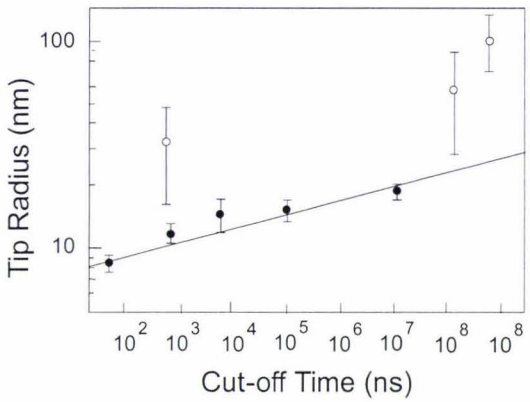

Figure 5.7: **Tip radius and the cut-off speed:** Delays in the cut-off will result in considerable tip blunting. The closed circles show the data recorded by Nakamure *et al.* The open circles show data from Ibe *et al.* which are not as sharp for the same cut-off speed. Presumably this is because the cut-off circuit was triggered by comparing the etching current with a reference so that extra etching occurs as in figure 5.6(a). This graph is reproduced from [36].

50 ns. In doing this they obtained tips with a radius of 8 nm. A graph was plotted of the tip radius and the cut-off time showing that for a tip radius of less than 10 nm a cut-off time of 1000 ns was needed. The radius of the tip was estimated using field ion microscopy (FIM).

This work appears to supersede what will be presented later. When this project was begun, the fastest cut-off time reported in the literature was 500 ns however, in section 5.7.1 the cut-off time will be given a little more attention.

The lower tip: limiting the etching area

As mentioned in section 5.2.2 use of the lower tip is simplified by limiting the etching area. This makes the shape more consistent and less reliant on other factors. Other solutions include surrounding the wire in a heat shrink tube [9], wax [25], using the lamellae technique [31, 34] or floating a small layer of electrolyte on some denser liquid, usually carbon tetrachloride [33][2].

Containing the etching in a small region is easily achieved by using the lamellae technique. The electrolyte is suspended in a small loop of the counter electrode, often platinum. This eliminates the problem of the lower tip being susceptible to extra etching, so its diameter is not reduced and less solution is used in the process. In essence this is the same as using the full immersion technique with a cover on the lower half of the wire, but the loop method is

[2]Due to its carcinogenic properties, working with carbon tetrachloride is to be avoided.

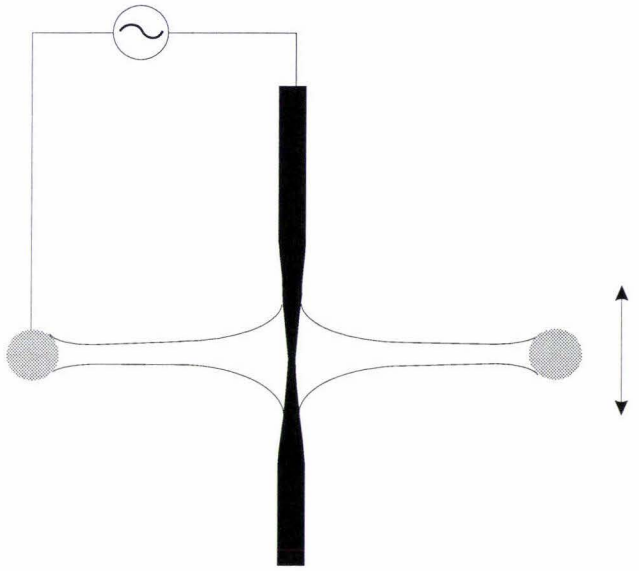

Figure 5.8: **The previous etching process:** A lamellae contained in a platinum ring was slowly moved up and down as the etching proceeded. An ac potential was used.

simpler. Generally the solution in the lamellae does not have to be replaced during the etching process. One disadvantage of the lamellae technique is that the lower tip has to be caught in some way without damaging it. In addition, the lower tip can be affected by the surface tension at the bottom of the lamellae and may break asymmetrically. To overcome this, a small weight can be fixed to the wire, but this affects the breaking in a detrimental way (see section 5.4.1). Nevertheless, the lower tips generally have a much poorer shape than the upper tips, being up to three times longer and with a non-reproducible tip curvature. However, because the etching stops immediately after fracture the tips are sharper.

Dr. Klank's technique was similar to this one. A solution of KOH was contained in a lamellae formed in a ring of platinum. The lamellae was slowly moved up and down during the etching process and eventually two tips were formed (see figure 5.8). No preference was given to either tip. Tips with a radius of less than 100 nm could be formed using this technique (see figure 5.9).

So far, no one has used the upper tip obtained from a lamellae etching process together with a cut-off technique. An alternative solution was proposed by Klein and Schwitzgebel [31]. Their idea was to flip the wire mid way through the etching process so that the nicely shaped tip was now at the bottom of the lamellae. This solution still has problems with catching the tip as mentioned earlier. Also, if the wire was flipped too early in the

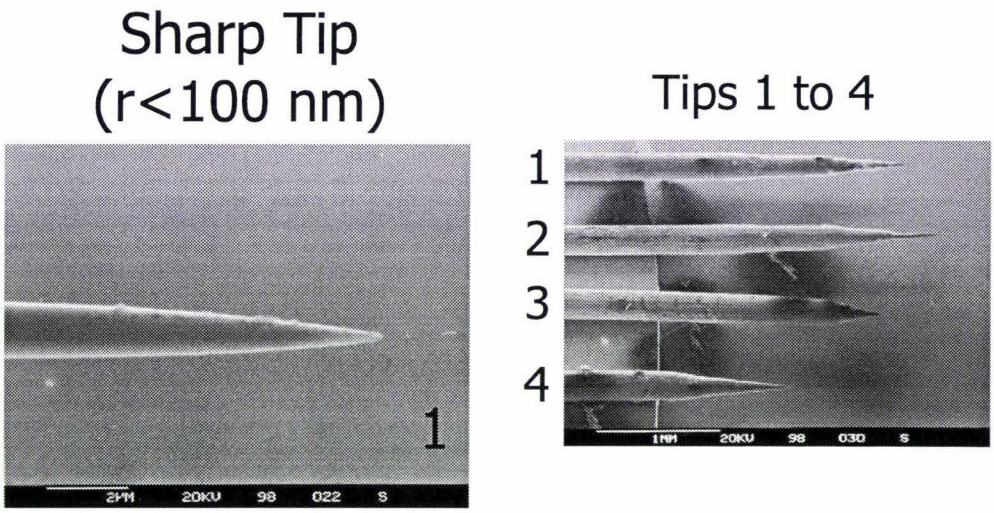

Figure 5.9: **Tips made by Dr. Klank:** This tip was successful in producing atomic resolution, unfortunately tips like this were not reproducible. The method used to produce these tips resulted in very inconsistent shapes.

etching process the nice shape would be undone as the lamellae slides down over the former upper tip. If the flip was performed too late in the etching process the wire might snap.

5.2.3 Etching parameters

ac or dc

The type of potential used has some effect on the shape of the tip [28]. Tips etched with an ac potential generally have a conical shape with a large cone angle, whereas the dc etched tips are sharper and have a more desirable hyperbolic shape [28]. However, ac is commonly used when etching tips from Pt-Ir [35, 31].

An ac potential causes gas to be evolved from the surface of the wire, which prevents an even etch. This problem is avoided with dc. However, in some cases an ac potential is preferable because it helps to clear away spent material which builds up when a dc potential [33] is applied. An ac potential is more commonly used in situations where a long taper is needed, such as FIM.

The bubbles formed at the tip during ac etching are usually considered to be a disadvantage, as they rise alongside the tip, protecting the tip unevenly from etching. This is the reason for the less desirable shape associated with ac etching. An idea presented by Fortino [22] was to use the bubbles formed by an ac potential to improve the tip quality. The tip was mounted upside

down in the solution and the bubbles served to sharpen the tips as they rose upwards along the tip. However, it was pointed out by Bourque and Leblanc [9] that this article contains no reference to the reproducibility of these tips or their ability to obtain atomic resolution.

Other factors

The choice of etchant is not critical. Common options include NaOH [28, 25, 22, 43, 9, 31, 2, 34] or KOH [10, 20, 27]. The effects of different solutions and concentrations were studied in detail by Oliva *et al.* [39] and it was found that KOH was the preferred etchant at a concentration of 2 to 3 M.

A voltagramme[3] shows three distinct regions, an almost ohmic region up to the reaction potential (around 2 V), a plateau spanning less than 10 V followed by a region in which the current increases very rapidly with voltage. The plateau region arises because the current is limited by mass transport and it is this region that is best for etching [39]. Above this plateau, the reaction becomes very violent which results in an uneven surface and the potential for unknown species to form in the reaction.

The value of this plateau current is determined by the configuration of the etching cell, i.e. the surface area of the wire and the counter electrode and the concentration of the etchant. Once these have been chosen, it is preferable to adjust the voltage until the current is in the plateau region. Plateau currents for etching tungsten range from 1 mA [10] to 70 mA [39]. Counter electrodes that are commonly used are platinum [31, 25], graphite [2, 20, 27], gold [9], copper [43] and stainless steel [28, 34, 39].

Is tungsten actually any good?

Generally tungsten tips are not recommended for use in air because of the oxide layer that forms as part of the etching process. The oxide layer will act as another potential barrier for the electrons to tunnel through, this causes extra noise and in some cases makes imaging impossible [27, 39]. If the oxide layer can be removed effectively, the tip can be used for around two to ten days before another oxide layer appears [39, 34]. Tungsten tips are routinely used for STM in ultra high vacuum (UHV). Pt-Ir tips are preferred for STM in air because of their chemical inertness and because they can be produced either by cutting or electrochemical etching.

The STM that we have been using is not in an UHV, but is in a prototype development stage and new tips are required quickly, easily and inexpensively. Pt-Ir tips, although superior, are too expensive to be used in an environment

[3] a current *vs* voltage plot for the etching cell.

where they could be damaged easily. For this reason it was decided to use tips fabricated from tungsten.

A common method for removing the oxide layer is by annealing the tip in a vacuum at approximately 800 °C. At this high temperature the surface oxides become volatile leaving only the tungsten behind [13].

Another method, reported by Hockett and Creager [27] is to dissolve the oxides of tungsten using a mineral oxide such as Hydrofluoric acid.

Müller *et al.* [34] claims that tungsten tips etched in dc are acceptable and says that an oxide layer is only formed a few days after the tip has been prepared.

5.2.4 Discussion

Although the argument about whether upper or lower tips are better has never been fully resolved, it is clear that some factors can be dismissed by containing the area of etching (section 5.2.2). This can be done by using the lamellae technique or by including some protection such as wax. The former appears to be the simplest method.

Although the lower tip will always be slightly sharper, for shape, consistency and to a lesser degree, ease of use, the upper tip is preferred if a fast enough cut-off circuit can be built. Only Müller *et al.* [34] disagrees and prefers the shape of the lower tip. The fastest method for cutting the etching current off is the differential approach suggested by Anwei *et al.*

The only thing that seems to be agreed on in making tips is that there is no one unique method that is superior to the others. Although the tips can be classified according to their length, radius and symmetry and they can be observed in micrograph images from electron microscopes, a tip is often considered unsatisfactory unless it can obtain atomic resolution. The two main standards of tip quality is to report the tip radius and more importantly evidence of atomic resolution, usually of highly orientated pyrolytic graphite in air [9, 39].

To obtain a superior technique for making tips two of the methods mentioned above will be combined. For consistently shaped tips, the etching current needs to be contained spatially and be predictable. The simplest way to do this is by using the lamellae technique. While most people have used this as a technique for utilising the lower tip we will use the technique's advantage of producing a predictable tip shape and use the upper tip. To do this a circuit needs to be designed to cut-off the etching current effectively.

5.3 The experiments

5.3.1 Standard drop-off technique

Experiments began with a set-up similar to that shown in figure 5.3. The etchant used was 4 M KOH and platinum was used as the counter electrode. The results were not reproducible, the necking effect and indeed the shape of the tip depends on the rate of material removal from the wire. This seems to be due to the non-uniform current density which is quite hard to control or predict. This occasionally manifested itself by producing the necking-in effect in two places while at other times the effect was not noticeable at all. To produce more consistent etching profiles the lamellae technique was preferred.

5.3.2 The lamellae technique

A small ring of platinum of approximately 8 mm diameter was sufficient to hold the solution and to act as the counter electrode. The etching area is now limited to a narrow region of the wire but now a new problem exists. For the etching to occur symmetrically around the wire, the corresponding reaction has to occur symmetrically around the ring. For the reaction at the ring to occur, nucleation sites must exist to enable the production of hydrogen gas. Such a surface is one that has coarse features on a microscopic scale. The ring was constructed by twisting the wire together (see figure 5.10) and doing this might have torn the surface of the metal slightly, providing sites for gas to evolve. The resulting effect is that it is easiest for the reaction to occur near the twist in the ring. This produces a reaction rate around the ring that is not symmetric and so the etching current density and consequently the shape of the tip will not be symmetric. This could be corrected for by placing the wire in the lamellae slightly off center where it could be assumed the current density would be symmetric. The symmetry is only important at the very apex of the tip, however a symmetric profile will produce shorter tips and a predictable shape is an advantage. Another solution is to etch the platinum in something, such as $CaCl_2$ first [31]. This would produce the necessary roughness on the surface of the platinum.

The wire beneath the lamellae was loaded with a small ball of blutak to prevent the lower tip from being affected by surface tension.

The experimental apparatus is shown in figure 5.11.

For different etching runs with similar initial conditions, the etching times varied considerably. On occasion the lamellae would break and the solution would need to be replaced (see figure 5.13).

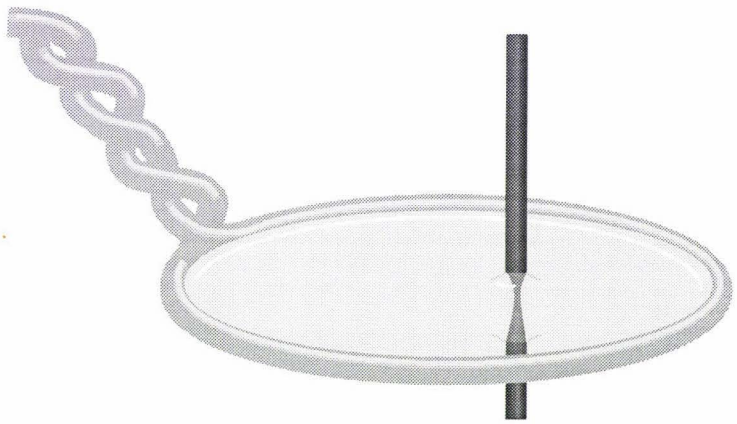

Figure 5.10: **The lamellae technique:** A small amount of 4 M KOH is held in a ring of platinum by surface tension forces.

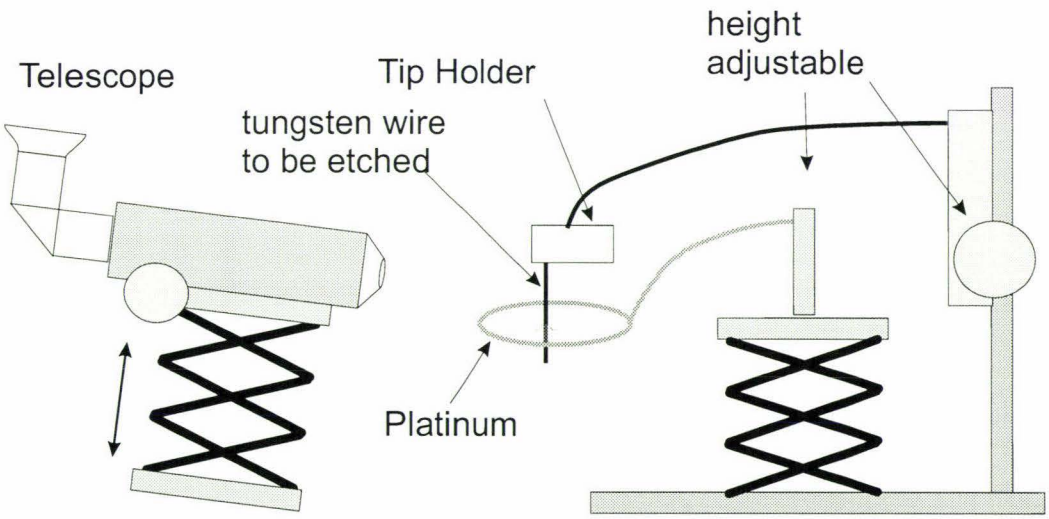

Figure 5.11: **Experimental setup:** The telescope was used to observe the meniscus on the wire. The tip holder and the ring are both adjustable to allow ease of positioning. They are not moved during the etching process unless the meniscus slides down the wire.

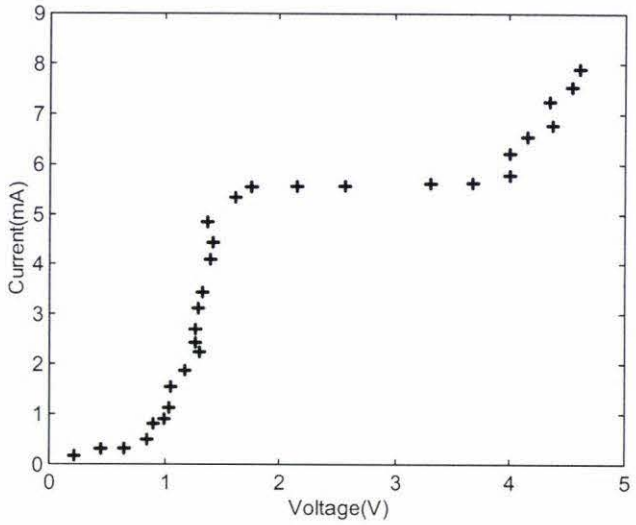

Figure 5.12: **Voltagramme for tungsten in a 4 M KOH lamellae:** The etching current increased rapidly at around 1.43 V, which is the reaction potential. The current then plateaus because the rate of reaction is limited by mass transport phenomena. The current increases above 4 V, but this is due to other unwanted reactions occurring. It is therefore desirable to etch in the plateau region.

The plateau region for this set up is between 1.6 V and 3.8 V for a dc current of about 5.5 mA (see figure 5.12).

Observing the etching current when the drop-off occurs shows a drop from around 2 mA to 1 mA over a period of about 5 ms (see figure 5.14). The sudden drop is due to the reduced surface area of the electrode when the lower portion of the wire drops off. Presumably the gradual drop is due to the reduction in surface area of the upper tip immediately after the drop-off.

5.3.3 Mechanical cut-off of etching current

Instead of an electrical cut-off circuit, the apparatus could be designed so that the upper tip removes itself from the lamellae after the drop-off. In section 5.2.2, a mechanical technique was dismissed as too slow. What follows in the rest of this section is an attempt to verify this.

The arm to hold the tungsten wire can be made out of a piece of copper wire. If a small mass is attached to the wire beneath the lamellae, the arm comes under tension. Once the lower tip drops off, the load on the arm is reduced and it springs up. This will remove the upper tip from the lamellae (see figure 5.15).

This method has two disadvantages, firstly, as will be seen later (section 5.4.1), adding extra mass to the wire beneath the lamellae will degrade

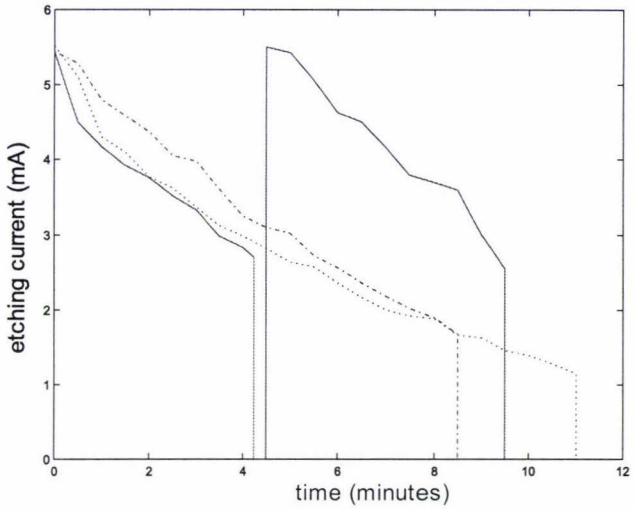

Figure 5.13: **Etching current for similar tips:** The drop-off current is different in each case, highlighting the advantages in using a differentiator to cut the current off. The area under each graph is related to the amount of material removed during etching and so it can be assumed that the etching profile for each etch was different. However, in all three cases the shape of the upper tip was consistent but the shape of the lower tip varied considerably. The solid line plot shows the lamellae being replaced after 4 minutes 15 seconds.

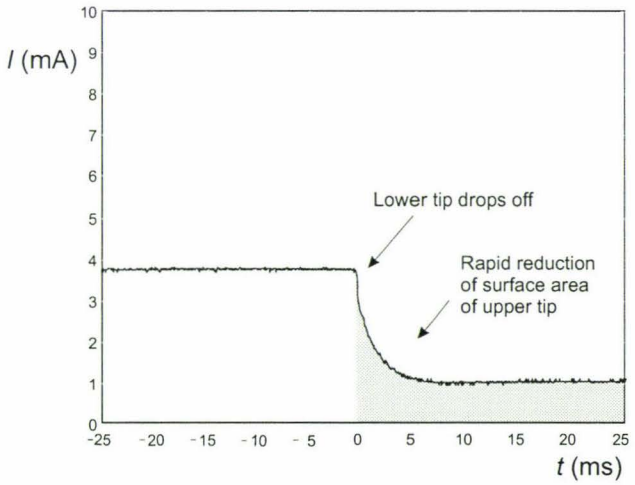

Figure 5.14: **Etching current when drop-off occurs:** The etching current drops very quickly due to the lower tip removing itself from the circuit. The current is then reduced further as the surface area of the upper tip is initially reduced dramatically and then plateaus at around 1 mA.

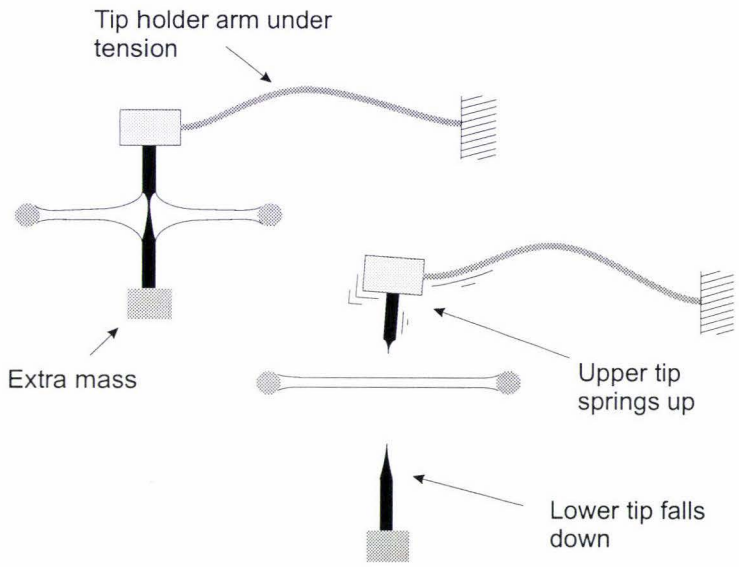

Figure 5.15: **Schematic of mechanical cut-off:** The large extra mass on the lower tip causes the upper arm to be under a little tension. When the drop-off occurs the tension is released and the upper arm springs up, removing the upper tip from the lamellae.

the upper tip. Secondly, as was suspected, the cut-off was too slow. Figure 5.16 shows that the upper tip was removed after 9 ms. With an electronic technique, the cut-off could be achieved in less than 1 μs. Further mechanical cut-off techniques were not considered.

5.3.4 Electronic cut-off

A block diagram of a cut-off circuit is shown in figure 5.18. For the differentiator to work effectively, the change in current needs to be known. Figure 5.17 shows that when the drop-off occurs there is a exponential-like change in current. Over about 750 ns the current drops by .5 mA. A cut-off circuit is designed to sense this drop (see figure 5.19).

To sample the current a 1 kΩ resistor was used in series with the tip. By monitoring the voltage across this resistor with an oscilloscope the etching current can be observed. Normally when using this approach, a small resistor is used so as to not load the circuit. However, this loading is not important because interest is only in the etching current and not the voltage required to produce this current. The voltage across this resistor is called V_{etch}.

An ac coupled transistor amplifier provided a fast way of differentiating V_{etch}. The biasing resistors and the sensing resistor determined the response of this amplifier. It was tuned to have a time constant of around 500 ns. The transistor amplifies the pulse and then a buffer amplifier drives the clock

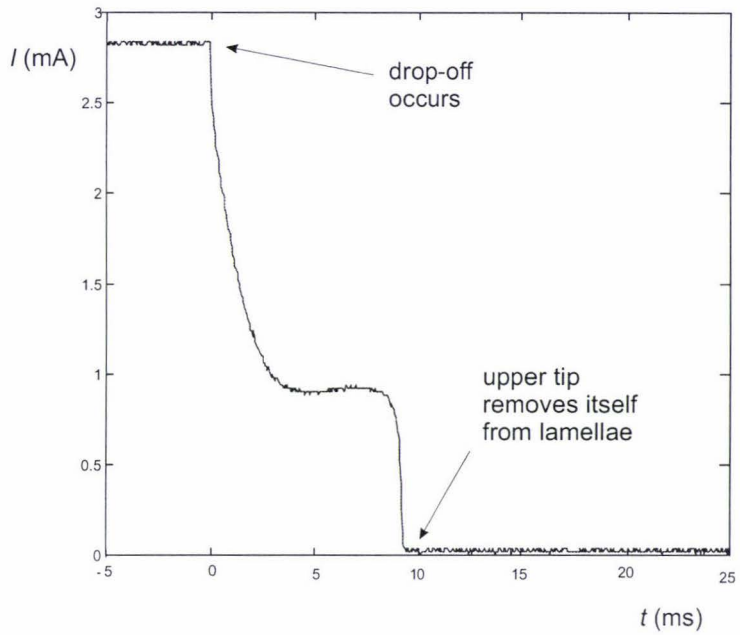

Figure 5.16: **Mechanical cut-off of etching current:** The lower half of the wire was weighted so that when the drop-off occurred, the holder would have spring up enough to remove the upper tip from the lamellae. This example illustrates the relatively slow speed of a mechanical cut-off technique.

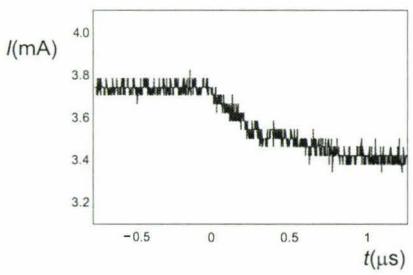

Figure 5.17: **The etching current on a finer time scale:** As the lower tip drops off a small exponential-like drop in current can be observed. A differentiator could be designed to respond to this drop.

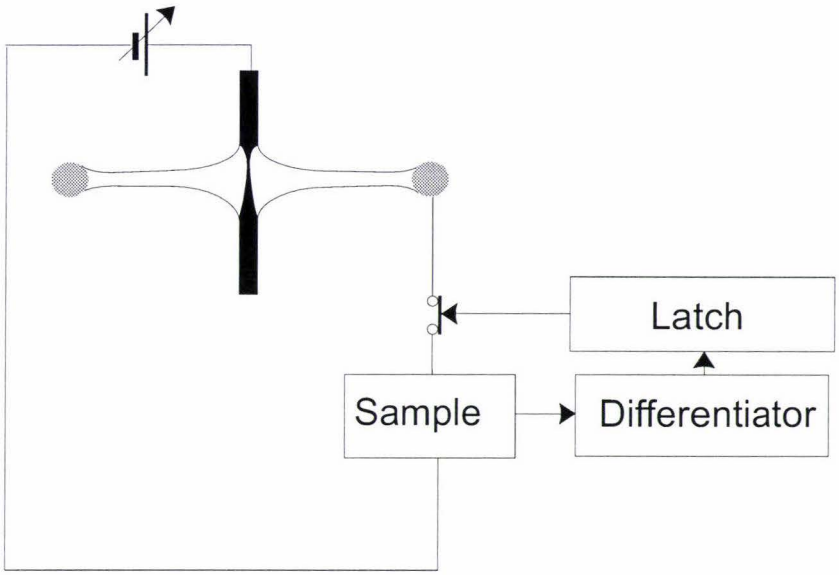

Figure 5.18: **Block diagram of cut-off circuit:** The etching current is converted into a voltage, this voltage is then differentiated so that a sharp change in etching current will trigger the latch to open the switch. This circuit is based on one presented by Anwei *et al.* [2].

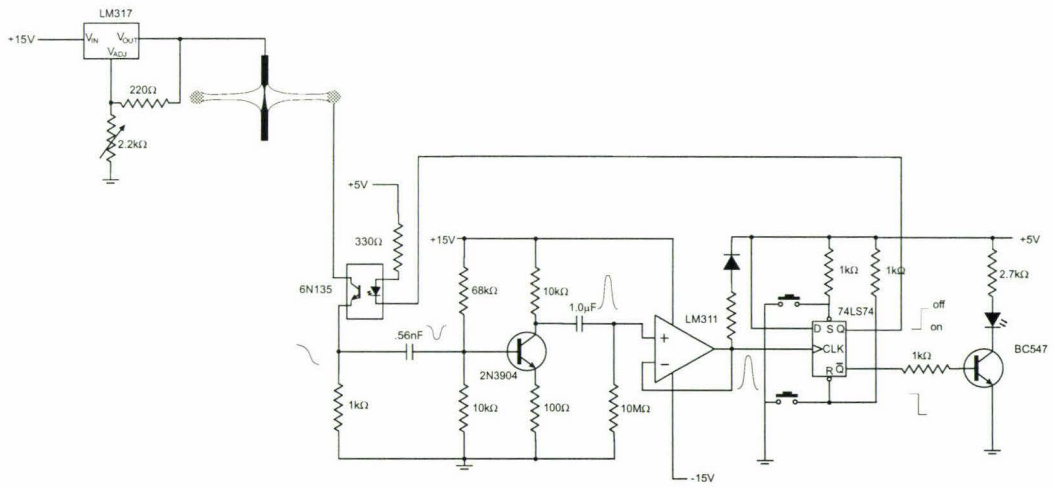

Figure 5.19: **Diagram:** The first attempt at making a cut-off circuit. The thin lines show the waveform as the drop-off occurs and then the circuit switched the current off.

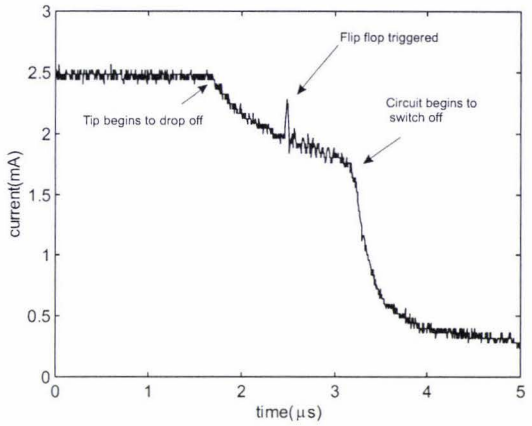

Figure 5.20: **Cutting off the current with an optocoupler:** Note: when the flip-flop triggers we see a small interference in the voltage across the current sensing resistor.

input of the flip flop. The D input of the flip flop is held high so that the output can be used to trigger a switch once the pulse reaches the clock input.

Since we wanted to be able to observe the etching current during cut-off the switch had to be placed between the etching cell and the resistor. An optocoupler was used to perform the switching since it has a rapid switching time of $\sim 500\,\text{ns}$.

5.4 Progress

After fabricating several tips, images of them were taken by a scanning electron microscope. This enabled us to look at the very ends of the tips down to a submicrometer scale. We saw that the overall tip shape was desirable but that the very ends of the tips were not sharp enough.

This could be because of extra etching that occurs. We know that any etching after the drop-off will blunt the tip and that our circuit cuts the current off within $2\,\mu\text{s}$ of this drop-off. Perhaps even this is not fast enough and the tip is blunted in this time. However, this does not seem to be the explanation, for the following reason. Looking at a micrograph of the tip, figure 5.22(a), it can be seen that there are still some small features that remain. If the tips were too blunt due to extra etching, these features would have been etched away too. This idea can be tested by making an intentionally blunt tip by including a large delay in the cut-off circuit (fig 5.22(b)). The tip is over etched to give a very smooth surface. This is not the case for the previous tip so it is concluded that the tip in figure 5.22(a) is not blunt from extra etching.

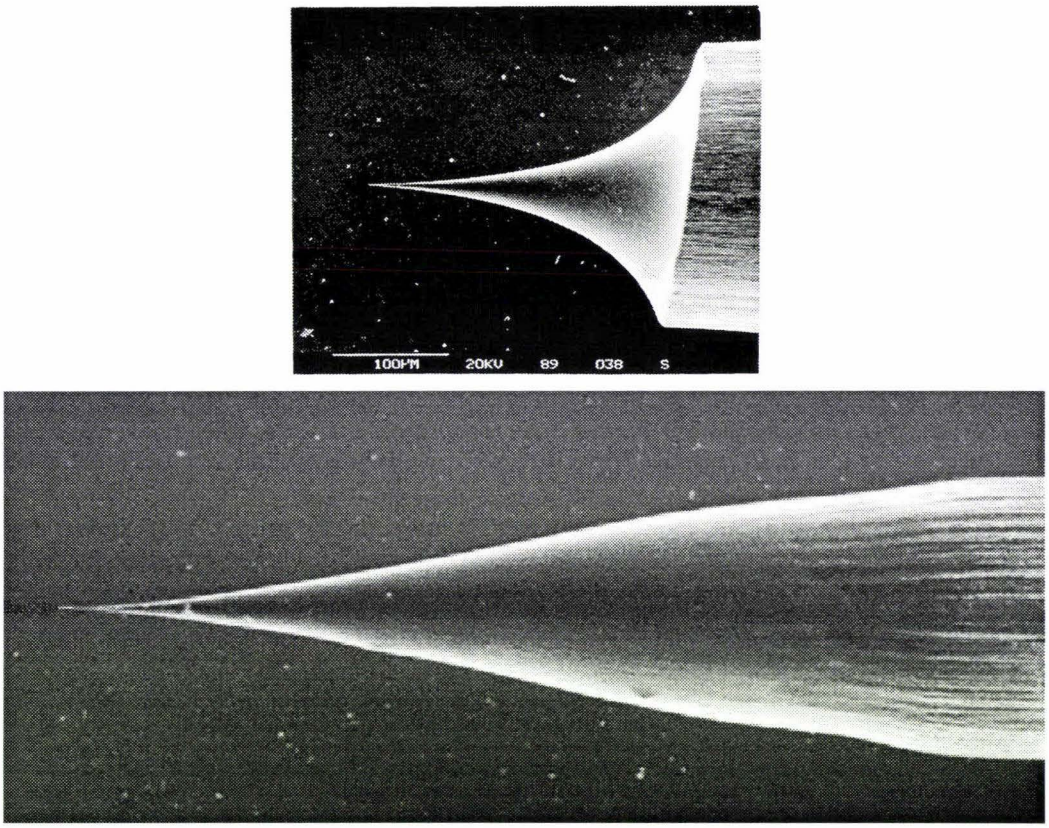

Figure 5.21: **SEM picture of tip:** (Upper picture)The overall shape of the tip is good because the taper is very short. However on a closer look at the apex it can be seen in figure 5.22(a) that this tip is not sharp enough. The lower tip, on the same scale as the picture above, exhibits a very different shape due to the shielding by the spent etchant.

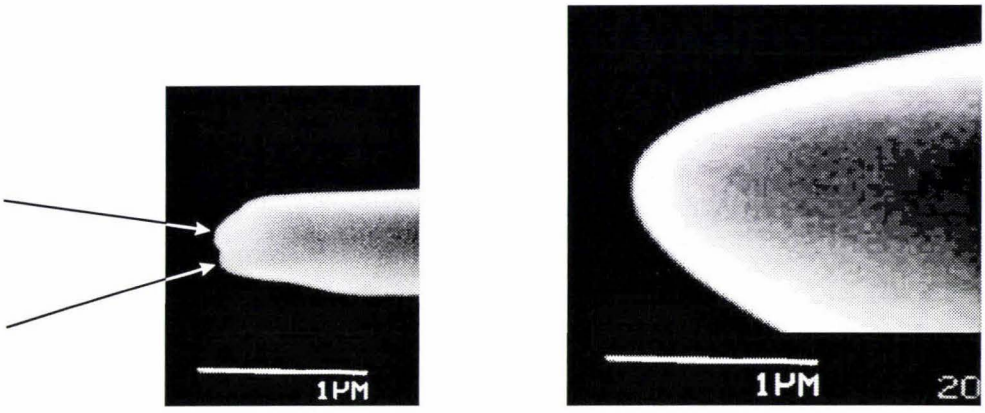

(a) (b)

Figure 5.22: **Etching features:** The tip in (a) was produced using the cut-off circuit and the tip in (b) was not. This shows that the effect of extra etching produces a very smooth well rounded tip as in (b). The tip in (a) does not display this smoothness, instead we can still see some small features (shown by the arrows). This suggests that this tip is not blunt from extra etching.

5.4.1 Uniaxial tension

The drop-off relies on the fact that the wire becomes so thin that it is no longer able to support itself. Obviously this will depend on the load that the wire is trying to support. So maybe we need to look at what happens when the wire fractures. If we look at figure 5.22 we might say that the wire had too much load on it and snapped before it could become thin enough due to etching. To test this idea we will look at the effects of placing a material under uniaxial tension.

As the wire is reduced in diameter, the strain in the wire is increased. As the strain becomes greater than the maximum tensile stress, a neck starts to form [14]. Figure 5.24 shows the elastic necking in a piece of copper under uniaxial tension. Because of the reduction in cross-sectional area, the strain increases further, the neck becomes more pronounced and the wire will fracture leaving a jagged surface behind.

To test this idea, a tip could be made with a large load on it, the neck should then be very pronounced and the area of the fractured surface should be larger.

A tip formed in this manner, together with the one in figure 5.22(a) are shown in figure 5.23. It can be concluded that the unsatisfactory tip apex is not due to extra etching but because the load on the wire was too great.

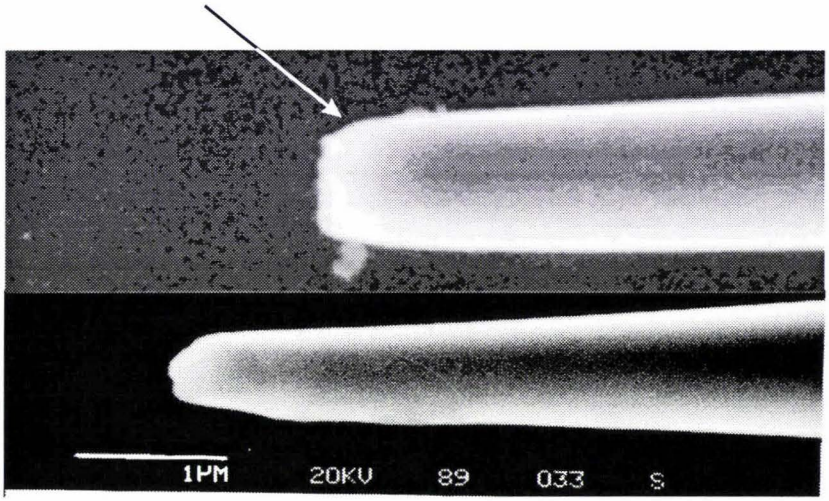

Figure 5.23: **Tips formed with different loads:** The top tip above was formed using a large load and the elastic necking can be seen (arrow). The final fracture area is larger than that of the tip below, which was formed using a smaller load.

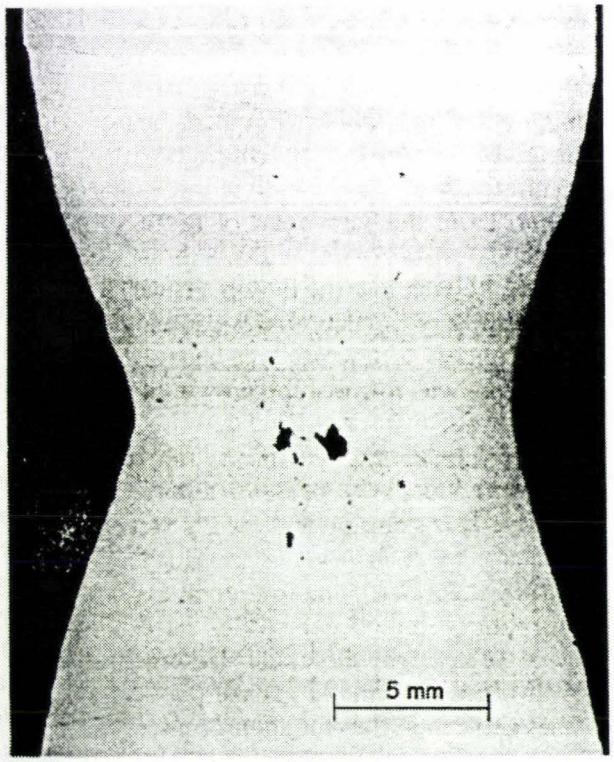

Figure 5.24: **elastic necking:** Section though a copper specimen that has a necked region from tensile deformation. Reproduced from [1].

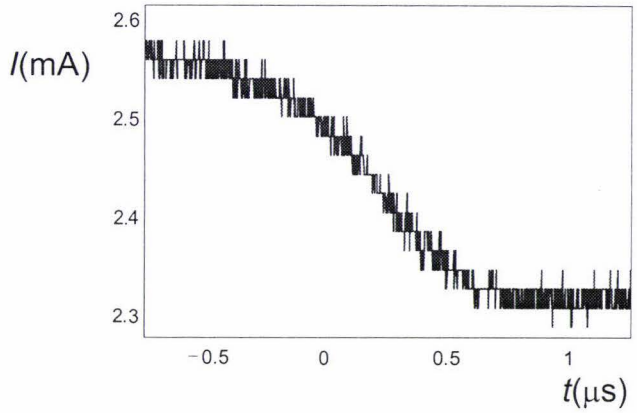

Figure 5.25: **A different etching current on a fine time and current scale:** When there is less wire placed beneath the lamellae, the above etching current is observed. This effect could be due to the increased resistance between the upper and lower tip immediately before drop-off.

5.5 Circuit Improvements

Following on from concluding that the tip had fractured too early, the apparatus was adjusted. Only a small amount of the wire was placed beneath the lamellae and the blutak was not used. When this was tried previously, the cut-off circuit would not trigger as the capacitor value was unsuitable. Now the capacitor in the differentiator had to be adjusted.

A transistor buffer was now used as this is faster than one based on an opamp. The dc level of the pulse was also adjusted so that it was only slightly below the triggering threshold of the flip-flop's clock input (see figure 5.26). A faster optocoupler was used as well. The cut-off time has now been reduced to around 200 ns (see figure 5.27).

This time the etching current when the tip was formed looked slightly different, instead of the exponential-like drop, there was a slower gradual drop (see figure 5.25). Maybe this drop occurs because as the tungsten gets very thin it begins to have a significant resistance $\sim 200\,\Omega$ and so the effective surface area of the tungsten is slightly less.

5.5.1 Tips produced

Several tips produced by this process had a radius that was difficult to see at the resolution of the SEM available to us. The radius was judged to be less than 20 nm (see figure 5.28).

It was hoped that if the circuit was fast enough, the etching could be switched off about 1 μs before the drop-off and then manually, short pulses,

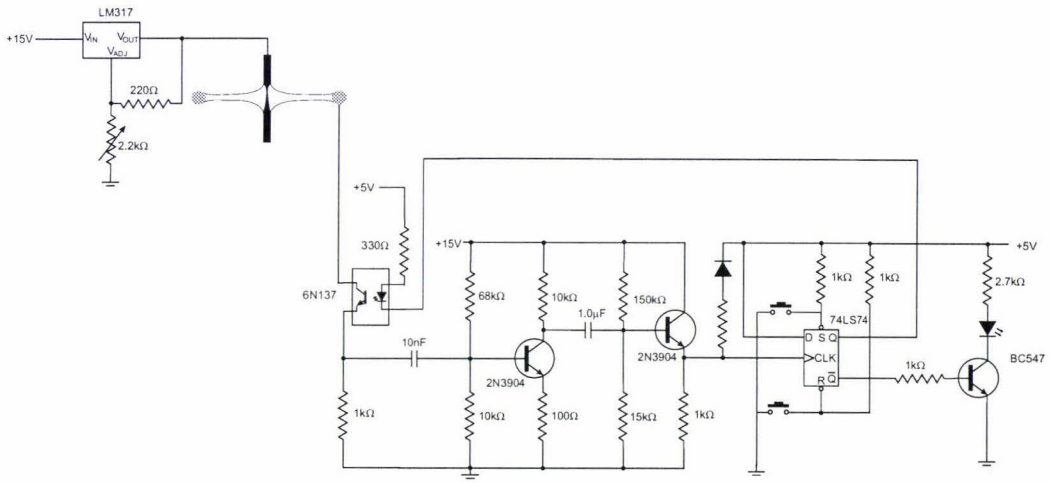

Figure 5.26: **Schematic diagram of the improved cut-off circuit:** A 1 kΩ resistor was used to sample the current and was switched off via an optocoupler. A transistor buffer was used as it has a faster switching time than the opamp used originally.

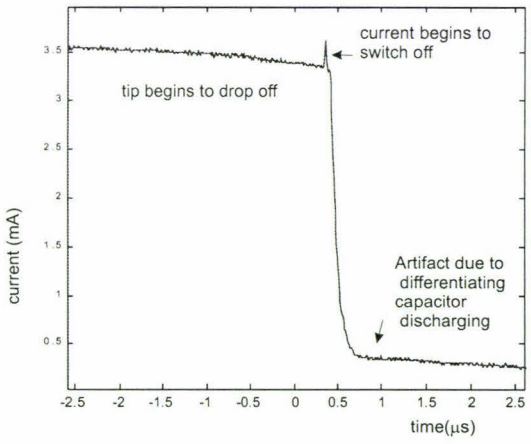

Figure 5.27: **Cutting off the current with a revised circuit:** This cut-off was produced using the circuit detailed in figure 5.26. Note: when the optocoupler is switched off the differentiating capacitor discharges through the sensing resistor.

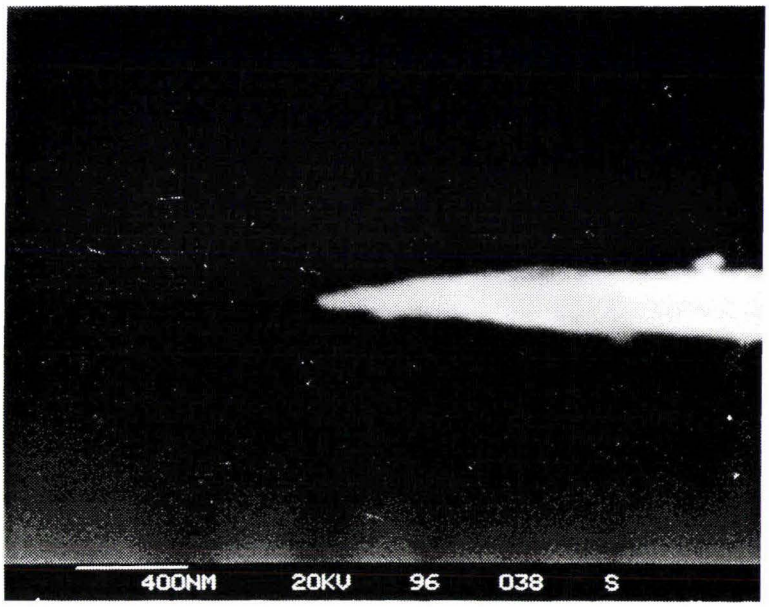

Figure 5.28: **A tip with a radius of less than 20 nm:** By reducing the amount of wire below the lamellae, tips such as this can be formed. Immediately before drop-off the wire begins to show an appreciable resistance, this is shown in the etching current which now shows a more gradual reduction (see figure 5.25).

(~ 200 ns), of very low current, ($\sim 200\,\mu$A) could be applied until the drop-off occurs. This should reduce the extra etching to almost nothing. Depending on the length and size of the current pulse this could take upwards of 100 pulses. Unfortunately, once the tungsten is this thin, the surface tension forces on the lower half are enough to tear it sideways.

Often the drop-off will not occur properly. The tension forces on the lower half become too great and the lower half of the wire flicks into the lamellae. This causes an increase in current due to the increased surface area. The circuit still triggers and cuts off the etching current and it can only be assumed that a sharp tip remains. However, the structure of the very end of the tip is unknown and the effective tip radius could be quite large (see section 6.3.1). In fact most of the tips manufactured using this technique and tested on the STM had this problem. It would seem that the current drop-off shown in figure 5.25 is a good indication of a sharp tip. However this effect using the lamellae technique has been difficult to reproduce. From here the standard drop-off technique could be investigated further to see if the characteristic drop-off current (as shown in figure 5.25) could be observed, thus indicating a sharp tip.

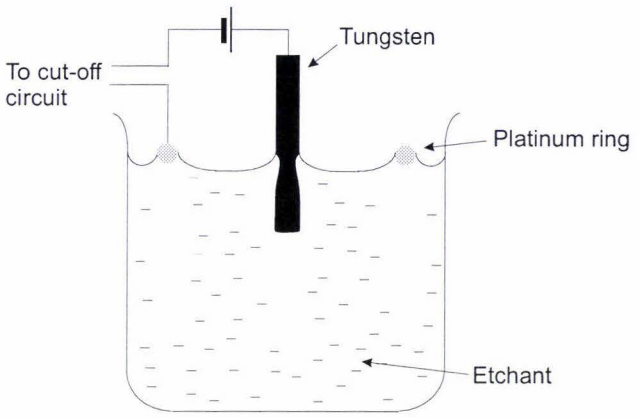

Figure 5.29: **The standard drop-off technique:** Dissatisfied with the results from the lamellae technique, the standard drop-off technique was investigated again. In an attempt to control the etching current the counter-electrode, a loop of Pt, was placed on the very surface of the etchant.

5.6 Return of the standard technique

The lamellae technique, while producing consistently shaped tips, has proved difficult to reproduce. The drop-off current that was assumed to be because of the drop in resistance between the upper and lower tips was only observed on occasion. All other times the lower tip would flip up into the lamellae and most likely bend the upper tip. This would not be acceptable.

To avoid this, the standard technique could be investigated further. Previously it was mentioned that this technique gave non reproducible results and inconsistent tip shapes. While this is still true, the underlying aim is to produce tips with a small radius and maybe the standard drop-off technique can provide this.

5.6.1 Containing the etching current

In an attempt to impede the etching current to the lower half of the wire, the counter electrode was placed on the very surface of the liquid (see figure 5.29). The wire was immersed 2 mm beneath the surface as suggested by Nakamura *et al.* [36].

The voltagramme for this setup shows a much higher etching current that for the lamellae(see figure 5.30). This is because of the greater surface area of both electrodes. In was mentioned above that it is desirable to perform the etching in the plateau region but for the standard drop-off technique this is not possible with the present circuit. An etching current of about 9 mA was used.

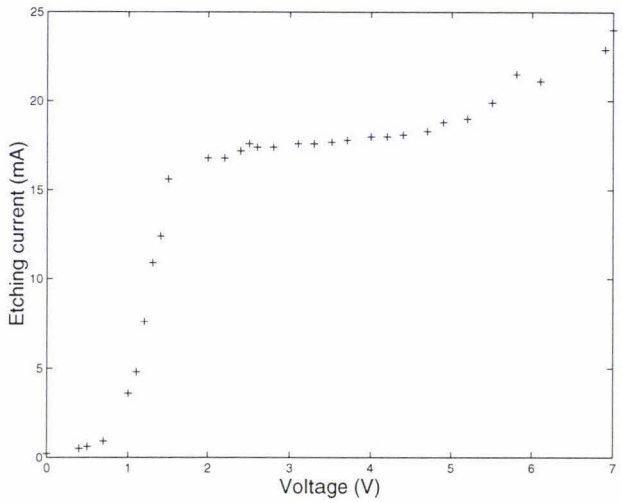

Figure 5.30: **Voltagramme for tungsten in 4 M KOH in solution:** Now that the surface area of both electrodes as been increased, the plateau current is considerable larger.

The etching current over time was more constant for the standard drop-off technique (see figure 5.31). This is possibly due to the spent etchant flowing to the bottom of the beaker while in the lamellae technique the WO_4^{2-} accumulated in the bottom of the lamellae and quickly reduced the effective surface area thus reducing the etching current. Sometimes a layer of material will form on the lower half of the wire which can be washed off by moving the wire up and down in the solution for about 2 s.

Figure 5.32 shows the variation in the shapes and lengths of the tips produced by this technique. It is envisioned that the consistency could be improved with careful attention of the various parameters. By contrast the shapes and lengths of the tips produced by the lamellae technique were very similar. Using the standard drop-off technique there is virtually no lower tip as it is almost completely etched away when the drop-off occurs.

At the drop-off the current looked very similar to that of figure 5.25 although in this case it occurred very consistently (see figure 5.33). This could be taken as an indication of potentially sharp tips. Other results (see section 6.3.2) also suggested that the tips were sharp. The overall shape of the tips were not very consistent and often the apex was quite long. However, this seems secondary to the requirement of needing sharp tips.

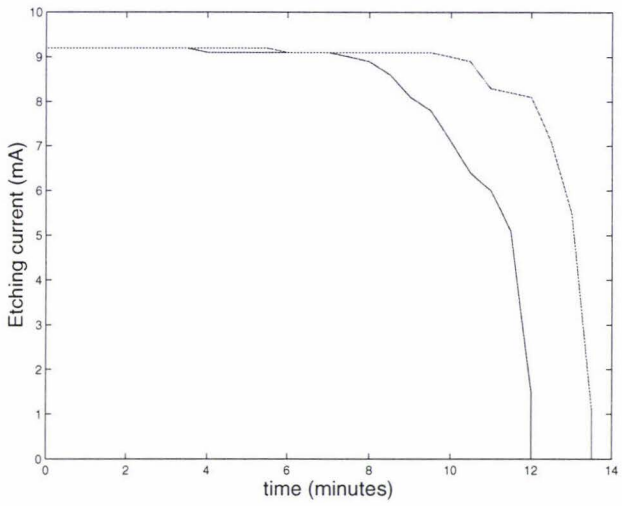

Figure 5.31: **Etching current for standard drop-off technique.:** The current will tend to stay constant for a long time. It appears that in the longer running one that there may have been more wire beneath the surface of the etchant.

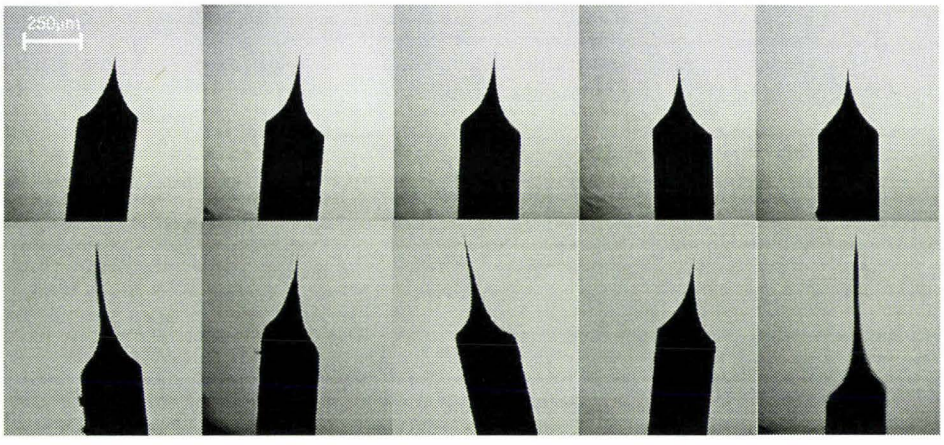

Figure 5.32: **Tip shapes produced using the standard drop-off technique and the lamellae:** The tips in the top of the picture were produced using the lamellae technique and so as a result the tips are shorter and have a consistent shape. The tips in the bottom of the picture were produced using the standard drop-off technique and as a result of the current density in the solution being hard to control, the tips produced are not of a consistent shape.

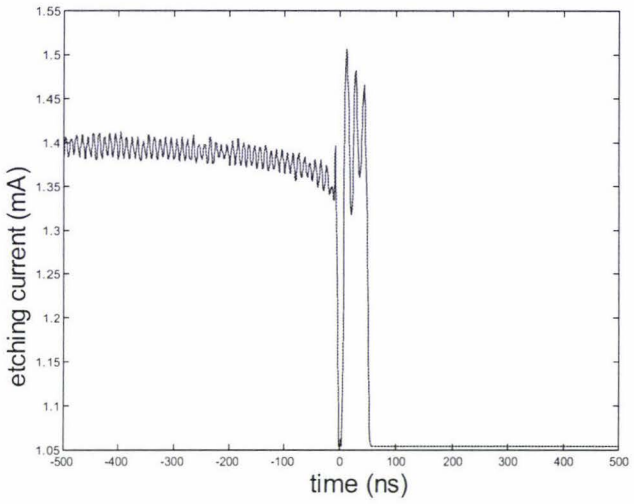

Figure 5.33: **Drop-off current using the standard etching technique:** This effect can be seen reliably using the standard drop-off technique. The reduction in etching current is thought to occur because as the wire gets very thin, it begins to have an appreciable resistance and so decreases the effective surface area of the lower half of the wire. This will then decrease the etching current. The interference visible on this graph is the local student radio station at 99.4 MHz. The glitch seen at time = 0 is due to interference from the flip flop triggering.

5.7 Further improvements

5.7.1 Cut-off times

It was stressed in section 5.2.2 that *any* extra etching after the drop-off will blunt the tip. An electronic circuit will switch the current off in a very short time but that is not what is important. The area under a graph of etching current *vs* time is related to the extra etching that occurs. That is, 1 mA current cut-off 100 ns after the drop-off, results in the same extra etching as 100 nA current cut-off after 1 s. This means that as a method for reducing the extra etching, the current could be smaller and so the demands of the cut-off circuit would not be so great. However, reducing the current would greatly lengthen the etching process and triggering a cut-off circuit would be more difficult.

Material removal from the tip will only stop when the etching current has reached exactly 0 A. All solid state switches will have some finite off-current. As much as the optocoupler tries to switch off, there may still be a slight current and even a small current will blunt the tip. This current was measured as 4.4 μA. To avoid this the etching cell could be shorted out at the same time that the optocoupler is switched off. This option is not described further because in this situation a current will flow due to unknown reactions

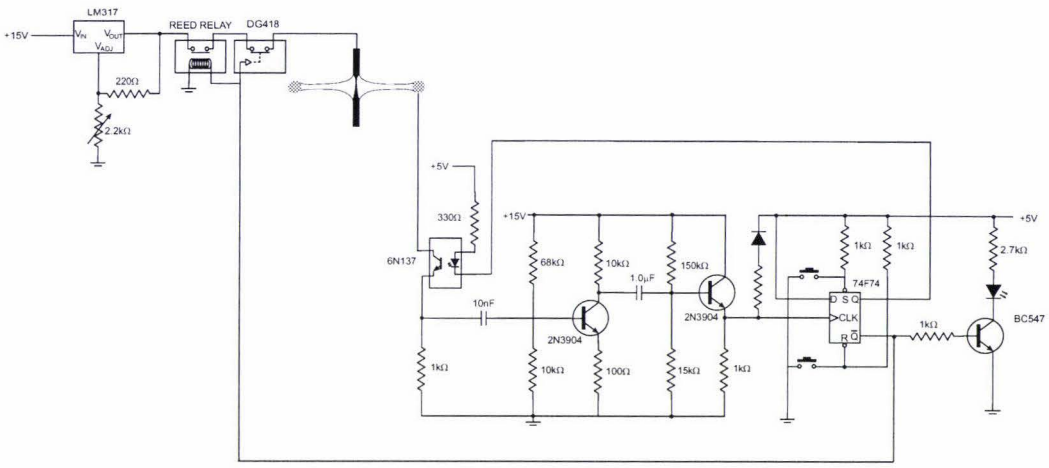

Figure 5.34: **Further improvements to the cut-off circuit:** A faster flip flop was used and two extra switches to reduce the leakage current. This circuit was used with the lamellae technique and the standard drop-off technique.

in the cell, such reactions could cause further etching or deposit unwanted materials on the tip.

In the circuit described above several additions were made to decrease the residual current. In series with the optocoupler an analogue switch was used. This is slightly slower than the optocoupler but the leakage current is reported to be less than 5 nA. Also in series was a relay, comparatively much slower than the other two switches but because it is a mechanical switch, the leakage current is zero (see figure 5.34). In addition, a faster flip flop was used. Referring to figure 5.20 we see that when the circuit switches off there is an artifact due to the differentiating capacitor discharging through the sensing resistor. To get an indication of the true cut-off time the capacitor can be disconnected and the circuit can be triggered using the reset pin on the flip flop. A graph recorded this way is shown in figure 5.35.

A new circuit was constructed with these changes in place and tips were produced using the lamellae technique and the standard drop-off technique. No pictures were produced with an SEM as the limiting resolution had already been reached.

5.8 Removing the oxide layer

It is accepted that an unwanted oxide layer forms on tungsten when electrochemically etched [16]. While it is still possible to obtain atomic resolution with these tips [34] it is desirable to somehow remove the oxide layer, then the tip will perform more reliably.

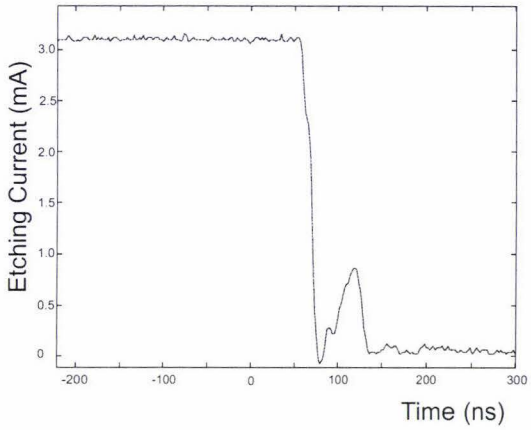

Figure 5.35: **The etching current with the differentiator capacitor disconnected:** When observing the cut-off current with an oscilloscope most of the current seen is from the differentiator capacitor discharging through the sensing resistor. By disconnecting the capacitor and switching the circuit off using the reset pin on the flip flop we can see the actual etching current cut-off time.

Methods for removing the oxide layer include annealing and the application of hydrofluoric acid, HF [27].

5.8.1 Chemically

Hockett and Creager [27] reported that all of the oxides of tungsten will be dissolved by concentrated hydrofluoric acid while tungsten is resistant. When etched tungsten tips were exposed for about 10-30 s, nine out of ten were able to produce atomic resolution of HOPG immediately.

Experiments performed showed that treating the tips with HF consistently reduced the noise of the tunnelling current to around 10 pA. As a test for oxide layer removal Hockett and Creager suggested that a V-I curve would go from a semiconductor type graph to one that looked ohmic (see section 6.3.1).

5.8.2 Annealing

Annealing is the process in which the tungsten tip, with its oxide layer is heated in a vacuum until the oxide layer sublimes along with other surface contaminants, leaving a clean metal surface behind.

Implementing the annealing process is not difficult as tungsten has such a high melting point (around 3000 °C). We have

$$2WO_3 + W \rightarrow 3WO_2 \uparrow .$$

Temperature, °C	Colour
500	red, just visible
700	dull red
900	cerise
1000	bright cerise
1100	dull orange red
1250	bright orange yellow
1500	white
1800	dazzling white

Table 5.1: **Temperature versus perceived colour:** An experienced user should be able to judge the temperature to within ± 50 °C [38].

At about 800 °C the WO_2 sublimes. The equation above states that some of the W will be removed from the tip. However papers detailing the annealing process make no mention of possible degradation of the tip [46, 13]. Therefore any W removal effects are assumed to be small.

Cricenti *et al.* [16] use a high vacuum (HV) chamber at a pressure of 2 $\times 10^{-6}$ mbar and anneal tungsten tips by electron bombardment at 1800 K for 30 min. This reportedly removed most of the oxide layer and subsequent *V-I* curves were more ohmic.

Methods of annealing have also been described for *in situ*. Scholz *et al.* [46] operate an STM inside a scanning electron microscope, therefore the tip cannot be disconnected easily for treatment. Direct heat is not an option as the piezoelectric material depolarises at 450 K. Instead the tip is pulsed at 1200 V for about 3 s with 30 s between each pulse. Heating is provided from the acceleration of the electrons and the pulses are short and far enough apart so that any extra heat will dissipate away. The pressure of the system 1 $\times 10^{-10}$ mbar, this will rise slightly as the annealing takes place.

Our Method

A chamber originally designed for sample preparation by vacuum deposition was used (see fig 5.36) at a pressure of 1 $\times 10^{-8}$ mbar. The tungsten tips were held by a nichrome jig through which a heating current was passed (see figure 5.37).

The temperature could only be estimated by observing the colour of the tips and referring to a pyrometry table (see table 5.1). Care had to taken to not increase the temperature too much because the nichrome would melt at 1100 °C.

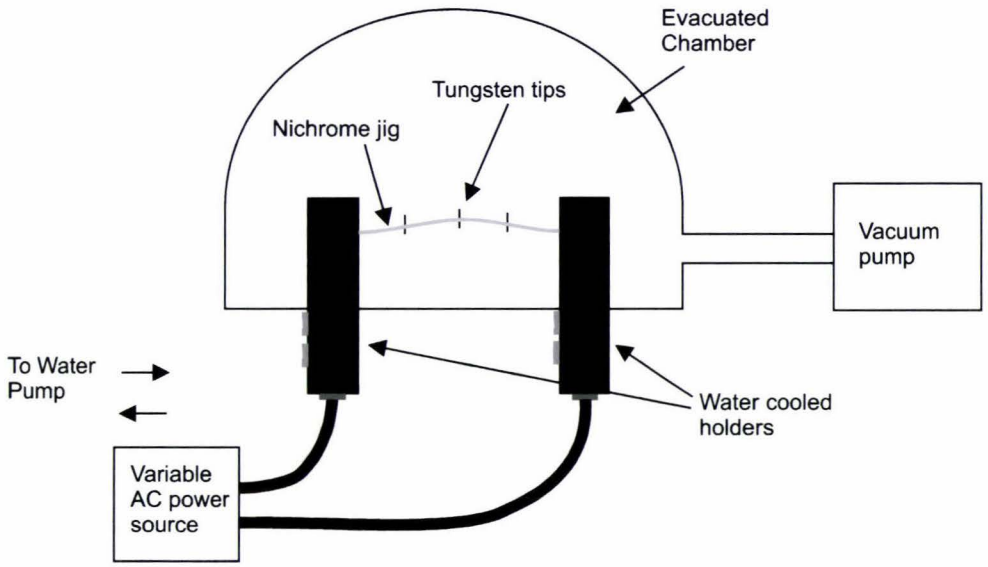

Figure 5.36: **Vacuum chamber:** The tips are held by a nichrome jig that is heated electrically and cooled at each end by water.

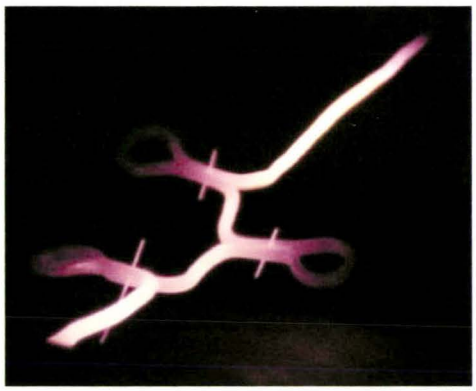

Figure 5.37: **Annealing the tips:** The temperature of the tips had to be estimated by observing the colour. The colour in this photo is not an accurate representation of the actual colour. Two of the three tips shown here are approximately 12 mm long and the longest one is around 20 mm.

5.9 Conclusion

The cut-off circuit has been shown to work very well for both the lamellae technique and the standard drop-off technique. Using a three stage cut-off technique it seems possible to cut the current off to less than 5 nA within 100 ns and then to zero amps after 150 μs. Despite the bias towards the lamellae technique with its advantage of nice shape, the standard drop-off technique possibly gives better tips. The etching current at the drop-off could give clues as to how good the tip is and if the current in figure 5.33 is an indication of a potentially good tip then the standard technique seems more reliable. The shapes and lengths of the tips are not consistent but this is considered a minor drawback.

Unfortunately we do not have access to a SEM with sufficient resolution to determine the radius of the tips produced.

Chapter 6

Results and conclusions

6.1 Overall project

When this masters was initiated, the original task undertaken by Henning Klank had been completed. A DSP based controller had been developed, software had been written to interface to the PC and images had been recorded. Henning Klank then went on to successfully defend his doctoral thesis in April of 2000.

For the microscope to perform reliably several changes had to be made. The PC interface needed to be improved as did some of the software in the DSP. This part was taken care of by Dr. Craig Eccles, the supervisor of this thesis (see appendix C). The very front end of the STM needed some attention too, in terms of the electronics, the preamplifier needed to be redesigned. Previously, the limiting factor in the overall performance was the input capacitance. Once this could be reduced the options of more gain, more bandwidth and better signal to noise are available.

At the front end of the hardware is the STM probe - the tip. It is vital to the performance of the STM that sharp tips are able to be produced reliably.

6.2 Preamplifier

As the first component in the electronics the performance of the preamplifier, or current-to-voltage converter, dictates the overall performance of the system. A circuit that was mounted on the probehead was successfully built and works well. Selection of an opamp with a low input bias current together with careful protection from leakage currents ensured a very small voltage offset. Careful choice of the feedback resistor gave a good frequency response, that is, a bandwidth of 5.5 kHz and near critical damping, when tested with

a 29 MΩ input resistor.

The major design aim was to reduce the input capacitance of 66 pF of the pre-existing current-to-voltage converter. The input capacitance of the new current-to-voltage converter is less than 10 pF, which is a considerable improvement.

The low noise and high gain enabled tunnelling currents as low as 5 pA to be measured reliably. Stable tunnelling currents as high as 7.5 nA were also recorded. The current-to-voltage converter can measure currents up to 17 nA.

Further improvements to the current-to-voltage converter could be made if the center piezo was to be redesigned. Initially, the size of the box that contains the current-to-voltage converter could be made considerably smaller, since it was originally designed to contain a glass-encased resistor 4.5 cm long. This should improve the mechanical stability of the probe. The tip holder, which is the input of the current-to-voltage converter could then be made smaller so there is less capacitance to ground. A shield could also be included to reduce the coupling between the current-to-voltage converter and the centre piezos.

6.3 Tip quality

A good tip, as defined in section 5.28, is one that can achieve atomic resolution. So far this has not been achieved. Micrographs of several tips obtained with an scanning electron microscope showed the tips have a radius of less that 20 nm. It is reasonable to assume that these tips might obtain atomic resolution. However, those particular tips were never tested in the STM and for accessibility reasons the SEM cannot be used to look at every tip that we place in the STM. Other methods for estimating the radius such as FIM [36] were not available to us.

It is also difficult to estimate the radius of a tip based on resolution. When imaging HOPG, if atomic resolution is not obtained then there are few other features on the sub 1 nm scale unless a terrace is found. These terraces tend to be about 3 nm high. Terraces were routinely found and imaged, suggesting a tip resolution of at least 1 nm.

6.3.1 The lamellae technique

Not everything is bad. The tips produced by using the upper tip from a lamellae and a cut-off circuit have proved to be very reliable. Consistently low tunnelling current noise of 20 pA rms, was achieved for a current set-

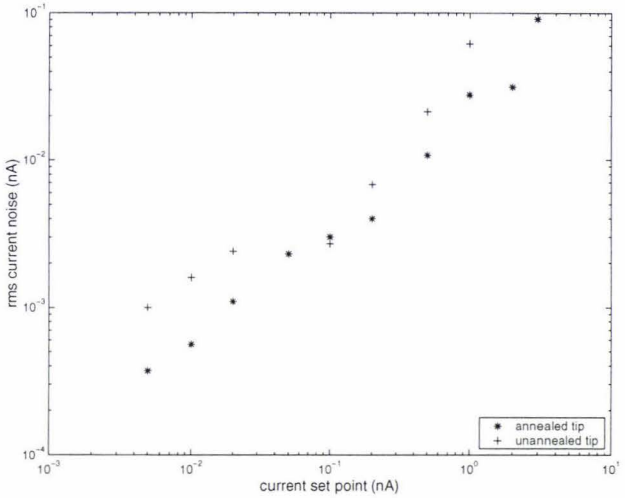

Figure 6.1: **Tunnelling current noise for annealed and unannealed tips:** The noise levels for unannealed tips were generally worse that those for annealed tips. The noise levels for unannealed tips also tends to be a little erratic. Although it is not shown on the graph at a set-point of 0.02 nA the rms noise for an unannealed tip ranged for 0.0009 nA to 0.0024 nA.

point of 1 nA and bias voltage of 0.2 V. A graph of current noise *vs* set-point was made (see figure 6.1). This noise level is considerably less than that reported by [27].

A series of graphs are also included which look at the tunnelling current for annealed and unannealed tips as a frequency spectrum (see figures 6.3 and 6.5). It seems that the annealed tips are less noisy for lower frequencies. The lack of well defined peaks in the frequency suggests that there is not much mechanical interference in the system.

V-I curves are reported to contain some information as to whether or not there is an oxide layer. After removal of an oxide layer we should see some change. Figure 6.6 shows a *V-I* curve for an unannealed tip. After removal of the oxide layer by touching the sample with the tip, the graph in figure 6.7 was produced. Due to the increased linearity of this graph, it would appear that the oxide layer has been reduced [27]. Similar graphs to figure 6.7 were obtained with annealed tips. Although the annealed tips had less curvature that the non-annealed tips they were never linear over a 1 V range.

Several results were not so well understood. A routine in the DSP called 'soft-touch' allows the control to be switched off and the tip extended toward the sample. As the tunnelling current rose exponentially it was assumed that this would give information about how far the sample was from the tip. In fact such curves were not so reproducible. The distances that the tip was able to move seemed, in many cases much further than we expected.

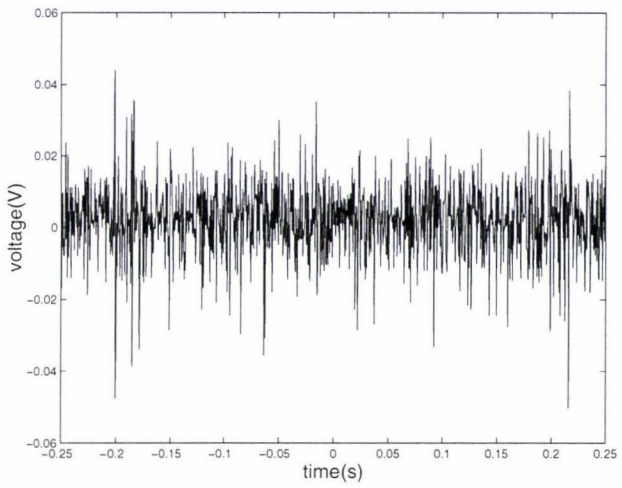

Figure 6.2: **Typical tunnelling current for an annealed tip:** This current was recorded with a set-point of 0.5 nA, bias voltage of 0.2 V and control terms of P=1 and I=0.05. Note 0.02 V $\equiv$ 0.02 nA.

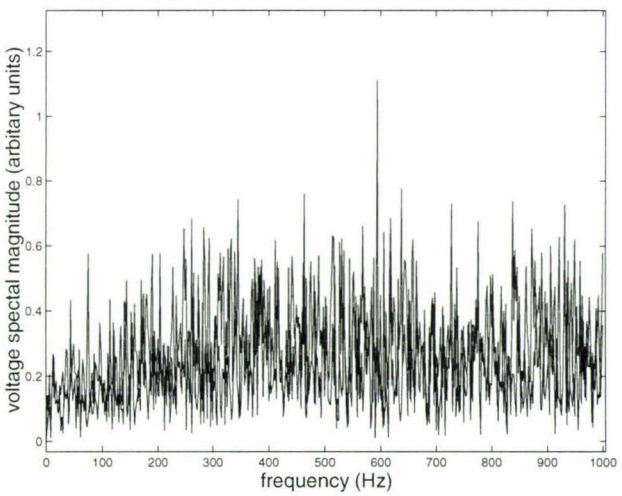

Figure 6.3: **Typical tunnelling current spectrum for an annealed tip:** This graph is a fast Fourier transform (FFT) of the data shown above. There appears to be less noise in regions of lower frequency.

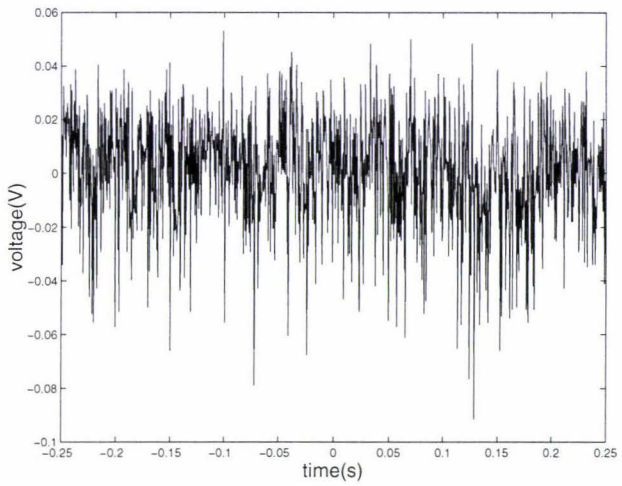

Figure 6.4: **Typical tunnelling current for an unannealed tip:** This current was recorded with a set-point of 0.5 nA, bias voltage of 0.2 V and control terms of P=1 and I=0.05. Note 0.02 V $\equiv$ 0.02 nA.

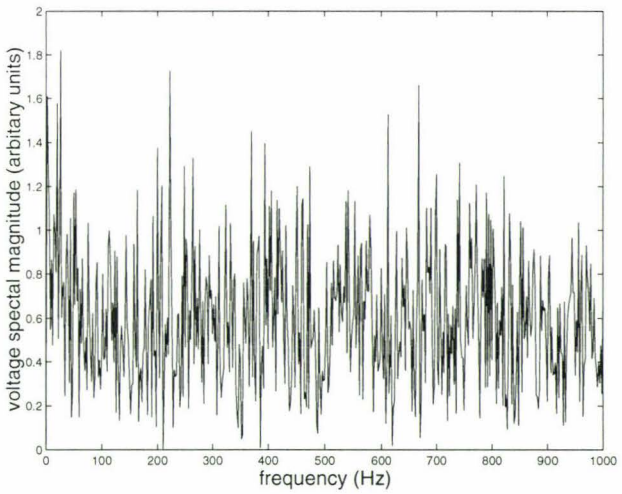

Figure 6.5: **Typical tunnelling current spectrum for an annealed tip:** This graph is a fast fourier transform (FFT) of the data shown above. In contrast to that of the annealed tip this noise appears to be consistent over a range of frequencies.

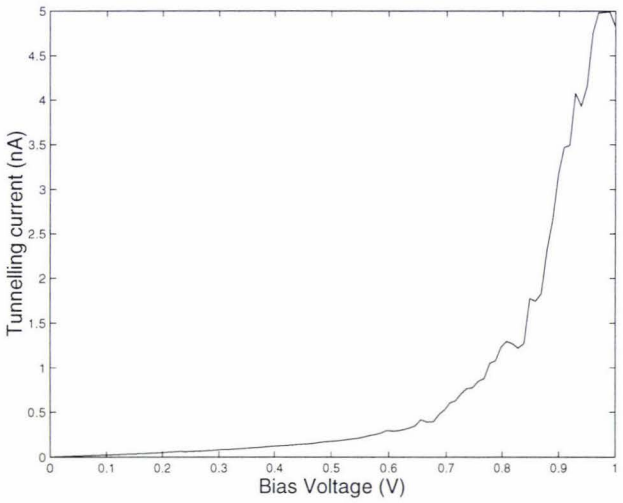

Figure 6.6: **A V-I curve recorded immediately after engagement:** A sharp rise in tunnelling current above 0.6 V indicates the presence of an oxide layer. The set-point for this curve was V_{bias}=0.5 V and $I_{\mathrm{set-point}}$=0.15 nA.

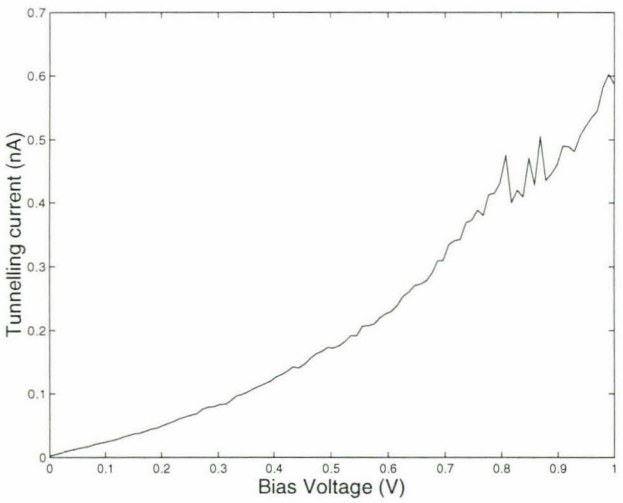

Figure 6.7: **A V-I curve recorded immediately after oxide layer removal:** A relatively linear response over a 1 V region suggests that the oxide layer has been removed. The set-point for this curve was the same as figure 6.6.

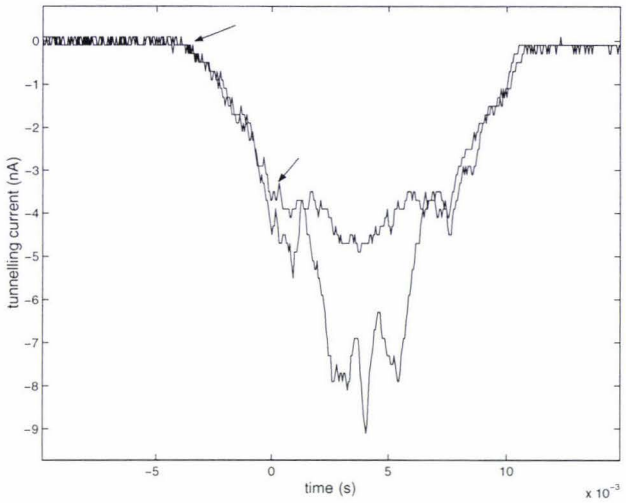

Figure 6.8: **Tunnelling current during 'soft-touch' routine:** Two consecutively recorded graphs show different results. The arrows show the beginning and the end of where the data is consistently the same. In this region the rise of the current is exponential which is expected. After this region the two graphs are not similar. Other graphs showed a tunnelling current of more that 17 nA. The set-point was .1 nA with a bias voltage of 0.1 V.

The tunnelling current was not even symmetrical between extending and retracting (see figure 6.8 and 6.9). Reasons for this are discussed below.

If the tip is very blunt, or broad due to the fracture effects discussed in section 5.4.1 then the tip could be assumed to be further away for a given set-point and bias voltage. This could explain why the apparent distances were so large. If the tip was unstable and somehow reconfiguring at the very apex then this could explain the asymmetry and the non reproducibility of these graphs. However, if a tip gives a stable tunnelling current it would seem that the tip is not reconfiguring.

If the tip has an oxide layer then the tip could be in contact with the sample and a tunnelling current could still be observed. Any attempt to lower the tip further would push the tip deeper into the sample (In the case of HOPG, lowering the tip may cause the graphite to flex, Bai [5] indicates that surface movements of up to 100 nm are not uncommon without tip penetration). All sorts of tunnelling sites would then occur and subsequent lowering of the tip would more than likely not give similar current pathways. Hysteresis effects may occur if the tip is touching the sample, indeed, forces between the sample and the tip could be significant when the tip is not touching. As the tip approaches, it may initially repel the surface and then as it gets closer still, the sample might be attracted to the tip. Such effects would give an asymmetric result for lowering and raising the tip.

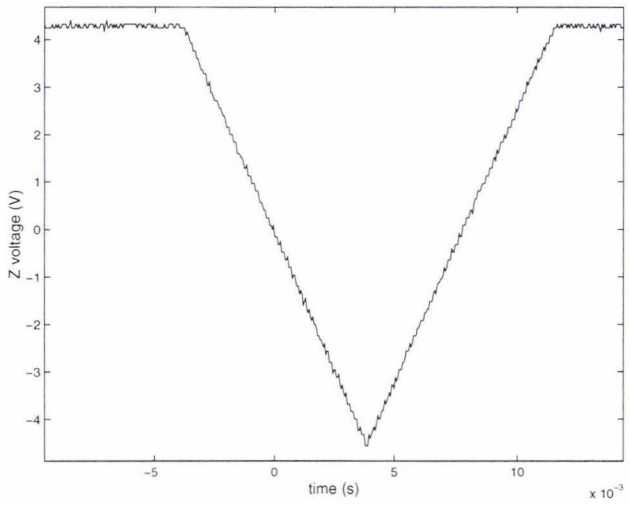

Figure 6.9: **Piezo voltage during 'soft-touch' routine:** The piezo extends while the DSP records the tunnelling current. The vertical calibration of the centre piezo is 3.36 V/nm. This means that during the routine the tip moved 30 nm closer to the sample. This suggests that the sample is flexing during the routine.

6.3.2 Standard technique

By performing a soft-touch we can get an indication of how close to the sample we are. The distance depends not only on the current set-point but also the effective radius of the tip. A tip with a large surface area will be further away than a very sharp tip for the same set-point. If each of these tips is moved closer to the sample as in the soft-touch routine, the current should rise steeper for the sharp one. Figure 6.10 shows the rise in current as the tip is moved down 400 pm. After some time of operation with this tip it would appear that it had been crashed and damaged since, on repeat of the soft-touch, it took 10 nm to repeat the same current(see figure 6.10).

It would seem that these tips are considerably sharper than those produced by the lamellae technique. This is evident from the soft-touch results and also that these tips are more sensitive to vibration for similar set-points which would suggest that they are closer.

One image (figure 6.15) using a tip produced from the standard drop-off technique showed an imaging artifact which suggested that there could have been two minitips present. While this effect is undesirable it could be an encouraging sign. If the tips made previously using the lamellae technique had a relatively large tunnelling area, they would be far from the sample for a given tunnelling resistance[1] and any minitip effects would be averaged

[1]determined by the bias voltage and the current set-point.

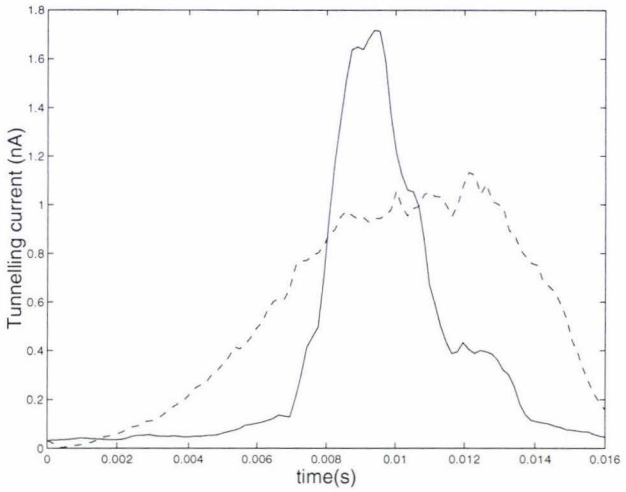

Figure 6.10: **soft-touch before and after crash:** When the tip was first engaged the soft-touch routine was instructed to move down 400 pm (solid line). This shows a very definite peak and the expected exponential result, however it is still not symmetrical. The dotted line shows the soft-touch routine performed after a tip crash. To get comparable results the tip had to be moved down 10 nm. This suggests that now the tip is about the same sharpness as those produced using the lamellae technique and so the tip, produced using the standard drop-off technique, was originally considerable sharper. This graph was recorded with the bias voltage opposite in polarity to that used to record the graphs in figure 6.8.

out. Now that we have possibly seen a minitip effect this might be further conformation that the tips produced using the standard drop-off technique are considerable shaper and therefore closer. Unfortunately time did not permit further experiments with these tips.

6.4 Terraces and nano manipulation

Figure 6.11 6.12 and 6.14 show many terraces that were imaged using tips made using the lamellae technique. The terraces seem to be well within the resolution of the tips. In the series of images in figure 6.11 and 6.12 we see evidence of nano 'manipulation'. This was achieved by driving the tip into the HOPG sample until is stuck to the tip. When the tip was disengaged pits were left behind. However there was usually some lateral movement during this process which meant that we could not control the position of the pits. Typical pit dimensions were a few nm, verifying the tip resolution estimates made from the imaging experiments (see figure 6.13).

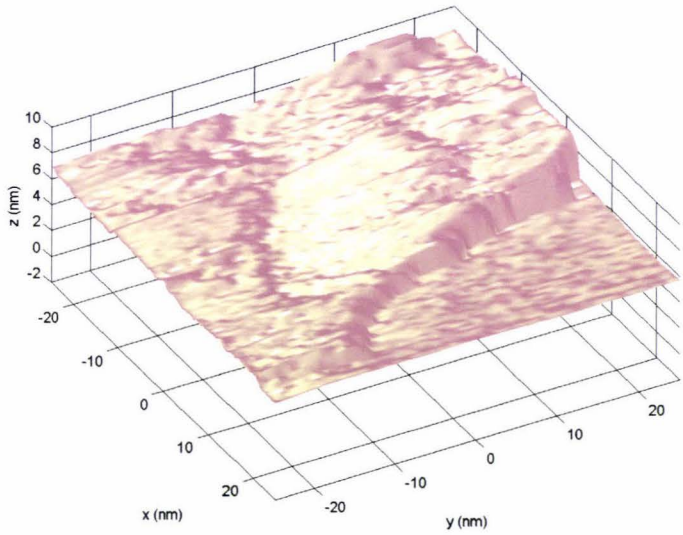

Figure 6.11: **Image of a HOPG terrace before manipulation:** A terrace that is around 3 nm high is imaged. The features on the upper terrace might have been produced by us during earlier experiments. The parameters for this image were $V_{\text{bias}} = 0.1\,\text{V}$, $I_{\text{set-point}} = 0.01\,\text{nA}$, $P = 1$, $I = 0.05$, samples per point = 200, step size = 2.5 pm and the image size is 100 by 100 points.

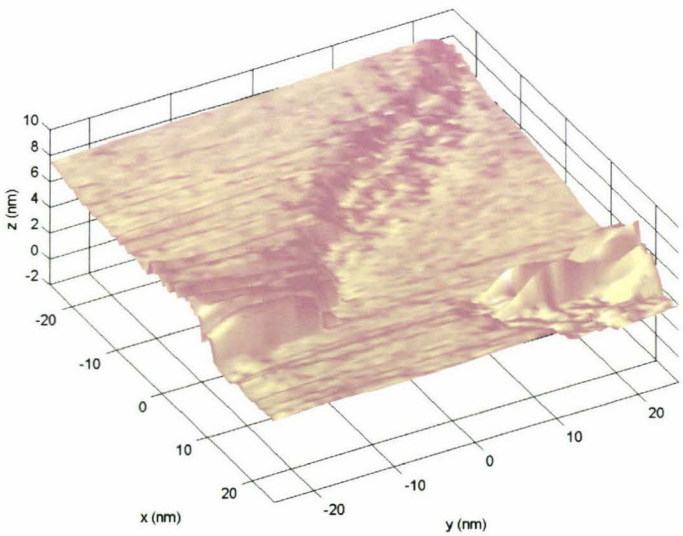

Figure 6.12: **Image of a HOPG terrace after manipulation:** By performing the soft-touch routine and scanning using the same parameters as above, the resulting image shows a new feature on the surface. The image has appeared to move laterally, possible due to bending of the tip.

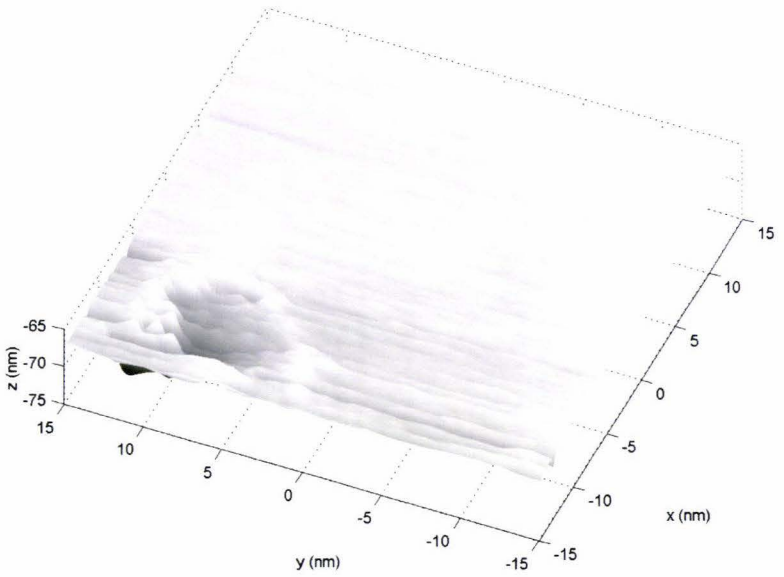

Figure 6.13: **Image of a dent:** This dent was produced using the soft-touch routine. Note that the horizontal and vertical scales are different, the dimensions of the dent are about 3 nm deep and 8 nm wide. The parameters for this image were $V_{\text{bias}} = 0.2\,\text{V}$, $I_{\text{set-point}} = 1\,\text{nA}$, $P = 0$, $I = 0.1$ and the image size is 100 by 100 points.

6.5 Further work and conclusions

All indications are that the microscope should now have considerably more potential with the improved current-to-voltage converter, stack isolation and high-voltage board modifications. (The gain and power supplies for the high voltage power supplies were reduced resulting in a 4 fold improvement in the noise level). Reproducible lateral resolution of about 1 nm is evident (see figure 6.11), while the vertical resolution is about 0.5 nm (see figure 6.15). It just remains to determine why we are not able to obtain the atomic resolution that had been obtained with the unimproved apparatus on one or two occasions in the past.

The critical element would still seem to be the tip, since tip noise still dominates the data. We could test this by trying the tips we have manufactured on a commercial STM to see if atomic resolution could be obtained. Conversely using a commercially produced Pt-Ir tip we could try and obtain atomic resolution in our system. These simple tests, which unfortunately could not be completed before the submission of this thesis, would quickly narrow down the source of the problem to either the tip or the rest of the microscope.

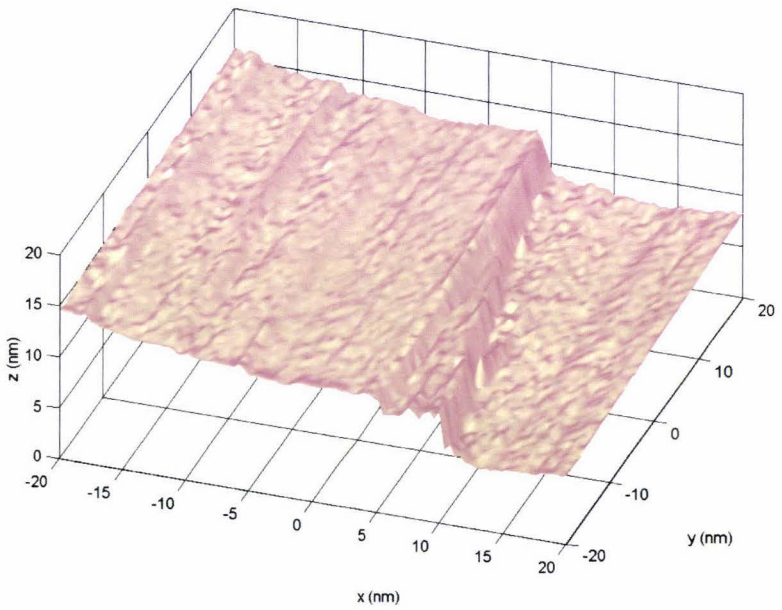

Figure 6.14: **Image of a terrace:** This HOPG terrace appears to be about 5 nm high. The parameters for this image were $V_{\text{bias}} = 0.2\,\text{V}$, $I_{\text{set-point}} = 0.05\,\text{nA}$, $P = 0$, $I = 0.05$ and the image size is 100 by 100 points.

More work needs to be done on the control loop to see if we can reduce the delay which occasionally results in image artifacts caused by overshoot (see figure 6.16). A suitable test sample with features on the nanometer scale would help to optimise the control feedback, however these tend to have rather coarse features (μm rather than nm) and are expensive.

Many tips were made and trialed during this work. A significant percentage of these were damaged before they could be used for STM purposes because of the difficulty in placing the tips into the probe head at a suitable distance (they must be manually positioned to within $\pm 0.2\,\text{mm}$.) An alternative probe head with a larger coarse approach range than is available with the "beetle" could therefore be a significant improvement.

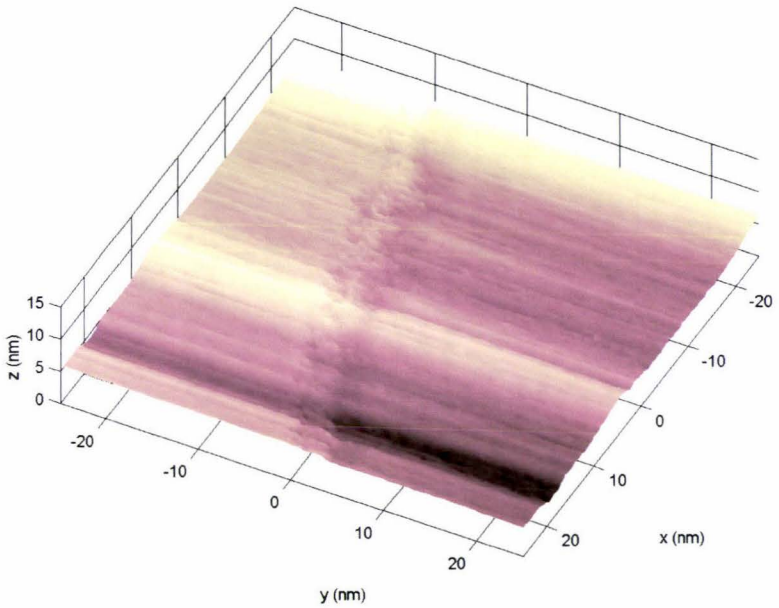

Figure 6.15: **Evidence of a double tip:** The double ridge in this image could be an image artifact of a tip possessing two minitips. The first minitip will see the ridge and then another might image it as well giving the effect in this image. This is an unwanted effect. However this ridge is very small with a height of only 0.5 nm. This gives an indication of the vertical resolution.

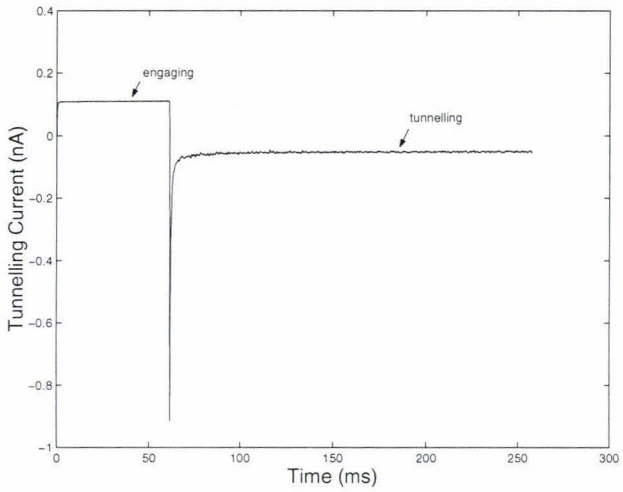

Figure 6.16: **Tunnelling current during engagement:** As the centre piezo expands the DSP is looking for tunnelling current. When the output reaches a threshold the piezo stops extending and the controller is switched on. This results in a rather large over-shoot of the set-point. Similar results are recorded when moving over a terrace or a pit. Note that the offset current initially, due to capacitive coupling from the centre piezo is larger that in figure 4.15 because a faster approach speed was used. For this engage the parameters were V_{bias} = 100 mV, $I_{\mathrm{set-point}}$ = -0.05 nA, P = 1 and I = 0.05.

Appendix A

Theory

A.1 Density of states

The 'density' is not a volume density but a number density over energy. Any particular metal will have many possible states available for its electrons. Each of these states may be at a different energy, governed by the Schrödinger equation. It is useful to know how many states are occupied in a given energy range. So the density of states is defined. If the number of quantum states, dN, are in a given energy range dE, the density of states is $\frac{dN}{dE}$.

To find the total density of states of a quantum system we must first integrate over all the possible quantum states with an energy E, or less. If we differentiate this expression with respect to E we get the density of states.

If we are interested only in a particular energy range we can simply sum up the number of states in a small energy range $E - \epsilon$ to E and divide by the range ϵ

$$\rho_1(E) = \frac{1}{\epsilon} \sum_{E_\mu = E-\epsilon}^{E} |\Psi_\mu|^2 , \tag{A.1}$$

if we were to include three dimensional position

$$\rho_1(\mathbf{r}, E) = \frac{1}{\epsilon} \sum_{E_\mu = E-\epsilon}^{E} |\Psi_\mu(\mathbf{r})|^2 , \tag{A.2}$$

Then we have the *local* density of states $\rho_1(\mathbf{r}, E)$.

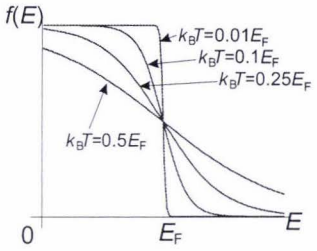

Figure A.1: **The Fermi-Dirac distribution:** As k_BT becomes small compared to the Fermi energy, E_F, the Fermi-Dirac distribution $f(E)$ can be approximated by a step function at E_F. When the temperature is low, almost all the states below E_F are filled and almost all the states above, are empty.

A.2 The Fermi-energy

The Fermi-Dirac distribution was developed by E. Fermi and P. A. M. Dirac independently in 1926. The distribution was built on Pauli's exclusion principle (only one electron is allowed in each state). The probability of an electron in a metal, at a temperature, T, occupying a state with energy E is

$$f(E) = \frac{1}{\exp[(E - E_F)/k_BT] + 1}, \tag{A.3}$$

where k_B is the Stefan-Boltzman constant. E_F is called the Fermi energy.

For the purposes of STM, when investigating two metals at room temperature the Fermi-Dirac distribution can be approximated as a step function at E_F [48] (see figure A.1). This can be interpreted as the metal having electrons with energies filled up to the Fermi level.

Appendix B

basic transimpedance amplifier

The circuit diagram of a basic transimpedance amplifier is shown in fig B.1. Although the tunnelling current is the parameter that we are measuring the junction is modelled as a constant voltage (the bias voltage) and a changing resistance (the tunnelling resistance). For ideal opamps this configuration has a very simple transfer function of $V_{out}/V_{in} = -R_f/R_t$. However, to get a more realistic model for the current-to-voltage converter we must consider the parasitic capacitances shown in fig B.2.

B.1 The superposition principle

For any linear circuit containing more the one voltage source or current source, the *superposition theorem* states that the total current in any part of the circuit equals the algebraic sum of the currents produced by each source separately. To calculate the current due to any one particular source, all other voltage sources are replaced by a short circuit and all other current sources are placed by an open circuit [47].

To find the potential at the inverting input, the superposition theorem can be applied by considering V_{bias} and V_{out} as voltage sources (see figure B.3).

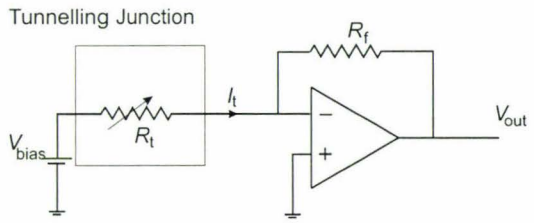

Figure B.1: **Ideal Preamplifier:** The tunnelling junction is like a variable resistance.

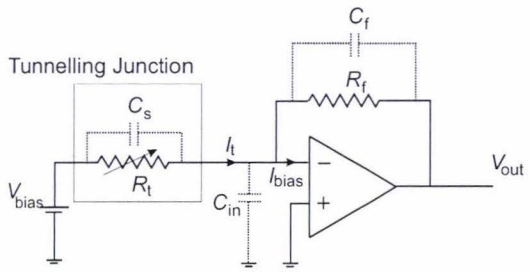

Figure B.2: **Real Preamplifier:** The current-to-voltage converter showing all the parasitic capacitances that have to be considered. $I_{\rm bias}$ is the input bias current to the opamp and can be ignored as it is much less than $I_{\rm t}$.

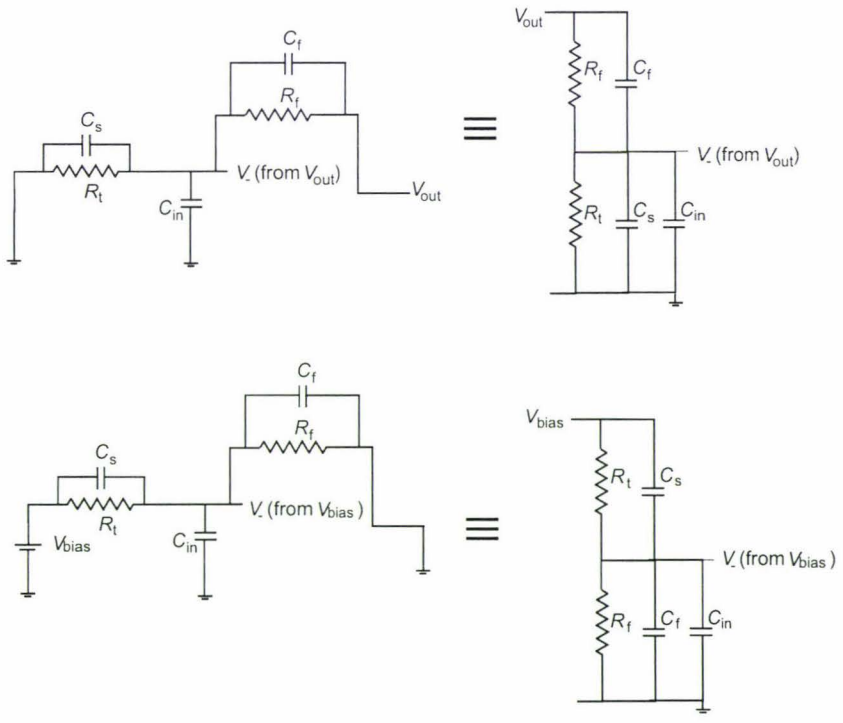

Figure B.3: **The Superposition Theorem:** If $V_{\rm out}$ and $V_{\rm bias}$ are considered ideal voltage sources, we can find their individual contribution to V_- by replacing the other with its ideal source resistance. The results can then be summed to find V_-.

V_- will then be equal to the sum of the voltages produced by each voltage source separately. Once V_- is found, and since V_+=0, we can use the opamp equation

$$V_{\text{out}} = A(V_+ - V_-), \tag{B.1}$$

to obtain an expression for $V_{\text{out}}/V_{\text{bias}}$. Replacing V_{bias} with a short circuit gives,

$$V_-(\text{from } V_{\text{out}}) = \frac{\frac{1}{\frac{1}{R_t}+j\omega(C_s+C_{\text{in}})}}{\frac{1}{\frac{1}{R_t}+j\omega(C_s+C_{\text{in}})} + \frac{1}{\frac{1}{R_f}+j\omega C_f}} V_{\text{out}}, \tag{B.2}$$

which, after some rearranging looks like

$$V_-(\text{from } V_{\text{out}}) = \frac{R_t}{R_t + R_f} \frac{1 + j\omega R_f C_f}{1 + j\omega (R_t || R_f) C_{\text{tot}}} V_{\text{out}} \tag{B.3}$$

where

$$C_{\text{tot}} = C_f + C_s + C_{\text{in}}.$$

similarly, replacing V_{out} with a short circuit gives

$$V_-(\text{from } V_{\text{bias}}) = \frac{R_f}{R_f + R_t} \frac{1 + j\omega R_t C_s}{1 + j\omega (R_t || R_f) C_{\text{tot}}} V_{\text{bias}}, \tag{B.4}$$

so from the superposition principle we can write V_- as

$$V_- = V_-(\text{from } V_{\text{out}}) + V_-(\text{from } V_{\text{bias}}) \tag{B.5}$$

$$V_- = \frac{R_t}{R_t + R_f} \frac{1 + j\omega R_f C_f}{1 + j\omega (R_t || R_f) C_{\text{tot}}} V_{\text{out}} + \frac{R_f}{R_f + R_t} \frac{1 + j\omega R_t C_s}{1 + j\omega (R_t || R_f) C_{\text{tot}}} V_{\text{bias}}. \tag{B.6}$$

The non-inverting input, V_+ is grounded so we can substitute the above expression into equation B.1

$$V_{\text{out}} = -A \frac{1}{R_t + R_f} \frac{R_t(1 + j\omega C_f R_f) V_{\text{out}} + R_f(1 + j\omega C_s R_t) V_{\text{bias}}}{1 + j\omega C_{\text{tot}} (R_f || R_t)}. \tag{B.7}$$

Rearranging to give $V_{\text{out}}/V_{\text{bias}}$ we have

$$\frac{V_{\text{out}}}{V_{\text{bias}}} = -\frac{\frac{R_f}{R_t+R_f} \frac{1+j\omega C_s R_t}{1+j\omega C_{\text{tot}} R_f || R_t}}{\frac{1}{A} + \frac{R_t}{R_t+R_f} \frac{1+j\omega C_f R_f}{1+j\omega C_{\text{tot}} R_f || R_t}}. \tag{B.8}$$

If the unity gain bandwidth is ω_{u}, the open loop gain, A, can be approximated as

$$A = \frac{\omega_{\mathrm{u}}}{j\omega}, \tag{B.9}$$

if $\omega < \omega_{\mathrm{u}}$, this gives

$$\frac{V_{\mathrm{out}}}{V_{\mathrm{bias}}} = -\frac{\frac{R_{\mathrm{f}}}{R_{\mathrm{t}}+R_{\mathrm{f}}}\frac{1+j\omega C_{\mathrm{s}}R_{\mathrm{t}}}{1+j\omega C_{\mathrm{tot}}R_{\mathrm{f}}||R_{\mathrm{t}}}}{\frac{j\omega}{\omega_{\mathrm{u}}} + \frac{R_{\mathrm{t}}}{R_{\mathrm{t}}+R_{\mathrm{f}}}\frac{1+j\omega C_{\mathrm{f}}R_{\mathrm{f}}}{1+j\omega C_{\mathrm{tot}}R_{\mathrm{f}}||R_{\mathrm{t}}}}. \tag{B.10}$$

This expression can be rearranged into a form which is similar to a *resonance curve* [52]. Such resonances are very common in mechanical and electrical systems and provide a convenient way of describing a system, in terms of the *resonant frequency*, ω_0 and *damping factor*, δ.

Rearranging the above equation some more we get

$$\frac{V_{\mathrm{out}}}{V_{\mathrm{bias}}} = -\frac{1 + j\omega C_{\mathrm{s}}R_{\mathrm{t}}}{\frac{j\omega}{\omega_{\mathrm{u}}}(1 + j\omega C_{\mathrm{tot}}R_{\mathrm{f}}||R_{\mathrm{t}})\frac{R_{\mathrm{t}}+R_{\mathrm{f}}}{R_{\mathrm{f}}} + \frac{R_{\mathrm{t}}}{R_{\mathrm{f}}}(1 + j\omega C_{\mathrm{f}}R_{\mathrm{f}})}. \tag{B.11}$$

Collecting like terms in ω gives

$$\frac{V_{\mathrm{out}}}{V_{\mathrm{bias}}} = -\frac{1 + j\omega C_{\mathrm{s}}R_{\mathrm{t}}}{\frac{R_{\mathrm{t}}}{R_{\mathrm{f}}} + j\frac{\omega}{\omega_u}(R_{\mathrm{t}}C_{\mathrm{f}}\omega_u + 1 + \frac{R_{\mathrm{t}}}{R_{\mathrm{f}}}) - \frac{\omega^2}{\omega_u}C_{\mathrm{tot}}R_{\mathrm{t}}}, \tag{B.12}$$

which can be written as

$$\frac{V_{\mathrm{out}}}{V_{\mathrm{bias}}} = -\frac{R_{\mathrm{f}}}{R_{\mathrm{t}}}(1 + j\omega C_{\mathrm{s}}R_{\mathrm{t}})\frac{\omega_0^2}{\omega_0^2 - \omega^2 + j\omega 2\delta}, \tag{B.13}$$

if

$$\omega_0^2 = \frac{\omega_u}{R_{\mathrm{f}}C_{\mathrm{tot}}}, \tag{B.14}$$

and

$$\delta = \frac{1}{2C_{\mathrm{tot}}}(\omega_u C_{\mathrm{f}} + \frac{1}{R_{\mathrm{t}}} + \frac{1}{R_{\mathrm{f}}}). \tag{B.15}$$

Equation B.13 gives the transfer function for the current-to-voltage converter. The fraction is a damped resonance with the characteristic frequency and damping factors given above. The extra term in the transfer function will have little effect (see section 4.4.1).

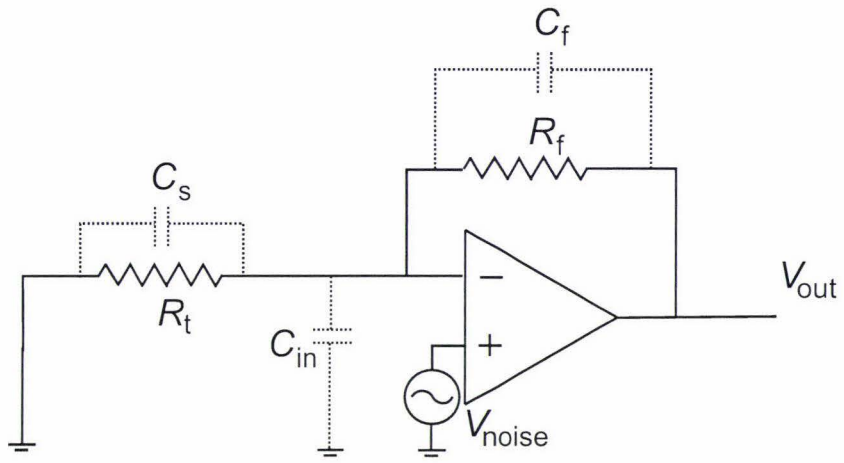

Figure B.4: **Noise model:** This configuration is used to model the noise for the preamplifier.

B.1.1 Noise gain

The noise gain of the circuit can be found by replacing the bias voltage with its ideal impedance and placing a noise generator on the non-inverting input (see figure B.4)[1]. Now the circuit becomes a non-inverting amplifier of v_{noise}, with the amplification determined by the feedback fraction.

We can write V_- from equation B.4

$$V_- = \frac{1 + j\omega R_f C_f}{\frac{R_t+R_f}{R_t} + j\omega R_f C_{tot}} V_{out}. \tag{B.16}$$

V_+ is equal to v_{noise} so we can use the opamp equation B.1 to write

$$V_{out} = A\left(v_{noise} - \frac{1 + j\omega R_f C_f}{\frac{R_t+R_f}{R_t} + j\omega R_f C_{tot}} V_{out}\right). \tag{B.17}$$

Rearranging and using equation B.9 for A, we get

$$\frac{V_{out}}{v_{noise}} = \frac{1}{\frac{j\omega}{\omega_u} + \frac{1+j\omega R_f C_f}{\frac{R_t+R_f}{R_t}+j\omega R_f C_{tot}}}. \tag{B.18}$$

This can be rearranged, using the same δ and ω_0 as in equations B.14 and B.15, to give

$$\frac{V_{out}}{v_{noise}} = \frac{R_f + R_t}{R_t}(1 + j\omega C_{tot} R_t || R_f)\frac{\omega_0^2}{\omega_0^2 - \omega^2 + j\omega 2\delta}. \tag{B.19}$$

[1]The input current noise can be ignored as it is so small.

This equation has a higher dc gain than the transfer function and in this case the extra term will have a considerable effect (see section 4.4.2).

B.2 The damped resonance equation

As mentioned previously the resonance term term arises frequently in mechanical and electrical systems, When fitting a model to data that are of this form, several properties can be utilised. A summary of these is given below.

The resonance equation with a magnitude of one at $\omega = 0$ is

$$\frac{\omega_u^2}{\omega_0^2 - \omega^2 + j\omega 2\delta}.$$

The damped resonance equation has three modes described by

- under damped $\delta < \frac{\omega_0}{\sqrt{2}}$,
- over damped $\delta > \frac{\omega_0}{\sqrt{2}}$,
- critically damped $\delta = \frac{\omega_0}{\sqrt{2}}$.

B.2.1 under damped

An under damped system will have a maximum in the transfer function and if very little damping is present this peak will occur at ω_0. As the system gets more and more damped the peak shifts to lower frequencies until the system is critically damped i.e. the is no peak. To find the frequency at which the transfer function is a maximum, the transfer function can be differentiated with respect to ω and then set equal to zero. This gives

$$\omega_{max} = \sqrt{\omega_0^2 - 2\delta^2}.$$

This equation is the origin or the criterion for determining which of the three modes the system is in.

By substituting this back into equation B.13 the magnitude of the transfer function maximum can be found as

$$\text{peak height} = \frac{\omega_0^2}{2\delta\sqrt{\omega_0^2 - \delta^2}}.$$

B.2.2 over damping

if the system is heavily damped i.e. $\delta >> \frac{\omega_0}{\sqrt{2}}$ then the transfer function can be approximated by

$$\frac{V_{\text{out}}}{V_{\text{in}}} = \frac{1}{(1+\frac{j\omega}{\omega_1})(1+\frac{j\omega}{\omega_2})},$$

where

$$\omega_1 = \frac{\omega_0^2}{\sqrt{2}\delta},$$

and

$$\omega_2 = 2\delta.$$

ω_1 is the approximate bandwidth of the system.

B.2.3 critical damping

This occurs when

$$\delta = \frac{\omega_0}{\sqrt{2}}.$$

If the system is critically damped (or close to it) we can write the transfer function as

$$\frac{\omega_0^2}{\omega_0^2 - \omega^2 + j\sqrt{2}\omega_0\omega},$$

and the 3 dB point is ω_0.

For any situation the 3db point is given by the rather ungraceful

$$\omega_{3\text{dB}} = \sqrt{\omega_0^2 - 2\delta^2 + \sqrt{\omega_0^4 + (\omega_0^2 - 2\delta^2)^2}}.$$

B.3 The resonance equation and out system

If we ignore the extra term in equation 4.1 we are left with a resonance term where

$$\omega_0^2 = \frac{\omega_{\text{u}}}{R_{\text{f}}C_{\text{tot}}},$$

and

$$\delta = \frac{1}{2C_{\text{tot}}}(\omega_{\text{u}}C_{\text{f}} + \frac{1}{R_{\text{t}}} + \frac{1}{R_{\text{f}}}),$$

The most desirable mode is when the resonance is critically damped. Once the circuit has been built, the feedback resistance chosen and the input

capacitance determined, the only way to increase the damping factor is to increase the feedback capacitance so that equation B.2.3 is satisfied. Substituting the above expressions for δ and ω_0 into equation B.2.3 we get a quadratic in C_f;

$$\omega_\mathrm{u}^2 C_\mathrm{f}^2 + \left(\frac{2\omega_\mathrm{u}}{R_\mathrm{t}}\right) C_\mathrm{f} + \left(\frac{1}{R_\mathrm{f}||R_\mathrm{t}}\right)^2 - \frac{2\omega_\mathrm{u}(C_\mathrm{in}+C_\mathrm{s})}{R_\mathrm{f}} = 0$$

It is desirable to have the resonance term critically damped for a wide range of tunnelling resistances. Solving the above equation for a range of tunnelling resistances gives us the feedback capacitance required for critical damping (see figure 4.21).

Appendix C

Software

C.1 Prospa for STM

Prospa (for Processing package), is derived from a UNIX and then a Macintosh program of the same name. Originally designed to handle NMR data it has been extended in this package with a module to control the STM built by Henning Klank.

The main aim of the package was to provide a user friendly interface, but still include the flexibility of a more powerful data processing package. To this end it has been modelled along the lines of Matlab but with a more specific user interface. Figure C.1 is a typical screen shot of the user interface for STM. Note that the interface is user definable e.g. one large window can be used rather than multiple windows shown.

Several windows are defined in this version. The command line interface (CLI) allows individual commands to be entered and executed. The 1D region displays data stored in vectors while the 2D region displays data stored in matricies. The STM control region contains buttons and text entry fields to interact with the DSP in the STM.

C.2 Operation

To obtain an image the user first presses the walk-down button. This causes the STM probe head to walk down the 0.4 mm ramp until tunnelling current is detected. The status line indicates the mode the STM is currently operating in. When tunnelling has been achieved the user can execute a variety of commands including:

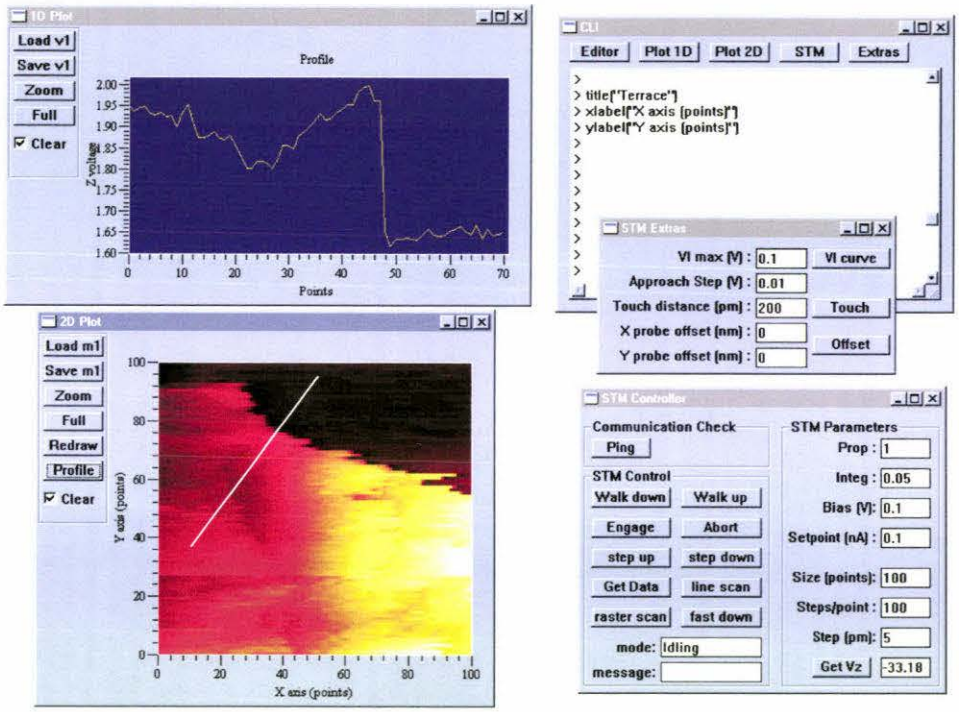

Figure C.1: **software interface:** A screenshot of the Prospa interface showing an image of a terrace of HOPG in the 2D window and a profile in the 1D window. The chosen profile is indicated by the white line in the 2D image.

Generate a V-I curve Here the tip control is temporarily terminated and the bias voltage is ramped from zero to some specified limit while the tunnelling current is recorded. The result will be displayed in the 1D display region. This command is used to check on the oxide level on the tip. An oxide free tip should have a linear V-I curve.

Perform the Soft-touch function Here the tip control is temporarily terminated and the tip is then dropped down towards the surface by a preset distance and then returned to its original position. The tunnelling current during this process is displayed in the 1D display region. This command is used to precondition a noisy tip or modify the surface.

Linescan The tip is scanned in the x direction using the specified steps sizes and number of data points. The data is then transferred to the PC for display in the 1D display region. (The method used is described below).

Rasterscan This generates a 2D image of the surface beneath the tip using the specified parameters. The tip is moved across the surface in small steps (5 pm in this case). During this process the tip is under constant current control and the tunnelling current and Z voltage at each step are summed. After a number of steps (100 here) these data are averaged and written into a line array. This is repeated a number of times (100 again). At the end of each line the data is transferred to the PC for display (i.e. the 2D image is built up in real time). The process is then repeated for the other 99 lines in the image.

Three other commands that are often used are:

Abort Retracts the tip as far from the surface as possible.

Engage Drops the tip down toward the surface until tunnelling current is found. (If not the tip is retracted).

Step up/Step down These raise or lower the probe head by one step (about 10 nm) using the outer piezo actuators. This should normally be done before imaging to ensure that the resting Z voltage is zero. This maximises the scan range and minimises creep. The Get V_z button allows the average Z voltage to be read to check the result of these functions.

While tunnelling the DSP continually checks to see if the tunnelling current is within a specified range. If it goes outside this range the tip will be retracted and the user if warned with an "$|I_t| > 10\,\mathrm{nA}$" message.

Additional commands can be built from these basic ones by writing script files or macros which are processed by the Prospa interpreter. For example the raster scan routine script is presented below:

```
v1 = matrix("real",100);          # Define a 100 point line vector v1
m1 = matrix("real",100,100);      # Define a  100*100 image matrix m1
stm("startrasterscan");           # Tell DSP to start rasterscan
for(i = 0 to 99);                 # Loop 100 times
   stm("rasterscan","v1");        # Get next row of data & store in v1
   m1[~,i] = v1;                  # Save v1 into m1
   displayrow(i,m1);              # Display row as it is loaded
   setpar(winSTM,15,"text",i);    # Update row number in message window
next(i);                          # Repeat until all rows collected
```

In addition to the PC interface the user is presented at all times with oscilloscope traces of the tunnelling current and the Z voltage.

Appendix D

Recent STM developments

D.1 Atomic manipulation

Ever since Gerd Binnig and Henrich Rohrer invented the Scanning Tunnelling Microscope (STM) in 1981, much excitement has been centred around the nanoscopic world of atoms. For the first time, surfaces could be probed on an atomic scale and many crystallography questions were answered and many more asked. For their efforts they were rewarded with a share in the 1986 physics Nobel prize[1].

The scanning tunnelling microscope had been used to modify surfaces as early as 1987 [6] but Eigler and Schweizer were the first to successfully position atoms with atomic precision. Using an STM in an ultra high vacuum at a temperature of 4 K they used a drag and drop technique, detailed in figure D.1, to move 35 xenon atoms on a surface of nickel(110) to spell out the letters IBM, figure see D.2. This technique shows the power of an STM as a research tool for potentially developing atomic sized circuits.

Another interesting demonstration of atomic manipulation was performed in 1993 by Crommie *et al.* Using a surface of copper(111), 48 Fe atoms were arranged into a circle, known as a corral (see figure D.3). The Fe atoms behave as a hard wall and inside the corral, surface electrons are trapped inside a two dimensional, circular, potential well. The STM image, which measures the local density of states (see appendix A.1), shows the electrons behaving like waves. Images of the corral under construction are shown in figure D.4.

Atomic manipulation was always performed at low temperatures and ultra high vacuum to avoid movement of the atoms through thermal excitation. In 1996, Jung *et al.* found a molecule that was suitable enough to manipulate

[1]The other share was awarded to Ernst Ruska for fundamental work in electron optics.

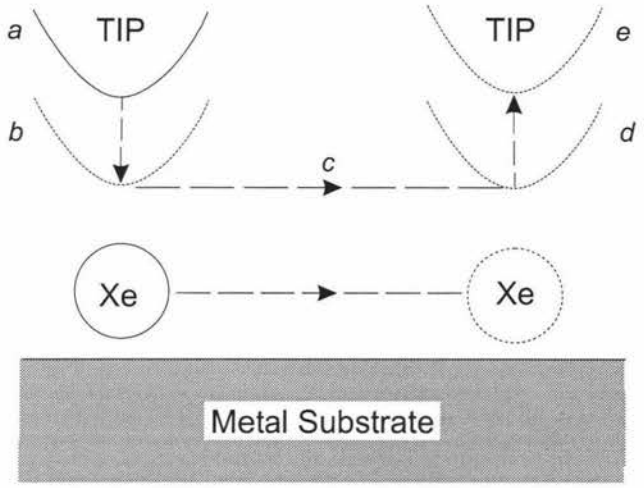

Figure D.1: **Atomic Manipulation:** (a) The tip is 'far' from the surface, in imaging mode. (b) The tip moves close to the atom so that the tip-atom forces become significant. (c) As the tip moves, the forces between the tip and the atom (presumingly van der Waals forces) are strong enough to drag the atom along. (d) The tip comes to rest where the atom is to be 'dropped'. (e) The tip retreats to where the tip-atom forces are insignificant.

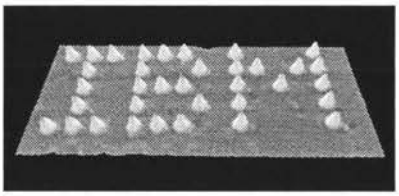

Figure D.2: **Xenon on Nickel:** These atoms were manipulated using an STM at low temperature and high vacuum. This picture appeared in [19].

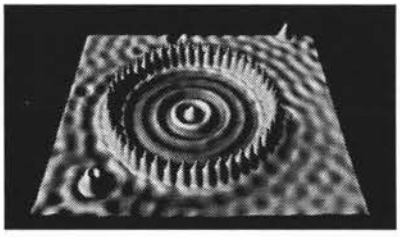

Figure D.3: **A quantum corral:** Fe on Cu(111). The atoms arranged in a circle give a startling picture of the wave-like behaviour of the electrons enclosed in the circle. This picture appeared in [17].

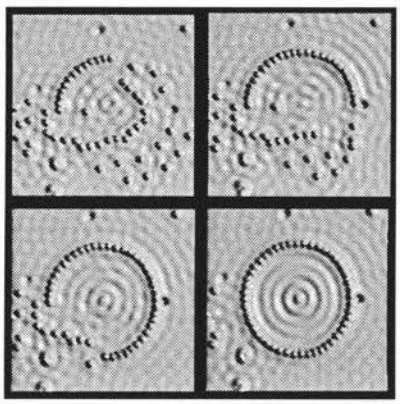

Figure D.4: **Constructing a quantum corral:** STM images are taken at various stages of construction of the corral.

at room temperature. The manipulation was performed on Cu(100) using a rigid molecule with four hydrocarbons attached as "legs". The interactions between the molecule and the sample were strong enough so that the molecule would stay attached at ambient conditions while still allowing the molecule to be "pushed around" by the tip. Similar effects have also been observed with C_{60} 'buckyballs', however, most atomic manipulation is still performed in an ultra high vacuum and at low temperature.

D.2 Quantum mirage

One very recent phenomenon observed as a direct result of atomic manipulation by an STM was reported in *Nature* in February 2000 [32]. Cobalt atoms were placed in an ellipse on a copper surface, making a quantum coral similar to those described above. Another cobalt atom was then placed at one of the foci of the ellipse. Cobalt was chosen as it possesses a net magnetic moment and displays a "Kondo resonance", which is an effect that can be observed with an STM.

When investigating the ellipse using a technique based on the Kondo resonance, a bright spot occurred at the foci with the atom and also at the other foci where there was no atom. This projection was dubbed a "quantum mirage". The 'phantom' atom displays the same energy states of its electrons as the real atom but its Kondo resonance is only about one third of the intensity. This phenomenon could be investigated to see if a real atom will bond with a 'phantom' one, or the quantum corral could be used to transmit information from the real atom to the 'phantom' one.

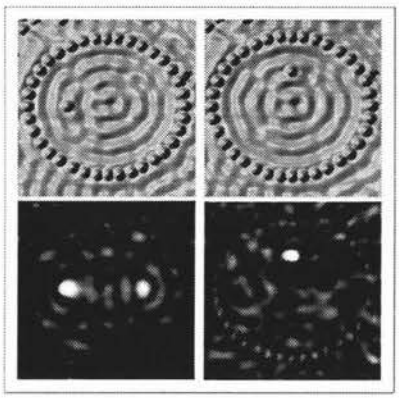

Figure D.5: **A phantom atom:** A measurement technique based on the Kondo resonance (lower pictures) shows the phantom atom at the other foci (lower left). However, when the atom is placed somewhere else (upper right) this effect is no longer observed.

D.3 Single molecule reactions

Reported in *Physical Review Letters* in September of 2000 by Hla *et al.* [26] was the use of an STM to create a chemical reaction between two molecules. The reaction was between two iodobenzene (C_6H_5I) molecules on a terraced copper substrate(see figure D.6). The two iodobenzede molecules were dissociated into phenyl (C_6H_5) and iodine, this is performed by applying a suitable bias voltage for a few seconds. One of the (C_6H_5) molecules is then dragged towards the other and once they are close, a suitable bias voltage is applied to bond the two together. To test if a bond has been made, one phenyl group is moved and the other should move with it. This technique of synthesising reactions at a molecular level could be useful for assembling many other designed molecules or similar nano-scale molecular engineering.

D.4 Summary

The scanning tunnelling microscope will continue to be a useful research tool as the need for smaller electronics continue. STMs have the advantage over AFMs in that they are sensitive to the electronic state of a sample. In areas of high density electronics, a method of transmission between a real atom and a phantom atom could be realised. More likely is the use of single molecules for wires or maybe a molecule could behave like a transistor. Conducting molecules are being investigated, with the help of an STM by Bumm *et al.* [11]. Other ideas include using an STM to manipulate C_{60} bucky balls in an atomic sized abacus [49], this would increase present storage

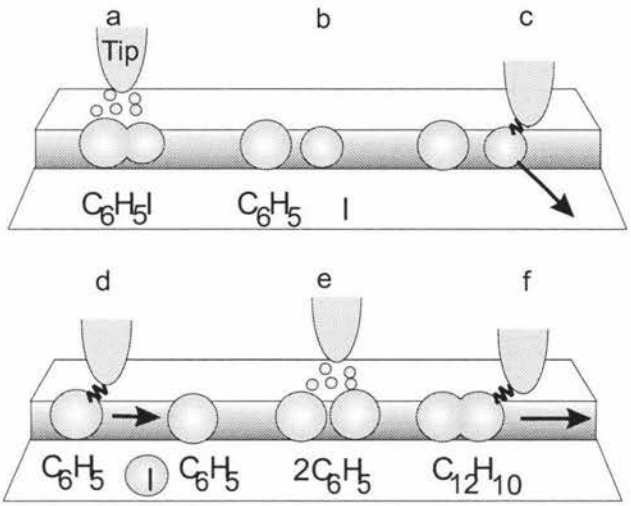

Figure D.6: **Single molecule chemistry:** (a) The STM probe dissociated a C_6H_5I on a copper terrace. (b and c) The iodine atom is drawn away. (d) the C_6H_5 molecule is drawn towards another previously dissociated one. (e) The two molecules are 'welded' together. (f) one C_6H_5 group is pulled to confirm the bond.

capacities by about one thousand. STM's have also been developed to study superconductivity at an atomic level at temperatures down to 240 mK and at fields of up to 7 T [40, 41].

Bibliography

[1] *McGraw-Hill encyclopedia of science and technology.*, volume 13. McGraw-Hill, 8 edition, 1997.

[2] Liu Anwei, Hu Xiaotang, Liu Wenhui, and Ji Guijun. An improved control technique for the electrochemical fabrication of scanning tunneling microscopy microtips. *Review of Scientific Instrumentation*, 68(10):3811–3813, October 1997.

[3] Neil Ashcroft and David Mermin. *Solid State Physics.* Saunders College Publishing, Philadelphia, 1976.

[4] David M. Auslander, Yasundo Takahashi, and Michael J. Rabins. *Introducing Systems and Control.* McGraw-Hill, 1974.

[5] Chunli Bai. *Scanning Tunneling Microsopy and its Application*, volume 32 of *Springer Series in Surface Sciences.* Springer, 1995.

[6] R. S. Becker, J. A. Golovchenko, and B. S. Swartzentruber. Atomic-scale surface modifications using a tunneling microscope. *Nature*, 325:419–421, 1987.

[7] K Besocke. An easily operable scanning tunneling microscope. *Surface Science*, 181:145–153, 1987.

[8] G. Binnig and H. Rohrer. Scanning tunneling microsocpy. *IBM Journal for Research and Development*, 30(4):355–369, 1986.

[9] H. Bourque and R. M. Leblanc. Electrochemical fabrication of scanning tunneling microscopy tips without an electronic shut-off control. *Review of Scientific Instrumentation*, 66(3):2695–2697, March 1995.

[10] P. J. Bryant, S. Kim, and R. Yang. Technique for shaping tunneling microscope tips. *Review of Scientific Instrumentation*, 58(6):1115, July 1987.

[11] L. A. Bumm, J. J. Arnold, M. T. Cygan, T. D. Dunbar, T. P. Burgin, L. Jones, D. L. Allara, J. M. Tour, and P. S. Weiss. Are single molecular wires conducting. *Science*, 271:1705–1707, March 1996.

[12] Burr-Brown. Ultra-low bias current *Difet* operational amplifier. Data sheet, 1994.

[13] Julian Chen. *Introduction to Scanning Tunneling Microscopy.* Oxford Series In Optical And Imaging Sciences. Oxford University Press, 1993.

[14] Thomas H. Courtney. *Mechanical Behavior of Material.* Mechanical and Industrial Engineering. McGraw-Hill, 1990.

[15] D. I. Crecraft, D. A. Gorham, and J. J. Sparks. *Electronics.* Chapman and Hall, 1993.

[16] A. Cricenti, E. Paparazzo, M. A. Scarselli, L. Moretto, and S. Selci. Preparation and characterization of tungsten tips for scanning tunneling microscopy. *Review of Scientific Instrumentation*, 65(5):1558–1560, May 1994.

[17] M. F. Crommie, C. P. Lutz, and D. M. Eigler. Confinement of electrons to quantum corrals on a metal surface. *Science*, 262:218–220, October 1993.

[18] K. Dickmann, F. Demming, and J. Jersch. New etching procedure for silver scanning tunneling microscopy tips. *Review of Scientific Instrumentation*, 67(3):845–846, March 1996.

[19] D. M. Eigler and E. K. Schweizer. Positioning single atoms with a scanning tunnelling microscope. *Nature*, 344:524–526, April 1990.

[20] R. Fainchtein and P. R. Zarriello. A computer-controlled technique for electrochemical STM tip fabrication. *Ultramicroscopy*, 42-44:1533–1537, July 1992.

[21] S. L. Flegler, Jr. J. W. Heckman, and K. L. Klomparens. *Scanning and Transmission Electron Microscopy. An Introduction.* Freeman, 1993.

[22] Mircea Fotino. Tip sharpening by normal and reverse electrochemical etching. *Review of Scientific Instrumentation*, 64(1):159–167, January 1993.

[23] Micheal Fourel. Private communicaiton, 1999.

[24] J Frohn, J F Wolf, K Besocke, and M Teske. Coarse tip distance adjustment and positioner for a scanning tunneling microscope. *Review of Scientific Instrumentation*, 60(6):1200–1201, June 1989.

[25] B. Hacker, A. Hillebrand, T. Hartmann, and R. Guckenberger. Preparation and characterization of tips for scanning tunneling microscopy of biological specimens. *Ultramicroscopy*, 42-44:1514–1518, 1992.

[26] S. W. Hla, L. Bartels, G. Meyer, and K. H. Rieder. Inducing all steps of a chemical reaction with the scanning tunnelling microscope tip: towards single molecule engineering. *Physical review letters*, 85(13):2777–2780, September 2000.

[27] Lisa A. Hockett and Stephen E. Creager. A convenient method for removing surface oxides from tungsten STM tips. *Review of Scientific Instrumentation*, 64(1):263–264, 1993.

[28] J.P. Ibe, P.P. Bey Jr., S.L. Brandow, R.A. Brizzolara, N.A. Burnham, D.P. DiLella, K.P. Lee, C.R.K. Marrian, and R.J. Colton. On the electrochemical etching of tips for scanning tunneling microscopy. *Journal of Vacuum Science and Technology*, 8(4):3570–3575, July 1990.

[29] Keithley Instruments, 28775 Aurora Rd., Cleveland, OH 44139, USA. *Low Level Measurements*, fourth edition, 1993.

[30] H. A. M. Klank. *Design of digital instrumentation for scanning probe microscopy*. PhD thesis, Massey University, 2000.

[31] M. Klein and G. Schwitzgebel. An improved lamellae drop-off technique for sharp tip preparation in scanning tunneling microcopy. *Review of Scientific Instrumentation*, 68(8):3099–3103, August 1997.

[32] H. C. Manoharan, C. P. Lutz, and D. M. Eigler. Quantum mirages formed by coherent projection of electronic structure. *Nature*, 403:512–515, February 2000.

[33] Allan J. Melmed. The art and science and other aspects of making sharp tips. *Journal of Vacuum Science and Technology B*, 9(2):601–608, May 1991.

[34] A. D. Müller, F. Müller, and M. Hietschold. Characterization of electrochemically etched tugsten tips for scanning tunneling microscopy. *Review of Scientific Instrumentation*, 70(10):3970–3972, October 1999.

[35] L. A. Nagahara, T. Thundat, and S. M. Lindsay. Preparation and characterization of stm tips for electrochemical studies. *Review of Scientific Instrumentation*, 60(10):3128–3130, October 1989.

[36] Y. Nakamura, Y. Mera, and K. Maeda. A reproducible method to fabricate atomically sharp tips for scanning tuneling microscopy. *Review of Scientific Instrumentation*, 70(8):3373–3376, August 1999.

[37] Peter G. Nelson. Technical background. Technical report, TMC Technical Manufacturing Corporation, 15 Centennial Drive, Peabody, Massachusetts 01960, USA, 1999. Internet: www.techmfg.com.

[38] J. V. Nicholas and P. R. White. *Traceable Temperatures, An Introduction to Temperature Measurement and Calibration.* John Wiley and Sons, 1994.

[39] A. I. Oliva, A. Romero G., J. L. Peña, E. Anguiano, and M. Aguilar. Electrochemical preparation of tungsten tips for a scanning tunneling microscope. *Review of Scientific Instrumentation*, 67(5):1917–1921, May 1996.

[40] S. H. Pan, E. W. Hudson, and J. C. Davis. ^{3}He refrigerator based very low temperature scanning tunnelling microscope. *Review of scientific instruments*, 70(2):1459–1463, Febuary 1999.

[41] S. H. Pan, E. W. Hudson, K. M. lang, H. Eisaki, S. Uchida, and J. C. Davis. Imaging the effects of individual zinc impurity atoms on superconductivity in $Br_2Sr_2CaCu_2O_{8+\delta}$. *Nature*, 403:746–749, February 2000.

[42] Sang-Il Park and C. F. Quate. Tunneling microscopy of graphite in air. *Applied Physics Letters*, 48(2):112–114, January 1986.

[43] M. V. H. Rao and B. K. Mather. Sharp tungsten tips for scanning tunnelling microscope prepared by electrochemical etching process. *Indian Journal of Pure and Applied Physics*, 31:574–576, August 1993.

[44] Kirsteen Rogers. *The Usborn Complete Book of the Microscope.* Usborne Publishing Ltd, Usborne House, 1998.

[45] M. Schmid and P. Varga. Analysis of vibration-isolating systems for scanning tunnelig microscopes. *Ultramicroscopy*, 42-44:1610–1615, 1992.

[46] R. Scoholz, M. Agne, O. Breitenstein, and H. Jenniches. Low thermal power electron beam annealing of scanning tunneling microscope tips. *Review of Scientific Instrumentation*, 68(8):3262–3263, August 1997.

[47] Robert Simpson. *Introductory Electronics For Scientists And Engineers.* Allyn and Bacon, Boston, second edition, 1987.

[48] J. Tersoff and D. R. Hamann. Theory and application for the scanning tunneling microscope. *Physical Review Letters*, 50(25):1998–2001, July 1983.

[49] J. A. Thomas. Atomic abacus. New Scientist, February 2000.

[50] R. Wiesendanger and H. J. Gütherodt (Eds.). *Scanning Tunneling Microsopy II*, volume 32 of *Springer Series in Surface Sciences.* Springer, 1995.

[51] Hugh Young. *University Physics.* Addison-Wesley Publishing Company, Reading, Massachusetts, eighth edition, 1992.

[52] D. G. Zill. *A first course in differential equations.* PWS publishing company, 5th, 1992.